The positive excess of cosmic ray muons at large zenith angles

Mackeown, P. K.

The Positive Excess of Cosmic Ray Muons at Large Zenith Angles

by

P.K. MacKeown, B.Sc.

A thesis submitted to the University of Durham, in support of an application for the degree of Doctor of Philosophy.

November, 1965.

Contents

Abstract

Details of two solid iron magnetic spectrographs, incorporating neon flash tubes, with m.d.m.'s. of 300 GeV/c and 1950 GeV/c are presented, as are the results on the μ^+/μ^- ratio in the zenith angular ranges 77.5° - 90°, and 82.5° - 90° based on samples of 10832 particles and 2167 particles respectively, obtained with these instruments. In the energy region where comparison with the work of other authors can be made agreement obtains. The overall results confirm, in general, previous values below 200 GeV but do not show any great evidence for a sharp minimum in the ratio in the region of 50 - 100 GeV as reported by some authors. At higher energies the present results do not show a rapidly increasing ratio, as was expected from an extrapolation of earlier measurements.

A review of all published measurements on the μ^+/μ^- ratio is presented, which suggests an approximately constant ratio from $E_\mu \sim 3$ - 10^3 GeV, of 1.20 - 1.25.

In an effort to give a theoretical interpretation of the results it is shown that pion production within the framework of a statistical model based on our knowledge of nucleon interactions at high energies will not account for the experimental data. The effect of, and evidence for, the production of kaons, subject to certain assumptions, is investigated and it is concluded that, under the assumptions considered, the adopted value of the K/π ratio is not sufficient to account for the data in the region E_μ = 10 - 50 GeV.

The effect of other dynamical models such as the isobar model and the O.P.E. model are considered. It is argued that the production of $T = \frac{1}{2}$ isobars with a slowly decreasing cross-section, combined with the other features of nucleon interactions as observed at accelerator energies, is sufficient to account for the present experimental position when the errors in the experimental data are taken into account, but none of several proposed models for particle

production in high energy interactions can be uniquely selected on the basis of the results.

Preface

The work reported in this thesis was carried out in 1963-1965 while the author was a research student, under the supervision of Professor A.W. Wolfendale, in the Cosmic Ray Group in the Physics Department of the University of Durham.

The author was responsible for the collection, analysis and interpretation of data obtained in an extended run of the spectrograph described by Pattison (1963), and for a modification of this instrument which involved its longitudinal extension and the introduction of an additional magnet and tray of flash tubes. With his colleagues he was also responsible for the operation of the modified instrument and the collection of data over a running period of 2100 hours and the subsequent analysis and interpretation of this data.

Interim reports by the author and his colleagues on the results have been presented at International Cosmic Ray Conferences, at Jaipur (1963) and London (1965), a note on the charge ratio was published by Ashton et. al. (1963), and a paper on the spectrum is in the press, Ashton et. al. (1965).

CHAPTER 1

INTRODUCTION

1.1 Cosmic Ray Research

From its initial discovery at the beginning of this century, the cosmic radiation has proved to be an extremely profitable field of investigation, and has attracted research workers in large numbers. These studies may be divided, if crudely, into two types. The first comprises studies of the primary radiation, with particular interest in such quantities as the energy distribution, particle composition, directionality, time variations and its interaction with the earth's geomagnetic field. This work, with a view to gaining information on the nature and origins of the radiation, we may classify as pure cosmic ray studies branching into astronomy and astrophysics. The second class of studies are more concerned with the fundamental interactions of the individual components of the radiation.

As the sole source of highly energetic particles in the 1930s the cosmic radiation proved invaluable in investigating the electromagnetic interaction at high energies and resulted in the discovery of the positron, while the detailed study of bremsstrahlung provided a remarkable confirmation of the then recently developed theory of quantum electrodynamics. Even today the cosmic radiation is used as a source of high energy particles to test the

validity of quantum electrodynamics at ultra high energies, e.g. Neddermeyer and Curtis (1963), and to investigate the so called nuclear interaction of muons in which photoproduction of pions occurs through the interaction of the virtual photon flux of the muon with nucleons e.g. Bull et. al. (1965). Even in the field of weak interactions, and despite the low fluxes, cosmic ray studies have become of great importance; the observation of neutrino induced interactions having recently been achieved by Achar et. al. (1965) at great depths under the earths surface using conventional cosmic ray techniques.

However, it is in the field of strong interactions that comsic ray studies have been outstandingly successful, from the original (if erroneous) discovery of the force quantum predicted by Yukawa to the discovery of the mesons and hyperons in the postwar years. The discovery of the π mesons and K mesons effectively created a whole new branch of physics, the field of elementary particles, which has attracted vast numbers of research workers. Not only did cosmic ray work provide the impetus for the construction of present day accelerators, but developed most of the techniques employed in 'machine physics.'

1.2 Nature of the Radiation

The primary radiation incident on the top of the earths atmosphere is composed almost entirely of nuclei with values of Z up to at least 26 of which the vast majority are protons, and a small, recently established, flux of electrons. The existence of high energy photons, γ rays, in the primary radiation, although of great interest has not yet been unambiguously established, but is under active investigation. Because of their finite

lifetime free neutrons do not form a part of the primary flux, neutrons only occurring as constituents of nuclei. Apart from perturbations due to the earths magnetic field, which are negligible at energies above a few tens of GeV, the incident radiation is isotropic at least up to energies of $\sim 10^{13}$ eV, and any anisotropy above this energy is small. Protons and neutrons occur in the primary radiation in the ratio 87/13, constant over a wide energy interval. The intensity of primary nucleons is a rapidly varying function of their energy, with an integral spectrum $N(>E_o) \propto E_o^{-2.6}$ and an intensity of 10^{-3} cm^{-2} sec^{-1} steradian^{-1} above an energy of 100 GeV. Energies as high as 10^{20} eV have been detected.

The primary nucleons collide with the air nuclei in the atmosphere, the interactions being characterised by a mean free path of ~ 80 g cm^{-2}, giving rise to the cascade, whose components are studied at various altitudes and at sea level. The characteristics of these interactions appear reasonably constant over a very wide range of energy; the dominant features being the production of π mesons, both charged and neutral, and the retention by the nucleon of a large fraction of its initial energy, resulting in an extended cascade down through the atmosphere. The charged pions produced in the interactions are subject to two competing mechanisms; interaction, which contributes further to the development of the cascade, and decay, whereby muons are produced, the former increasing in importance with increasing energy and depth in the atmosphere. The neutral pions, having a very short lifetime ($\tau_{\pi^o} = 1.8\ 10^{-16}$ sec), all decay giving rise to photons which materialise into electron pairs, and these in turn radiate more photons, and by this method the electron-photon component develops. Because of their relatively

long lifetime (τ_μ = 2.20 10^{-6} sec), and the fact that they do not have a strong interaction, most of the muons above 1 GeV survive to sea level, gradually losing energy along their path. Since the total vertical depth of the atmosphere is 1030 g cm^{-2} the flux of nucleons at sea level above a given energy is very much smaller than the primary flux, and at this depth the flux is dominated by the secondary components, mainly muons and electrons.

1.3 Studies of the Interactions

Depending on the features being studied and the energy range of interest the techniques used in cosmic ray studies are very diverse. In the early work the cloud chamber was the instrument responsible for the most important discoveries. A significant advance in the study of interactions induced by cosmic rays took place with the development of the nuclear emulsion, which could be flown at great altitudes where the flux of energetic nucleons is greatest, and it was by this means that several of the 'elementary' particles were discovered. More recently the development of spark chambers has produced new results, especially when used in conjunction with scintillation counters in the 'ionisation calorimeter', which enables the interaction of very high energy cosmic rays to be studied in considerable detail at mountain altitudes. At the very highest energies, $E_o \gtrsim 10^{15}$ eV, localised interactions of nucleons cannot be studied because of the very low particle fluxes, and the only way these interactions can be investigated is from observations on the secondary products of the interaction in extensive air showers.

While at lower energies, $E_o \lesssim 10^{14}$ eV, the fluxes are sufficient for emulsion studies to be made, it is convenient, and of interest, to complement such studies with similar indirect studies of the secondary components. This

arises since, if the theory of propagation of the secondary component in the atmosphere is known, one can work backwards to infer the properties of the interactions. That studies of this type should still be of value, so many years after the introduction of accelerators, is due to the fact that the maximum energy attainable with these accelerators is not sufficiently high for all the characteristics of the interaction to be manifested, i.e. they are not in the so called asymptotic region as was at one time believed; recent theoretical considerations indicate that strong interactions acquire new features at energies where $\ln(E_0/M) \gg 1$, where M is the nucleon mass, Chernavsky and Feinberg (1963), and this quantity is only ~ 3 at $E_0 = 30$ GeV. Evidence in this direction has been accumulating from cosmic ray work for some time, especially from the analysis of jets in emulsions, which encourages cosmic ray studies at a fractional cost of accelerator work.

Since the muon sea level flux is of reasonable intensity and studies at sea level are relatively simple a considerable effort has been devoted to investigating this component in the past. Among the properties of the muon beam that can be studied are its energy spectrum, charge composition and polarisation, and its variation with altitude and zenith angle. Apart from confirming the results of localised studies of interactions these indirect methods are capable of investigating quantities which cannot easily be measured by the other methods e.g. the charge composition.

1.4 Muon Studies

The quantity of greatest interest pertaining to the muon flux is its energy spectrum and many efforts have been devoted to its determination over the years. Using the spectrograph technique one can measure the momentum

of positive and negative muons separately and thus investigate the charge composition of the muon beam, and it turns out that the investigation of the muon charge ratio, defined as the ratio of the number of positive muons to the number of negative ones in a given momentum interval in the incident flux, $R = N(\mu^+)/N(\mu^-)$, is of no less interest than the spectrum itself. The particular importance of this quantity μ^+/μ^- - henceforth $\mu^\pm$ will denote the number of $\mu^\pm$ etc., where no confusion is likely to arise - arises from the fact that, as will be discussed later, it is very closely related to the primary nucleon interaction.

Spectrographs have been subject to much modification over the years, each new design having its own advantages, and, more particularly its own sources of bias. Many of the early spectrographs incorporated a cloud chamber between the pole faces of an airgap magnet. This arrangement suffered from several disadvantages, not least of which, as was pointed out by Hyams et. al. (1950), was the very inefficient use of the deflecting volume of the magnetic field, and these authors developed the general principles for the design of a spectrograph where the deflection and detection regions were separated. These authors constructed such a spectrograph using Geiger counters as detecting elements, having a maximum detectable momentum of $\sim$ 30 GeV/c - a similar instrument was independently developed by Caro et. al. (1951). While the resulting increase in resolution and increased collecting power were a great improvement, the inability to study events in detail due to the absence of visual detectors was sorely felt. Extensive spectrum measurements were made with instruments of this type and they contributed significantly to the establishment of the vertical muon spectrum and charge

ratio, but they were all subject to an unknown bias due to the necessary rejection of accompanied particles, and those producing knock-on showers in traversing the instrument. The reintroduction of visible detectors at the detecting levels, cloud chambers by Pine et. al. (1959), Holmes et. al. (1961a), and the more versatile flash tube (Conversi tube) by Brooke et. al. (1962a), not only increased the resolution but made more definite intensity measurements possible. Using these techniques, the muon momentum spectrum in the vertical direction was measured up to several hundred GeV/c. by Hayman and Wolfendale (1962b).

The investigation of muons at high energies is limited by two factors; the momentum resolution possible with conventional spectrographs and the low flux of particles. Among other attempts to overcome the first limitation we may mention the introduction of spark chambers at the measuring levels by Allkofer (1960), who investigated the spectrum up to 60 GeV/c, and the emulsion spectrograph of Allen and Apostolakis (1961). Both these instruments while in principle capable of very good resolution, suffered from small collecting power. Other methods of studying muons at high energies are the investigation of electromagnetic bursts produced by muons, e.g. Higashi et. al. (1964), and measurements of intensity as a function of depth underground, e.g. Miyake et. al. (1964), but while these methods enable a determination of the muon spectrum to be made, no information on the charge composition can be obtained. On the other hand the results of Hayman and Wolfendale (1962b) indicate that both good resolution and large apertures can be obtained using simple flash tube arrays.

When one is specifically interested in high energy muons the enormously greater flux of low energy particles in the vertical direction is a con-

siderable complication in the measurements and analysis. At large zenith angles the muon spectrum has a very different shape at low energies where the relative intensity of low energy particles is very severely reduced with a resulting much higher mean momentum of the muons in the flux. Also at very large zenith angles the overall intensity of muons with energy greater than ~ 100 GeV is greater than in the vertical direction, and combined with the fact that at a given sea level energy one is investigating considerably higher production energies, studies of the primary interactions at high energies via the muon component are best carried out at large zenith angles. These features of the spectrum arise from the fact that at large angles the path length traversed, and thus the energy loss of the muon, is very much greater than in the vertical direction, ~ 36 times more matter at $\theta = 90^{\circ}$ then at $\theta = 0^{\circ}$; and the properties of the atmosphere at the production level are very different at the large zenith angles such that pion decay successfully competes with pion interaction up to much higher pion energies. Measurements up to $\theta = 60^{\circ}$ were carried out by Moroney and Parry (1954), and extended to the extreme zenith angles by Jakeman (1956), who studied muon intensities in the angular range $88^{\circ} - 90^{\circ}$ with a view to determining the lifetime of the parents of the muons, and Wilson (1959) who studied the isotropy, time variation and angular distribution of muons in the range $86.5^{\circ} - 90^{\circ}$. These early studies either only measured integral intensities or did not extend to sufficiently large zenith angles.

Apart from the purity of the incident beam and the augmented flux of high energy particles, the investigation of muons at large zenith angles is of additional interest from the fact that by a comparison with the vertical

spectrum, some characteristics of the particles giving rise to the muons may be inferred, in particular the contribution of particles other than pions to the muon flux, provided the characteristics of propagation are known. Mindful of the calculations of Smith and Duller (1959), Maeda (1960, 1964), and Zatsepin and Kuzmin (1961), on the expected spectrum at large zenith angles and following the interesting results of Hayman and Wolfendale (1962a), which indicated an appreciable charge ratio up to a few hundred GeV, for which confirmation would be desirable since this quantity plays an important role in the interpretation of high energy interactions, two groups undertook muon studies at large zenith angles since only here could the necessary statistics be built up in a reasonable period of time. At Durham a hodoscoped geiger counter spectrograph using a solid iron magnet to study muons at 80° was constructed, Ashton and Wolfendale (1963). A similar instrument at 78° was developed by the Nagoya group, Kamiya et al. (1963). The replacement of air gap magnets by solid iron ones enables large acceptance apertures to be used since in this case a uniform field over a large volume can be obtained, and the induction can be made quite large with modest power supplies. Also because at low energies the spectrum is much softer at large zenith angles the effect of coulomb scattering in such an instrument is not as pronounced as at the vertical. More recently spectrum measurements at 83° - 90° have been carried out by Judge and Nash (1965) using a spectrograph and by Borog et. al. (1965) studying muon burst production at $\theta > 60^{\circ}$.

1.5 The Present Work

The Durham instrument was modified by Pattison (1963) who introduced flash tubes at the four measuring levels and reorientated it to detect

muons in the range 77.5 - 90°. The first half of the present work is concerned with the measurement of the muon charge ratio in the range 77.5 - 90° with this instrument, to be known as Mk 1, the modification of this instrument to increase its resolution, the modified version to be known as Mk 2, and the determination with the latter instrument of the muon charge ratio in the range 82.5° - 90° up to muon energies of $\sim 10^3$ GeV. The second half of the work will be devoted to a review of all charge ratio measurements, and an investigation of the properties of high energy interactions relevant to its interpretation. Finally, conclusions are drawn on the most likely explanation of the present experimental situation.

CHAPTER 2

The Spectrographs

2.1 The principles of a momentum spectrograph

By virtue of the fact that a particle of charge e, traversing a magnetic field of strength B, experiences a force given by

$$F = e\,\underset{\sim}{v} \wedge \underset{\sim}{B}, \text{ or } |F| = p.v/\rho$$

we have $$p = mv = \rho e\,\underset{\sim}{v} \wedge \underset{\sim}{B} = B\rho \sin\theta \frac{ds}{d\varphi}$$

where $\rho = \frac{ds}{d\varphi}$ is the radius of curvature of the path. Then the total angle of deflection on traversing the field is,

$$\varphi = e \int \frac{B \sin\theta \, ds}{p}$$

$$= e \int \frac{B \, d\ell}{p}$$

where $d\ell$ is an element of path perpendicular to the magnetic field. If we can ignore the energy loss, and thus varying momentum, in traversing the field we have, for B in gauss, ℓ in cm and φ in radians

$$p = \frac{300}{\varphi} \int B \, d\ell \quad \text{eV/c} \qquad \ldots\ldots\ldots(2.1)$$

To determine high momenta one must therefore have maximum resolution in the deflection φ, though it must necessarily be compromised with the aperture because of the low flux of high energy particles. In the present case the two features most serious in limiting the resolution are:-

(i) the finite size and efficiency of the flash tubes and the accuracy of their alignment, and

(ii) the multiple coulomb scattering suffered by the particle in traversing the instrument. Further, for spectrum measurements, which require absolute intensities, several other factors arise, notably the knowledge of the detection

efficiency and the degree of bias introduced by the selection criteria used; a detailed analysis of the spectrum determination will not however be presented here.

The deflection is obtained from a number of measured co-ordinates along the track of the particle, and an uncertainty in the momentum, increasing relatively with increasing momentum, will arise from uncertainties in these co-ordinates. Since for high resolution the locating levels must be widely separated the alignment of the co-ordinate system becomes a considerable problem.

Superimposed on any magnetic deflection there will occur a projected angle of scattering in the deflection plane, which becomes particularly serious for the present work because of the great amount of matter traversed by a muon in passing through the spectrograph. The root mean square projected angle due to coulomb scattering is given by

$$\langle \psi \rangle = \frac{K}{\beta p \sqrt{2}} \sum t^{\frac{1}{2}}$$

if the momentum is assumed constant throughout the path. $\sum t$ is the total thickness of material traversed in radiation lengths and β the relative velocity of the particle. Since in the present work the scattering outside the magnetic field region is small compared with that in the iron magnet $t \propto l$ whence we have the ratio of magnetic deflection to r.m.s. scattering deflection

$$\varphi / \langle \psi \rangle \propto \sqrt{l} \quad , \quad \text{for } \beta \to 1 \quad \ldots\ldots\ldots (2.2)$$

which is seen to be independent of momentum. The more general theory, taking the continuous energy loss into account is considered by Ashton and Wolfendale (1963), where it can be seen that this relation holds, to a good accuracy, down to quite low energies.

Where a solid iron magnet is used the energy loss in traversing the field becomes important at low energies, because of the rapidly varying spectrum being measured. The resulting angular and linear deflections have been considered by Ashton and Wolfendale (1963), who find that the momentum on entering the magnet is given by

$$p = \alpha l / (1 - \exp - (\frac{\alpha \varphi}{300B}))$$

instead of expression (2.1), for constant B, where α is the mean momentum loss per unit of path length. For analysing the data the simple relation (2.1) will be used, and the necessary correction at low momenta may be applied to the observed intensities to find the incident spectrum.

2.2 The Spectrographs

The Mk 1 spectrograph consisted of a solid iron magnet, with the deflecting plane vertical, flanked on each side by two vertical trays of Geiger counters whose axes were parallel to the field. Each of these Geiger trays was shadowed by a tray of neon flash tubes with their axes parallel to the Geiger counters. An additional, horizontal, Geiger tray was placed above the instrument to reject extensive air showers. A schemetic diagram of the instrument is given in fig. 2.1. Geiger trays A,B,C,D are connected to a four-fold Rossi coincidence circuit which in turn feeds into an anticoincidence gate. Also input to the anticoincidence unit are the pulses from the rejection tray E. The registration of an event is thus effected by an ABCD$\bar{E}$ coincidence. When this condition is satisfied the anticoincidence unit triggers the high voltage unit which supplies the voltage across the electrodes in the flash tube trays, whereby those tubes through which a charged particle has passed glow, and are photographed. The gate also paralyses the Rossi circuit, and

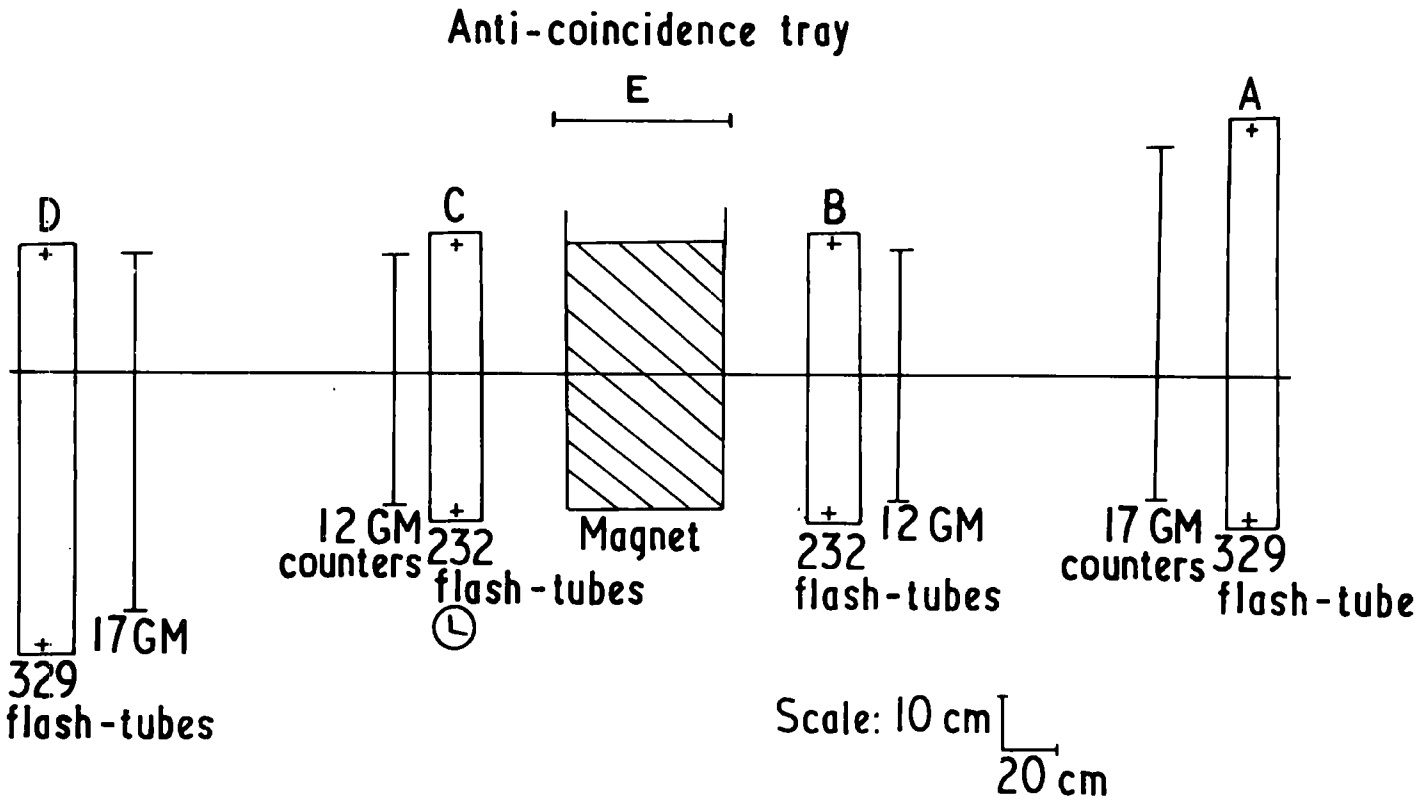

Fig. 2.1 - Schematic diagram of the M.I.T. spectrograph.

triggers a cycling system, of 3 sec period, which illuminates fiducial lights on the flash tube trays, and a clock, and winds on the film in the camera in readiness for the next event.

2.3 The deflection and detection elements

The magnet, described in detail by O'Connor and Wolfendale (1960), is in the shape of a large transformer core, and consists of 50 iron laminations - (of composition 99.04% Fe, 0.36% Mn, 0.2% Cu, 0.11% Ni with traces of other elements) - of nominal thickness 0.5 inches each. These plates are mounted vertically in an iron cradle and the gaps between the plates reduced to a minimum by the pressure of retaining bolts. The excitation coils consist of 250 turns of 14 SWG double cotton covered copper wire on each limb, of total resistance 5.70 ohms, and self inductance 250 mH. The current is supplied from a mains rectifier and a reversing switch is incorporated in the circuit. The magnetic induction as a function of excitation current is shown in fig. 2.2a. The volume uniformity of the field was studied in detail by the authors cited above and is uniform to $\sim 2\%$. Thus for a given excitation current $300 \int B \, d\ell = \text{const.} = C'$ and we have

$$p = C'/\varphi \qquad \ldots\ldots(2.3)$$

Each Geiger counter was fitted with its own switch, and set at a voltage such that a variation of $\pm$ 30 volts did not affect its counting rate. The Geiger counters are of the type 20th Century Electronics G60, of sensitive length 60 cm and internal diameter 3.35 cm. The Geiger counters, with their axes parallel to the magnetic field were arranged in ladder formation in vertical frames, small air gaps remaining between the tubes. Groups of four counters were attached to a quenching unit, included, although the tubes are self quenching, to reduce and make more definite the dead time, from which the

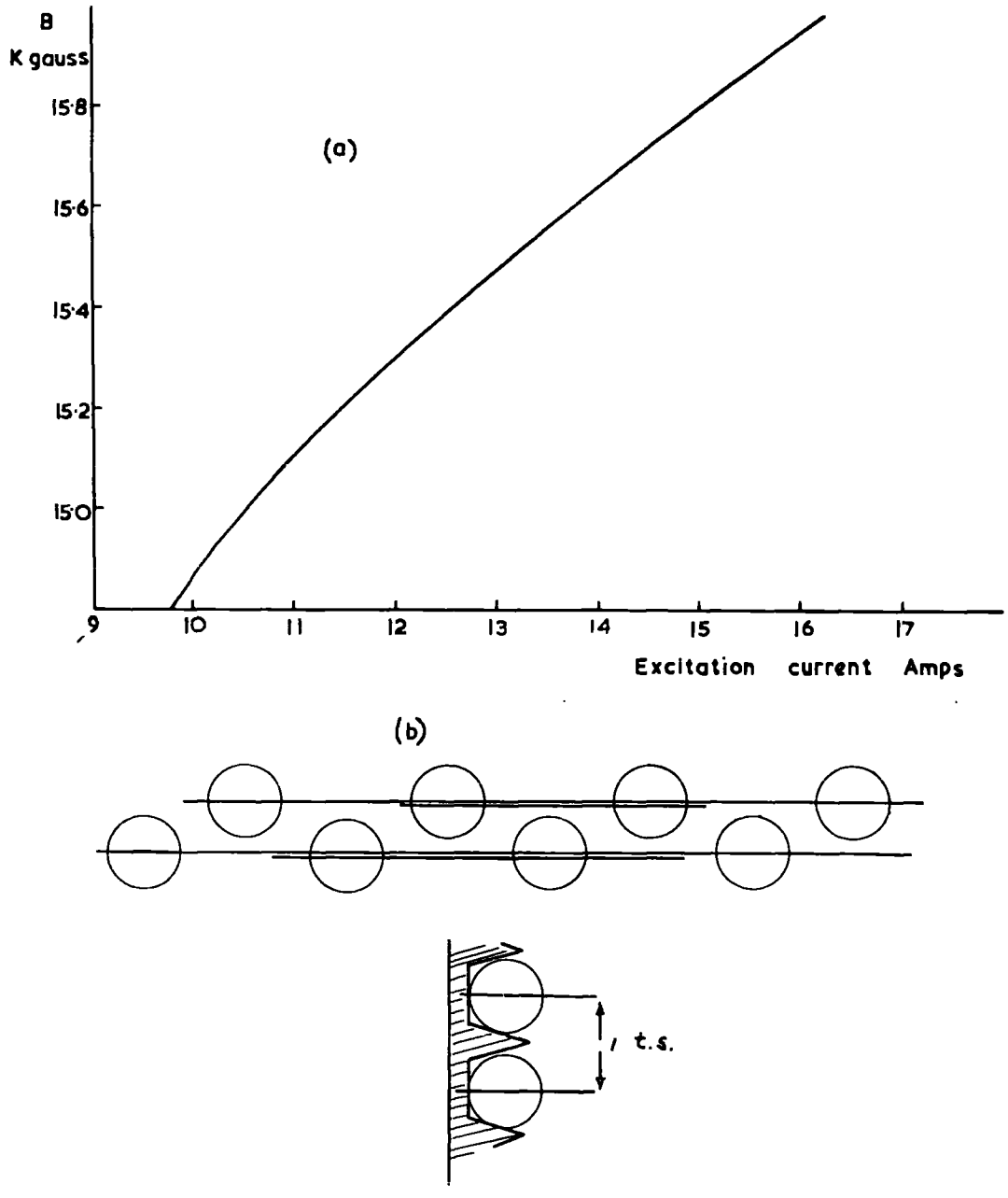

Fig.2.2 (a) Magnetic induction vs current.
(b) The arrangement of the flash tubes.

output pulses are taken.

Each Geiger tray had a tray of flash tubes shadowing it which served as the display elements. Detailed investigations into the characteristics of these tubes have been carried out by Gardner et.al. (1957) and Coxell and Wolfendale (1960), and the theory of their operation has been discussed by Lloyd (1960). The tubes, of the type described by Coxell (1961), are ~80 cm in length and 1.5 cm external diameter made of soda glass and filled with Neon to a pressure of 60 cm Hg with a plane window at one end. These tubes are the result of a detailed investigation by Coxell (1961) into the characteristics and optimum design of such tubes. The rate of spurious flashing of the tubes is 0.6 per 1000 pulses at the operating voltage. Each of the four trays of flashtubes contained eight columns of tubes, a column in trays A and D containing 41 tubes and one in trays B and C 29. The columns were interleaved with aluminium electrodes, alternate ones being connected together, the outermost ones being earthed. The tubes were supported in frameworks of slots accurately milled in identical tufnol rods, see fig. 2.2b, and arranged so that any bow in the tubes was in the horizontal plane, so as to minimise uncertainty in location in the vertical direction due to non uniformity of the tubes. The individual columns were staggered relative to each other, fig. 2.2b, such that at least four tubes per tray are traversed by a particle; in the majority of cases not less than six tubes were observed to flash in a tray along the path of a particle. The vertical separation of adjacent slots is 1.905 $\pm$ 0.002 cm, a unit henceforth to be referred to as a 'tube spacing' and abbreviated to t.s. The mean column efficiency under the operating conditions was 78%. The horizontal separation between columns is 2.8 cm. Each flash tube tray was fitted with two fiducial lights which were flashed when a particle was registered and served to locate the positions of the trays on projection of the film.

All four trays were photographed on the same frame on red sensitive 35 mm film (Ilford HP3) via a system of plane mirrors. Also registered on the same frame were the fiducial lights on each tray and the illuminated dial of a clock to record the time of each event.

The high voltage unit consisted of a small thyratron which was triggered by the anticoincidence unit. This in turn triggered a large hydrogen thyratron via a pulse transformer which in turn triggered four triggatron valves. The pulses from the triggatrons were delivered to the tray electrodes via pulse transformers. The delays in the electronic circuitry were such that the pulse reached the electrodes ~9 μsec after the particle traversed the instrument, such a time delay being fully compatible with the efficiency vs. time delay characteristics of these tubes. The final H.T. pulse had a rise time of 0.8μ sec, to a maximum of 8 kV and a width of ~2.5 μsec, producing a field across the tubes of 2.86 kV/cm.

2.4 Alignment of the instrument

For accuracy of measurements it is vital that all the flash tubes be accurately parallel to each other throughout the instrument and that their relative vertical positions be known. In this respect the alignment of a horizontal instrument, of considerable length - Mk 1 is 4.5 m long - is more difficult than for a vertical instrument.

The frameworks supporting flash tube trays B and C were affixed to the magnet cradle, while trays A and D were supported in frames firmly fixed to the floor of the laboratory. Each tray was suitably fitted with adjusting screws such that it could be positioned in its frame in the three perpendicular directions during alignment.

Alignment in the longitudinal direction was effected as follows: to each of the flash tube frames four plates each containing a small hole were affixed in identical positions. Through these plates tensioned cotton threads were run, and the trays then adjusted such that the threads were judged to pass through the centres of the holes. The degree of alignment in the vertical plane was also checked by measuring the separation of corresponding points on the trays, at top and bottom, The degree of horizontality of the tubes was checked by three methods; optically, by removing a flash tube and using a cathetometer and telescope focussing through the groove to the other side, secondly by using a sensitive spirit level and thirdly by replacing a flash tube by an identical closed glass tube containing a small amount of mercury.

When the instrument was aligned it was necessary to measure the constants of the spectrograph, The important ones were a_o, b_o, c_o and d_o as shown in fig. 2.3, these being the distances from a horizontal reference level to arbitrary origins of co-ordinates in each tray. The origin of co-ordinates in all the trays was taken as the centre of the lowest tube in the fourth column from the north. The reference level was defined by two tensioned cotton fibres stretched the length of the spectrograph, supported on knife edges at each end, the latter having been set in the horizontal plane by means of a cathetometer, with which the constants were also measured. This procedure was carried out by three independent observers. Corrections were applied for the catenary effect on the fibre, different tensions being used as a check on this. The final values, along with the longitudinal dimensions are given in table 2.1. An alternative procedure for measuring the constants was adopted for the Mk 2 spectrograph and will be described later. The best check on the

Table 2.1

Adopted values of the Geometrical Constants

	Mk 1		Mk 2	
Dimension	cm	ts	cm	ts
ℓ_1	149.15 ± 0.02	78.29 ± 0.01	334.5	175.59
ℓ_2	74.54 ± 0.04	39.13 ± 0.02	146.4	76.85
ℓ_3	71.95 ± 0.03	37.77 ± 0.02	146.7	76.85
ℓ_4	150.44 ± 0.05	78.97 ± 0.03	334.5	175.59
a_o	25.643 ± 0.003	13.461 ± .002	26.547	13.935
b_o	25.864 ± 0.002	13.577 ± .001	25.884	13.587
c_o	25.512 ± 0.002	13.392 ± .001	24.919	13.081
d_o	0 ± 0.002	0 ± .001	0	
x_o	-		25.559	13.417

1 ts = 1.905 cm

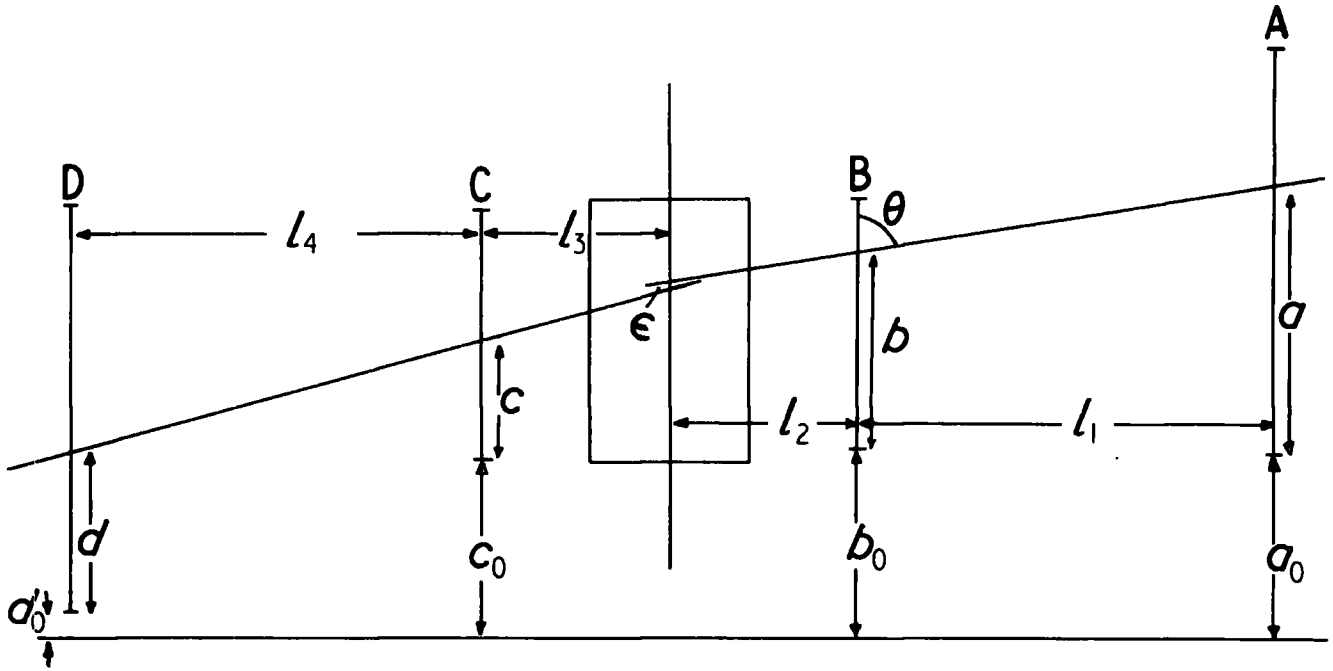

Fig.2.3 The measured coordinates in the Mk.1 spectrograph.

accuracy of the quoted constants would be to do a series of measurements with no magnetic field in the instrument, but since the magnet was fixed this proved to be impracticable in the present case and the simplest check possible is from an investigation of the discrepancies in the measured tracks of detected particles and this is considered later in the chapter.

The Geiger counters were aligned in a similar manner, the tubes being positioned parallel to the magnetic field.

2.5 The Mk 2 Spectrograph

In view of the results obtained with the Mk 1 instrument, especially the apparent confirmation of the work of Hayman and Wolfendale (1962a) on the charge ratio of muons in the region of 200 GeV, it was felt desirable to have an instrument of better resolution. The desire for better resolution must however be compromised with the low flux of particles at the large zenith angles. Considering these facts, and mindful of the fact that the ratio of magnetic to scattering deflection varies as $\ell^{\frac{1}{2}}$, equation (2.2), it was decided that the desired resolution could best be obtained by the inclusion in the instrument of another magnet, and a tolerable extension of the longitudinal dimensions for a reasonable collecting power. A schematic view of the Mk 2 spectrograph is shown in fig. 2.4. An additional tray of flash tubes identical with trays B and C is placed symmetrically between the two magnets.

The new magnet, II, positioned parallel to the original one, I, is identical with it, and is wound similarly, the coil having a total resistance of 5.64 ohms, and both are supplied from the same rectifier through rheostats to maintain the appropriate current in each one. A simple comparison of the inductions indicates that they are equal to within 3%.

The Geiger counters were arranged in the four trays in an overlapping

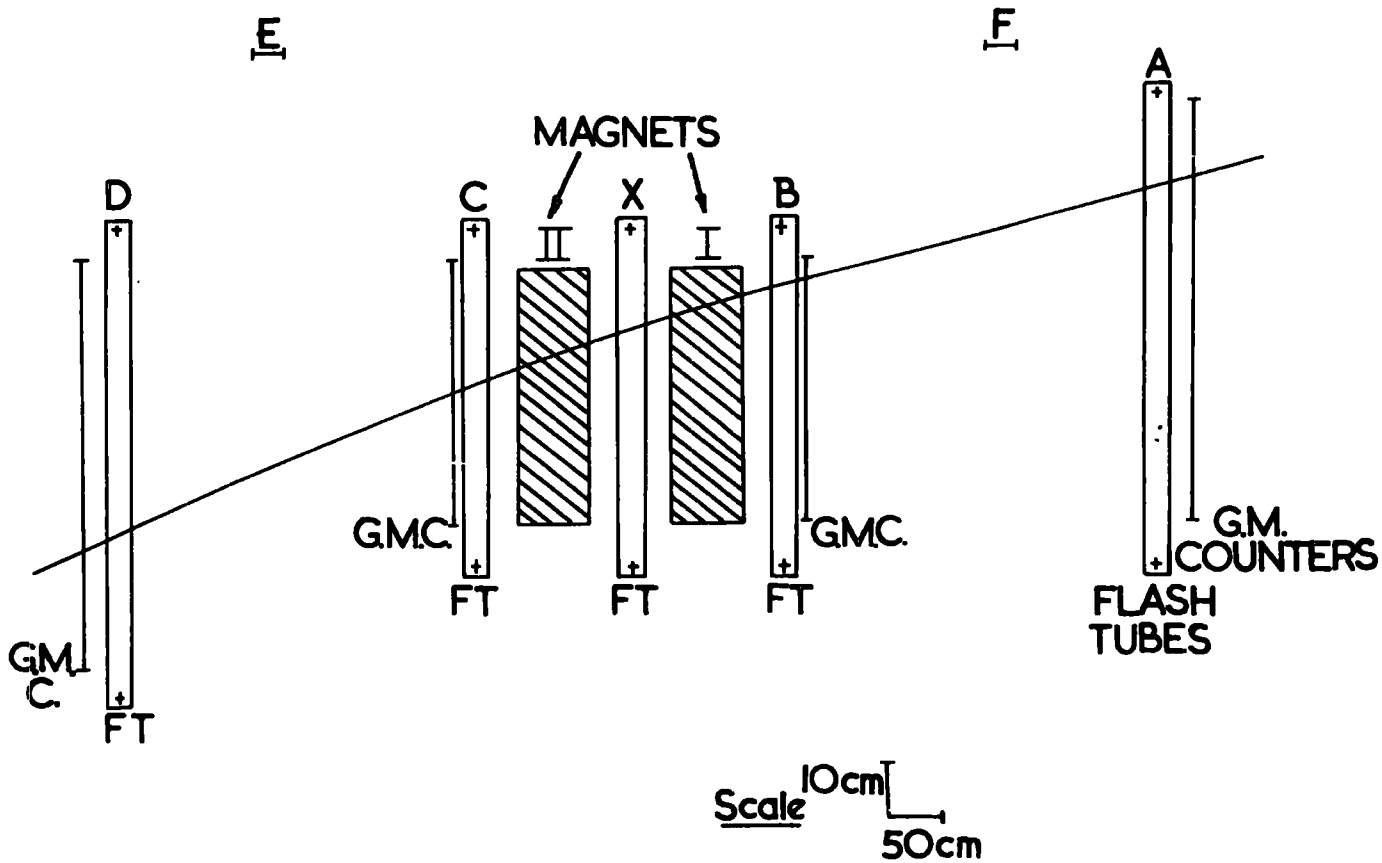

Fig.2.4 A schematic diagram of the Mk.2 spectrograph.

manner, such that the gaps between tubes in the previous arrangement were covered by an additional tube. All the quenching units were replaced by new ones of a more robust and reliable type, but having similar characteristics, and, as before, groups of four counters - alternate ones being grouped to reduce the probability of neighbouring tubes being dead simultaneously from a quenching pulse - were connected to a quenching unit. Two trays of Geiger counters E and F were arranged symmetrically over the instrument and connected to the others in anti-coincidence to eliminate extensive air showers.

Many of the original flash tubes were replaced by newer, but similar, tubes, and further to reduce the spurious flashing, due to light radiation triggering off neighbouring tubes through cracks in the paint, all the trays were interleaved with black 'Fablon' material such that no tube was directly visible to another. Several new monitoring meters were incorporated to keep a check on the constancy of the behaviour of the instrument. The insertion of the fifth flash tube tray necessitated a change in the position of the mirrors and the camera, and besides the clock, a facility was provided for photographing a serial number of the film and the direction of the field, on the same frame.

2.6 Alignment of the Mk 2 Spectrograph

The longitudinal dimension of the Mk 2 instrument is greater than 10 meters, which increases the difficulty of making reliable measurements of the constants. The alignment was carried out as for the Mk 1 spectrograph, the whole instrument was made symmetric about a plane midway between the two magnets as shown in fig. 2.5. As a horizontal reference line from which the constants were measured after alignment a free water surface was used. In

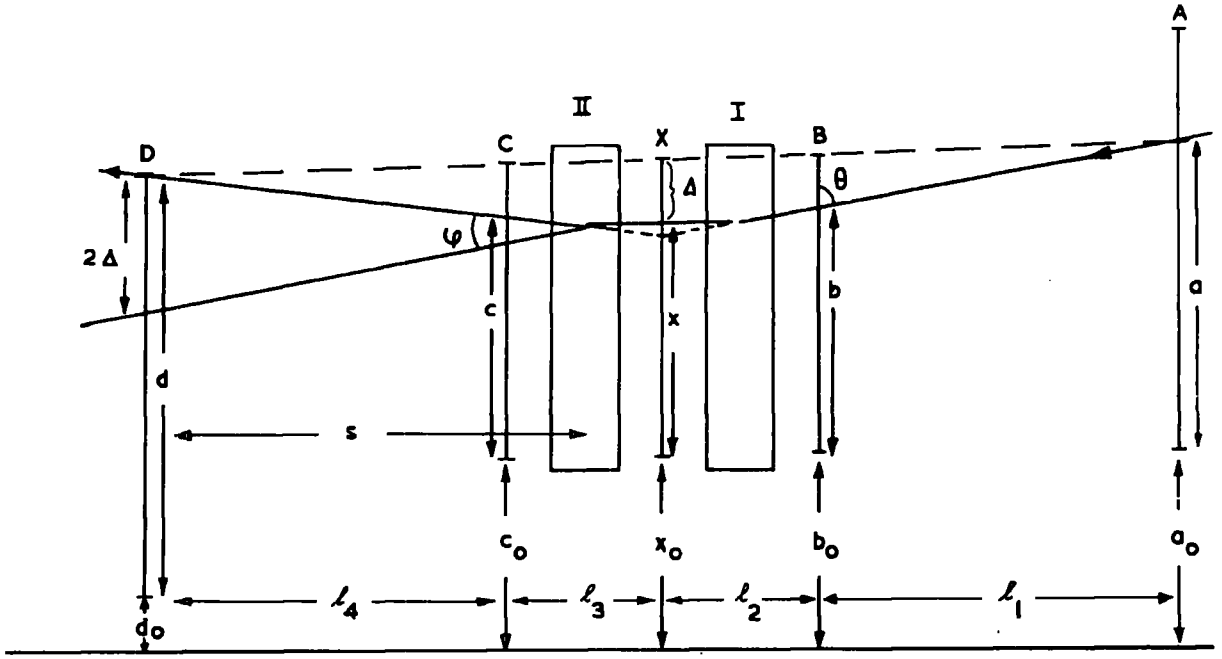

Fig.2.5 The measured coordinates for the Mk.2 spectrograph.

the absence of a long through, large beakers of water connected to each other by a siphon were placed underneath each tray, and on both sides. By this method, using a cathetometer, consistent values of the constants could be obtained provided suitable precautions, such as leaving the cathetometer to settle for some time after moving it from the vicinity of one tray to another, were taken. Because of evaporation the same water level could not be assumed for more than ~2 hours, which restricted the measurement of the constants to three at a time. They were measured on each side of the spectrograph, by three observers and the adopted values of a_o, b_o, n_o, c_o, d_o and the longitudinal dimensions are given in table 2.1. The Geiger counter trays were aligned as before.

The axes of both spectrographs coincide and lie on a line 7.8°E of the geomagnetic meridian. This is so as to minimise the amount of material through which particles at very large zenith angles have to pass in coming from the north direction. On the south side of the laboratory there is a large landmass corresponding to a path of $\sim 3\ 10^4$ g cm^{-2} at 82° and $\sim 2\ 10^5$ g cm^{-2} at 90°, which severely attenuates the flux from this direction. Also the Geiger trays are geometrically arranged such as to be strongly biassed in favour of particles arriving from the north. The effect of contamination by particles travelling from south to north will be discussed later.

2.7 Operation of the Spectrographs

The counting rate of all quenching units, and their pulse shapes were checked daily, and the counting rates of the individual Geiger tubes were checked weekly. For the Mk 2 instrument a continuous record was kept of the counting rates of each Geiger tray. A recording barometer was also kept running in order to correlate variation in the counting rates of selected events with

atmospheric pressure. During scanning of the films an eye was kept on flash tubes which failed to flash when expected to do so, and faulty ones were immediately replaced. The direction of the magnetic field was reversed daily to reduce the effect of any sources of bias slowly varying with time. The operation of both spectrographs was relatively simple and faults were usually quickly detected and rather trivial, though all films during which any doubtful operation occurred were not analysed, and the quality of the records obtained was very good.

2.8 Collection and Analysis of Data

2.8.1 General

In terms of the co-ordinates denoted in fig. 2.3 for Mk 1 we can write the deflection, using the small angle approximation

$$\varphi = ((a + a_o) - (b + b_o)) \ell_1^{-1} + ((d+d_o) - (c+c_o))\ell_4^{-1}$$

whence

$$\ell_1\varphi = ((a-b)- \frac{\ell_1}{\ell_4} (c-d)) + ((a_o-b_o) - \frac{\ell_1}{\ell_4} (c_o-d_o)) \equiv \Delta \quad \ldots.(2.4)$$

and by (2.3)

$$p\Delta = C \text{ where } C = 300\ell_1 \int Bd\ell$$

Thus the momentum is obtained in terms of the quantity Δ, directly determined by the co-ordinates of the trajectory a,b,c and d. For a mean excitation current $\langle i \rangle$ = 13.35 amps, B = 15.5 K gauss and C = 23.12 GeV/$_c$ t.s. or

$$p\Delta = 23.12 \text{ GeV/}_c \text{ t.s.} \quad \ldots\ldots(2.5)$$

A quantity which also follows from the measured co-ordinates is the discrepancy at the centre of the field ,

$$\epsilon = (b+b_o) - (c+c_o) - \frac{\ell_2}{\ell_1} ((a+a_o) - (b+b_o)) + \frac{\ell_3}{\ell_4} ((d+d_o)-(c+c_o)) \quad \ldots..(2.6)$$

The origin of this discrepancy has three sources:

(i) errors in location at the measuring levels and uncertainties in the positions of the tubes;

(ii) multiple coulomb scattering in the instrument and

(iii) energy loss in traversing the magnet at low energies.

From the work of Ashton and Wolfendale (1963) we see that for the present magnet the ratio of the r.m.s. scattering deflection $\langle\psi\rangle$ to the magnetic deflection φ is

$$\langle\psi\rangle/\varphi = 0.30 \qquad \ldots\ldots(2.7)$$

If we assume equal errors in location, σ_i, at all the four measuring trays then the error in the calculated deflection follows from (2.4) and is

$$\sigma_\Delta = K_1 \sigma_i$$

where the constant K_1 depends on ℓ_1 etc., and is equal to 3.964.

Similarily from (2.6) the distribution observed in ϵ is characterised by

$$\sigma_\epsilon = K_2 \sigma_i$$

K_2 another geometrical constant, $K_2 = 4.913$. This is the case if most of the contribution to ϵ comes from errors in track location. Then we have

$$\sigma_\Delta = \frac{K_1}{K_2}\sigma_\epsilon = 0.899\,\sigma_\epsilon$$

and the location error in a tray is

$$\sigma_i = \sigma_\epsilon / 2.216$$

The error in the deflection Δ enables us to define a quantity known as the maximum detectable momentum, (m.d.m.), of the instrument, which is that momentum which corresponds to a deflection equal to the error on the deflection

$$\text{Pmdm} = C/\sigma_\Delta$$

or alternatively the momentum which corresponds to a deflection equal to the most probable error on the deflection

$$Pm.dm. = {}^{C}/0.675\sigma_{\Delta} = \frac{23.12}{.675\,\sigma_{\epsilon}} \text{ GeV/c} \quad \ldots\ldots\ldots\ldots (2.8)$$

and this definition will be used.

The meaningfulness of the quantity thus defined depends on the assumption that at high energies the contribution to ϵ from non-magnetic scattering is vanishingly small and this needs consideration. The probability that a particle of momentum p will undergo a (projected) angular deflection and a projected linear displacement y in traversing a thickness of t radiation lengths has been shown by Rossi and Greisen, (1941) to be

$$P(\psi,y,t,)dy\ d\psi = \frac{\sqrt{3}}{2\pi}\ \frac{\omega^2}{t^2}\ \exp\left(-\omega^2\left(\frac{\psi^2}{t} - 3y\ \frac{\psi}{t^2} + 3y^2\frac{\psi}{t^3}\right)\right)dy\ d\psi$$

where $\omega = 2\beta\, p/E_s$ and $E_s = 21$ MeV.

With reference to fig. 2.6, where a particle is assumed scattered through angles α_1 and α_2 in trays B and C, (exaggerated in the figure), and an angle ψ in the magnet, the distribution in $(y - l\psi/_2)$ from the above equation is found to be Gaussian with a standard deviation $l\langle\psi\rangle/\sqrt{12}$ where $\langle\psi\rangle$ is the r.m.s. projected angle of scattering in the magnet. Then due to scattering $\epsilon_s = l_1(\alpha_1 + \alpha_2) + (y - l\psi/_2)$ is Gaussian distributed with a standard deviation $\sigma_\epsilon^2 = 2\,l_1^2\ \sigma_\alpha^2 + \frac{l^2}{12}\langle\psi\rangle^2$.

Now σ_α = constant . Δ and $\langle\psi\rangle/\varphi$ = constant (=0.30 for Mk 1)

whence $$\sigma_{\epsilon_s}^2 = \text{const}\ \Delta^2$$

Then the total standard deviation in ϵ, including errors in alignment and track location is

$$\sigma_\epsilon^2 = \text{const}\ \ \Delta^2 + \sigma_o^{12} \quad \ldots\ldots (2.9)$$

which becomes constant at high momenta, $\Delta \longrightarrow 0$.

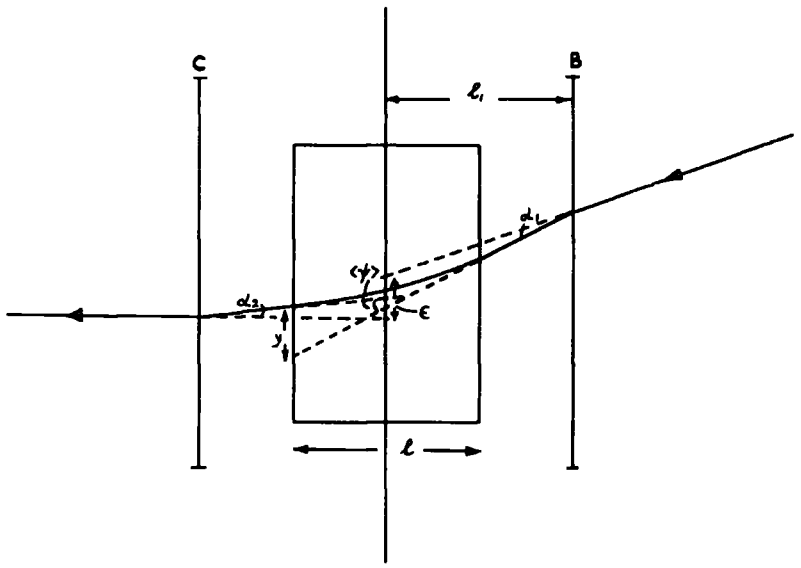

Fig.2.6 Displacements due to scattering.

For the Mk 2 instrument we have, referring to fig. (2.5)

$$\varphi = 2\Delta/s$$

and $$\Delta = \frac{a + d + a_o + d_o}{} - x - x_o \qquad \ldots\ldots(2.10)$$

Also the discrepancy at the centre is[2]

$$\epsilon = Xab - Xcd \qquad \ldots\ldots(2.11)$$

where $$Xab = b - \frac{l_2}{l_1}(a-b) + (b_o - x_o) - \frac{l_2}{l_1}(a_o - b_o)$$

$$Xcd = c - \frac{l_2}{l_1}(d-c) + (c_o - x_o) + \frac{l_2}{l_1}\ Co$$

are the intersections at the centre line expected from the measured co-ordinates. This instrument was run at a mean current $\langle i \rangle$ = 13.6 amps giving B = 15.58 K gauss whence

$$p\Delta = 63.52 \text{ GeV/c t.s.} \qquad \ldots\ldots(2.12)$$

and $p\varphi$ = 0.5936 GeV/c radians. From equations (2.10) and (2.11) we get $\sigma_\Delta = 0.575\ \sigma_\epsilon$ whence

$$Pmdm = \frac{63.52}{.387\ \sigma_\epsilon} \text{ GeV/c} \qquad \ldots\ldots(2.13)$$

and $\sigma_i = \sigma_\epsilon/2.122$. Since the length of the scattering region, ignoring contributions other than from the magnets, has been doubled we have by (2.2)

$$\langle\psi\rangle/\varphi = \frac{0.3}{\sqrt{2}} = 0.212$$

2.82 Analysis of data from Mk 1

Using the Mk 1 instrument the data were collected in two series, a preliminary run of 1300 particles discussed by Pattison (1963), and a more extended run. Comparison of the two series show no significant inconsistancies and so they have been grouped together. In a total running time of 1508.56 hours, exactly half of it on each field direction, a total of 10,080 acceptable

particles were detected in the angular range 77.5° - 90° with momenta p 3.7 GeV/c ($\Delta <$ 6.24 t.s.).

The measured rates of events were as follows:

4 fold coincidences, (ABCD) : 37.36 ± 0.14 hr^{-1}

5 fold coincidences, (ABCD$\bar{E}$) : 15.92 ± 0.09 hr^{-1}

Despite the anticoincidence requirement a significant fraction of the photographs showed weak extensive airshowers and the rate of acceptable particle events observed on the films was 7.9 ± 0.4 hr^{-1}, but at these large angles the loss of particles through accompaniment by E.A.S. is negligible. An analysis was made of the separation in arrival times of over 1000 of the particles and the resulting plot indicated excellent agreement with a Poissonian distribution in the separation intervals.

To analyse the data, a projection board, on which was accurately drawn the outline of the positions of all the flash tubes in the instrument, and the fiducial markings, was prepared. A scale marked in tube separations, with origin at the centre of the lowermost tube, was drawn in the centre of the fourth column of tubes from the north, on each tray. Each event was projected on to this board and the four co-ordinates a,b,c and d found by placing a cursor across the tubes which had flashed, judging a best estimate of the track, and reading the scale at its intersection with the cursor. In the majority of cases the co-ordinates, reading to 0.1 t.s., as measured by three independent scanners agreed, and seldom varied by more than $\pm$ 0.1 t.s. In cases where alternative tracks were available in one or more trays, which were not easily distinguishable, all possibilities were considered and the most likely combination chosen after calculation on the basis of a minimum discrepancy ϵ. It should be noted that the information available, in principle,

on the angles of the tracks in the trays is not used in this simple method. For each event its zenith angle θ, deflection Δ and discrepancy ϵ were computed. This method of analysis will be referred to as the 'projector method'.

Those particles having a nominal deflection $\Delta < 0.4$ t.s., ($p > 56$ GeV/c), were remeasured more accurately using the 'track simulator' device. This device, described in detail by Hayman (1962), consists of an accurate scaled version of a section of a flash tube tray, enlarged by a factor 2.5 in the vertical direction and diminished by a factor of 0.716 in the horizontal direction, the vertical axes of the tubes only being drawn. A scale was drawn on the fourth column of tubes as before. In using this device the information available on the angles of incidence and emergence of tracks in the trays is incorporated. These high energy events were rescanned and the position of the flashed tubes in each tray noted down and transferred to the track simulator. A cursor, its angle determined by the co-ordinates, was moved along the scale until an optimum path through the tubes was found, and its intersection with the scale read. From these more accurate co-ordinates θ, Δ and ϵ were again calculated. Events having large values of the discrepancy ϵ were reinvestigated and if no improvement occurred those with $\epsilon > 3\langle|\epsilon|\rangle \approx 0.66$ t.s., were rejected as being accidental coincidences of separate tracks, or very large scattering.

From § 2.8.1 we see that the distribution in ϵ is a measure of the accuracy of location and scattering, and affords a comparison of the relative accuracies of the two methods of analysis, the projector and track simulator methods. The symmetry of this distribution also reflects the accuracy of alignment of the instrument. Fig. 2.7 shows a typical distribution in ϵ for

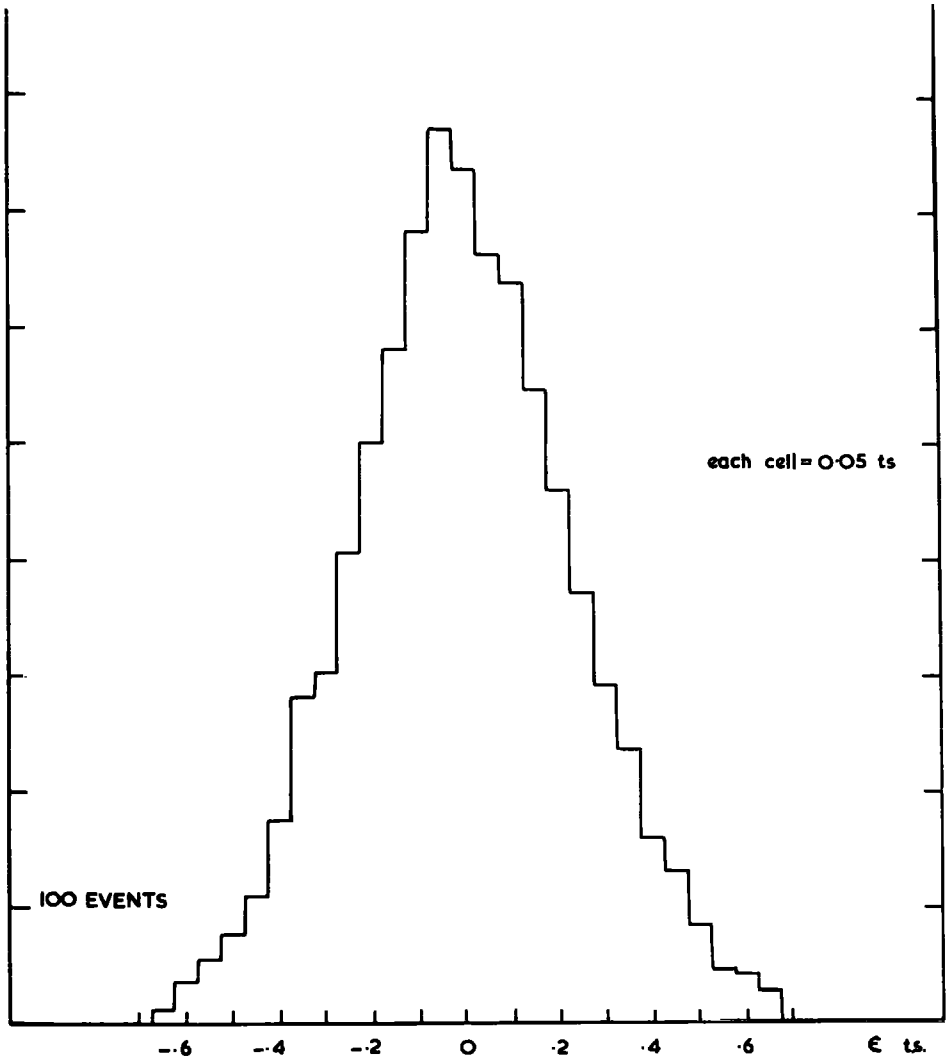

Fig. 2.7 The ε distribution for the projector data for the Mk.1 series.

data of all momenta as measured by the projector method, here the two field directions have been combined after verifying that an identical behaviour obtained for both. For the whole series $\langle \epsilon \rangle_{proj} = 0.0024 \pm 0.0057$ t.s. indicating a high degree of symmetry. The standard deviation on ϵ for the series is $= 0.217 \pm 0.0089$ t.s. resulting in a standard deviation on Δ,

$$\sigma_\Delta = 0.195 \pm 0.008 \text{ t.s.}$$

from which the maximum detectable momentum is

$$P_{mdm} = 176 \text{ GeV/c} - \text{projector method.}$$

The improved accuracy obtained by using the track simulator device can be seen from figs. 2.8a and 2.8b which show the ϵ distribution for a sample of events having $\Delta < 0.4$ t.s. as computed from the projector and track simulator data. The reduced width of the track simulator distribution is significant. Using the track simulator data, for the whole series, ($P \gtrsim 56$ GeV/c) we get $\langle \epsilon \rangle_{t.s.} = -0.0414 \pm 0.0049$ t.s. and $\sigma_\epsilon = 0.130 \pm 0.0067$ t.s. whence

$$\sigma_\Delta = 0.117 \pm 0.006 \text{ t.s.}$$

resulting in a maximum detectable momentum

$$P_{mdm} = 294 \text{ GeV/c} - \text{track simulator method.}$$

As can be seen the distribution in ϵ from the track simulator data is significantly shifted towards negative values. That this is not entirely due to errors in the track simulator diagrams was verified by investigating the distribution in difference between the co-ordinates as found by the projector and track simulator methods for each tray and also subdivided by field direction. It can only be concluded that the shift, which also appears sensibly independent of zenith angle or deflection in the high momentum region is due to an error in the alignment of the instrument, but since it

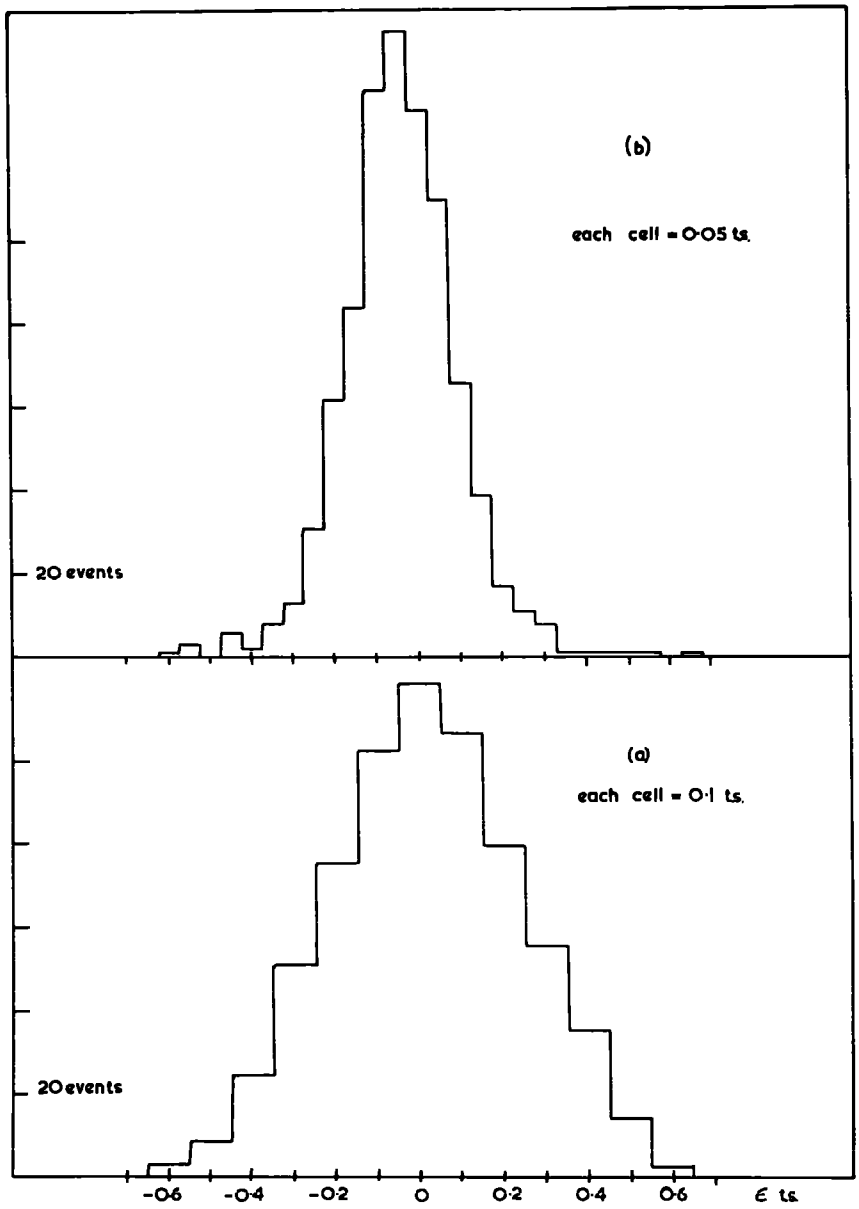

Fig.2.8 The ϵ distribution for a sample of events from the Mk.1 series, (a) before and (b) after track simulation.

corresponds to a momentum of about four times the m.d.m. it is not serious in the analysis provided one does not try to interpret results at momenta well beyond the m.d.m. From σ_ϵ we also obtain the error at each locating level σ_i = 0.0587 t.s. = 1.12 mm. As expected from the considerations in § 2.8.1 the dependance of σ_ϵ on Δ was shown to be weak. For those particles having $\Delta <$ 0.050 t.s., ($p >$ 460 GeV/c), σ_ϵ = 0.111 $\pm$ 0.007 t.s. leading to an m.d.m. of 344 GeV. Mindful of the negative shift in ϵ, the m.d.m. will be taken as 300 GeV.

The rejection of particles having $\epsilon >$ 0.66 t.s. after examination is a bit too severe, since they will not all be due to accidental coincidences of unrelated tracks. While some suitable, Δ dependant, correction is necessary to obtain the true intensities no bias is introduced into the charge ratio measurements by this. The arrangement of the selecting trays is such as to strongly favour the acceptance of particles travelling from north to south, and the spectrum and charge ratio is based solely on these particles. Because of the topography of the terrain to the south of the laboratory, as mentioned in § 2.6, there is an energy loss of ~90 GeV at $\theta = 82^\circ$, ~370 GeV at 86° and ~750 GeV at 90°. The flux from this direction will thus be enormously smaller than from the north especially at the larger angles. At the smaller angles there is a measurable flux of which those travelling down in trays B and A can be immediately identified and rejected. The rejection of the remaining ones i.e. those deflected above the horizontal in B and A, is vitally important because they have the effect of neutralising any charge excess in the beam. As a rejection criterion, because of the rapid fall off of intensity with θ, it was decided to reject all particles which had a smaller zenith angle in trays C and D than in trays A and B,

i.e. those for which $\varphi > 2\theta$, while minimising any effect on the charge ratio this criterion will create a bias in the intensity measurements, and an appropriate correction factor was derived for this.

2.8.3 Analysis of data from Mk 2.

Because of the reduced rate, this sample consists of only 2167 particles in the angular range $82.5 \leq \theta \leq 90^{o}$ collected in a period of 2097.6 hours, half of it on each field direction. The rates of detected events are as follows:

4 fold coincidences, (ABCD) : 27.8 hr^{-1}

5 fold coincidences, (ABCD$\bar{E}\bar{F}$) : 4.5 hr^{-1}

and the rate of acceptable single particle events was 1.03 hr^{-1}, a factor of ~8 down on the Mk 1 instrument.

A projection board was constructed as before and the five co-ordinates a,b, x, c,d determined. In distinction to the earlier instrument, the rate of events being considerably less, the information available on the angles of the tracks was taken into account in this analysis. Again the deflection Δ, using only three co-ordinates, (2.10), the discrepancy ϵ, (2.11), and the zenith angle θ were computed. Particles having a momentum greater than 100 GeV/c, ($\Delta < 0.635$ t.s.), were reconsidered. Those with $100 < p < 200$ GeV/c were recomputed using a least squares fit to the five co-ordinates, while those with $p > 200$ GeV/c were remeasured in a manner similar to the track simulator method described in § 2.8.2., but taking also into consideration small differences between the flash tube trays and the variation of the probability of a tube flashing with the line of traversal, both inside and outside the tube. These particles were also calculated using a five point least squares fit. Figs. 2.9a and 2.9b show the distribution in ϵ for 1500 particles, as calculated by the initial projector method, and for the

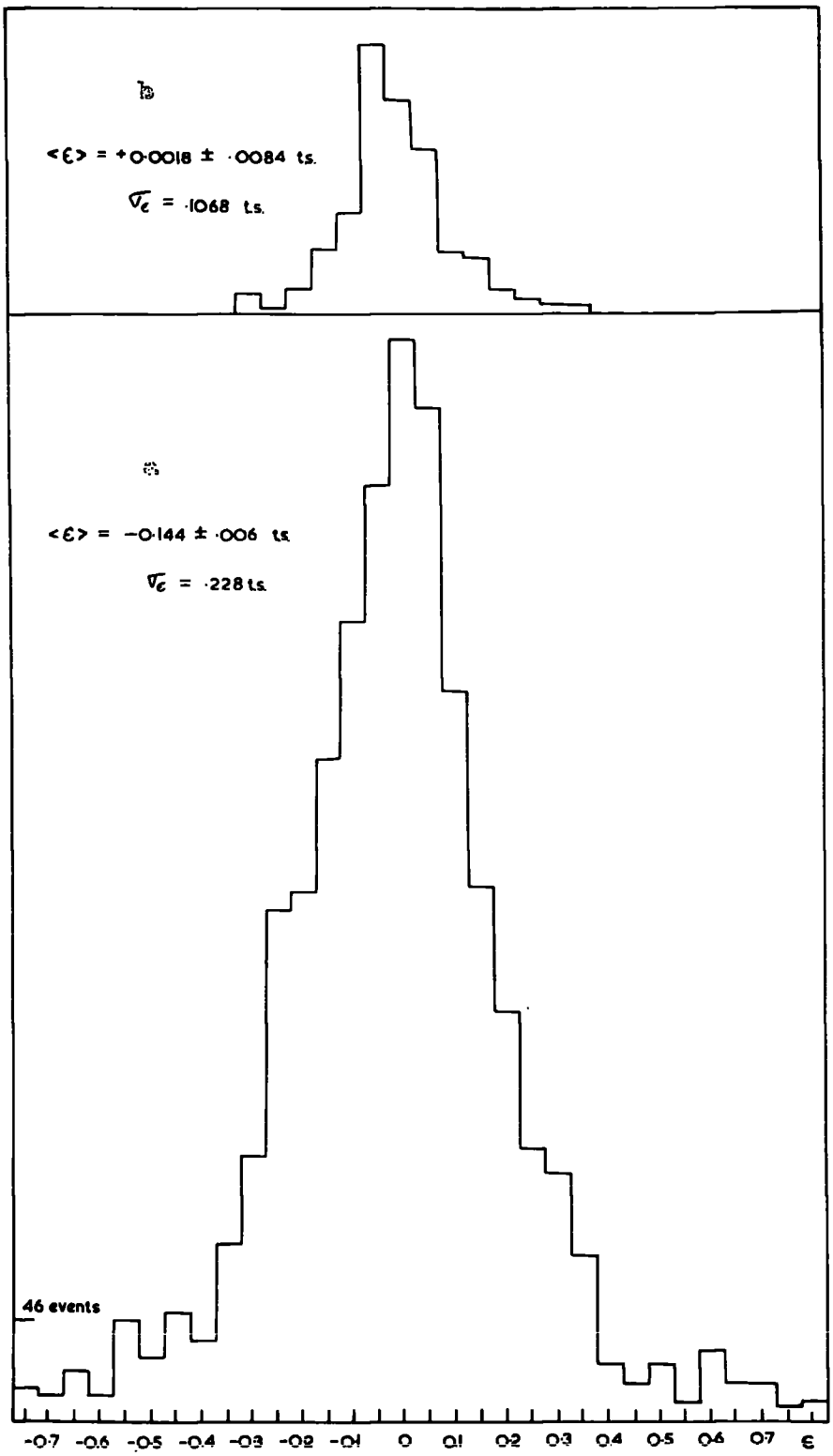

Fig. 2.9 The ϵ distribution for the Mk.2 series, (a) from the initial measurements, (b) after refined analysis.

associated particles with $p > 200$ GeV after the refined analysis. For the projector measurements we have $\langle \epsilon \rangle = -.0144 \pm .006$ t.s. and $\sigma_\epsilon = 0.228$ t.s. resulting by (2.13) in an m.d.m.

$$p \text{ m.d.m.} = 720 \text{ GeV/c.}$$

For the high energy particles after reanalysis we get $\langle \epsilon \rangle = +0.0018 \pm 0.0084$ t.s. and $\sigma_\epsilon = 0.1068$ t.s. resulting in an m.d.m.

$$p \text{ m.d.m.} = 1520 \text{ GeV/c}$$

From σ_ϵ we find the location error in a tray $\sigma_i = \sigma_\epsilon / 2.122 = 0.956$ mm., a 15% improvement on the value found in the Mk 1 series. Since the momenta were in fact determined from a five point least squares fit to the co-ordinates the actual m.d.m. will be in excess of the value quoted above. From σ_i the consequent improvement factor turns out to be 1.28 whence

$$P \text{m.d.m.} = 1945 \text{ GeV/c.}$$

As before, particles with large values of ϵ were reinvestigated and if in the projector data $\epsilon > \sqrt{0.09 + 0.0225 \Delta^2}$ or in the refined analysis $\sum_{i=1}^{5} \delta a_i^2 > 0.045$ t.s.^{2} the particles were rejected, where $\delta a_i = a_i - \bar{a}_i$ where $\bar{a}_i$ is the co-ordinate predicted by the least squares fit and a_i the observed co-ordinate.

2.9 The basic data and the spectrum

The basic data observed with the Mk 1 instrument in $\theta = 77.5^\circ - 90^\circ$ divided into cells of Δ and zenith angle θ are presented in table 2.2, and again data for the Mk2 series being given in table 2.3. The experimental data are compared in figs. 2.10 and 2.11 for the two series with the theoretical differential spectra derived via the vertical spectrum of

Table 2.2. Basic Data: The Momentum Distribution for Mk 1 series

Δ t.s.	P_μ s/l (GeV/c)	$\langle p \rangle$ (GeV/c)	77.5-80°	80-82.5°	82.5-85°	85-87.5°	87.5-90°
3.99-6.25	3.7-5.8	4.72	192	211	158	54	14
2.36-3.99	5.8-9.8	7.49	292	348	243	119	40
1.156-2.36	9.8-20	13.9	524	752	543	284	98
.746-1.156	20-31	24.7	338	448	410	214	88
.451-.746	31-51.3	38.9	308	487	466	321	153
.313-.451	51.3-73.8	60.9	191	231	338	258	125
.108-.313	73.8-215	114	114	310	329	303	169
<.108	>215	447	60	124	148	153	92

Table 2.3. Basic Data: The Momentum Distribution for Mk 2 series

Δ t.s.	p_μ s/l GeV/c	$\langle p \rangle$ GeV/c	82.5-85°	85-87.5°	87.5-90°
3.19-6.52	9.8-20	14.2	56	166	77
2.06-3.19	20-31	25.3	42	174	75
1.25-2.06	31-51.3	39.5	42	220	93
.866-1.25	51.3-73.8	61.4	14	128	83
.297-.866	73.8-215	121	29	295	232
.128-.297	215-500	290	3	84	82
.0628-.128	500-1000	605	1	20	18
<.0628	1000	1750	1	8	9

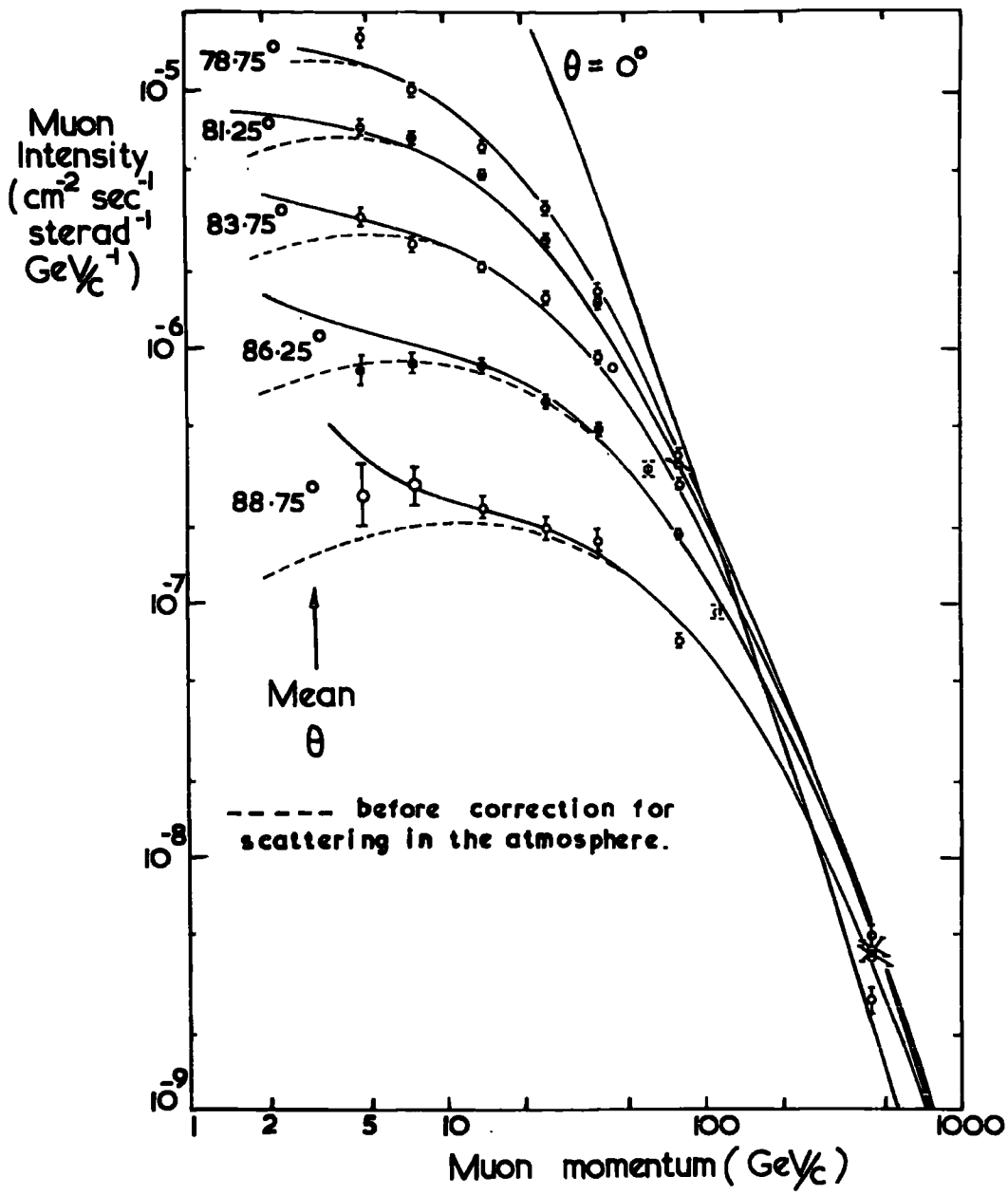

Fig. 2.10 - comparison of the observed data with the predicted spectra, after Osborne (1964, p.c.), for the Mk.1 series.

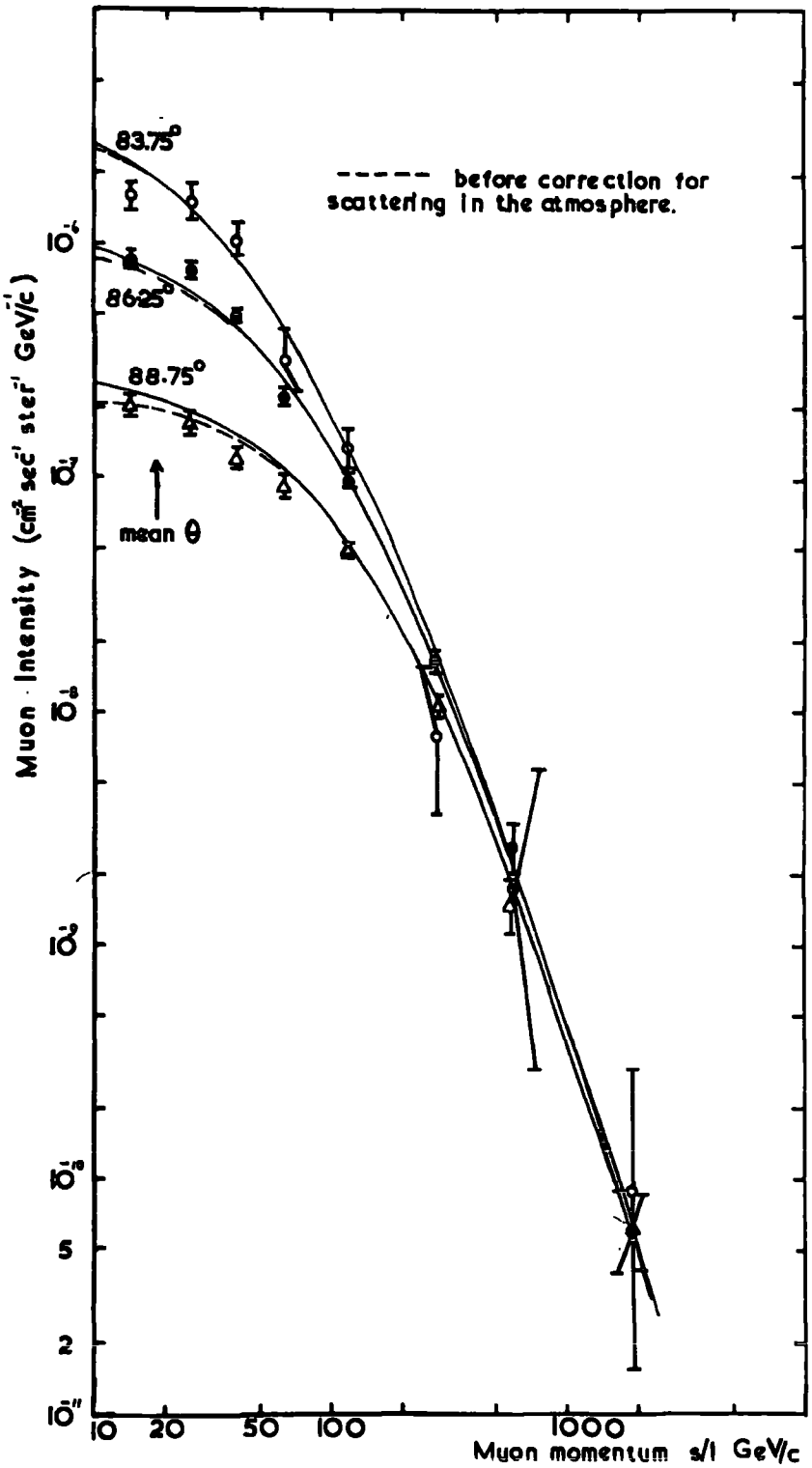

Fig. 2.11 A comparison of the observed data with the predicted spectra, after Osborne (1964, p.c.), for the Mk.2 series.

Osborne et.al. (1964) for the case of all pions as parents of the muons, as computed by Osborne (1964, private communication). The comparison in each case is effected by multiplying the theoretical intensity at the mean energy point of each of the cells by the ratio of the observed to the predicted numbers in that cell, where the predicted numbers, in a running time t is given by

$$N(\Delta_{1,2}, \theta_{1,2}) = t \int_{\Delta_1}^{\Delta_2} \int_{\theta_1}^{\theta_2} \int_{-\infty}^{\infty} N(\Delta', \theta) F(\Delta', \theta) Q(\Delta', \Delta) d\Delta' d\theta d\Delta \qquad \ldots.(2.14)$$

where $N(\Delta', \theta)\, d\Delta'$ is the incident differential displacement spectrum. $F(\Delta', \theta)$ is an 'acceptance' function, consisting of terms for geometrical limits, Geiger tray sensitivities, quenching unit dead times, paralysis of the Rossi circuit, loss of particles due to large ϵ values and accompaniment by large knock-on showers, the too severe rejection of 'south-north' particles and the effect of scattering in so far as it effects geometrical acceptance of a particle. $Q(\Delta', \Delta)$ is a distribution function representing the effects of scattering and errors in track location on the observed intensities; it is the probability that a particle of momentum corresponding to the deflection Δ' will be observed as having a deflection Δ and may be represented by a Gaussian distribution

$$Q(\Delta', \Delta) = \frac{1}{\sigma(\Delta')\sqrt{2\pi}} \exp\left\{ - \frac{(\Delta' - \Delta)^2}{2\,\sigma^2(\Delta')} \right\}$$

where by (2.9) $\sigma(\Delta') = \sqrt{\sigma_0^2 + k^2 \Delta'^2}$, which at high momenta $\rightarrow \sigma_0$, the error due to track location. Expression (2.14) can now be written in the form

$$N(\Delta_{1,2}, \theta_{1,2}) = t \int_{\Delta_1}^{\Delta_2} \int_{\theta_1}^{\theta_2} N(\Delta, \theta) F(\Delta, \theta) S(\Delta, \theta)\, d\theta\, d\Delta \qquad \ldots.(2.15)$$

where $S(\Delta, \theta) = \frac{1}{N(\Delta)} \int_{-\infty}^{\infty} Q(\Delta', \Delta) N(\Delta', \theta)\, d\Delta'$

$$= \frac{1}{N(\Delta)\sqrt{2\pi}} \left\{ \int_{-\infty}^{\infty} \frac{N(\Delta')}{\sigma(\Delta')} \exp\left(-\frac{(\Delta'-\Delta)^2}{2\sigma^2(\Delta')}\right) d\Delta' + \int_{-\infty}^{\infty} \frac{N(\Delta')}{\sigma(\Delta')} \exp\left(-\frac{(\Delta'+\Delta)^2}{2\sigma^2(\Delta')}\right) d\Delta' \right\}$$

which, since $N(\Delta') = N(-\Delta') = N(|\Delta'|)/2$ gives

$$S(\Delta,\theta) = \frac{1}{N(\Delta,\theta)\sqrt{2\pi}} \int_{0}^{\infty} \frac{N(|\Delta'|)}{\sigma(\Delta')} \left[\exp\left(-\frac{(\Delta'-\Delta)^2}{2\sigma^2(\Delta')}\right) + \exp\left(-\frac{(\Delta'+\Delta)^2}{2\sigma^2(\Delta')}\right) \right] d\Delta'$$

$S(\Delta,\theta)$, which shows the effect of scattering and noise on the intensities, is shown in fig. 2.12a for Mk 1 where σ_0 = 1.22 t.s. and k = 0.30, and in fig. 2.12b for Mk 2, where σ_0 = 0.061 t.s. and k = 0.212. The predicted numbers have also been corrected for the energy loss in the magnets, at low energies.

In the Mk 1 series a rather large cell viz. 51.3 - 215 GeV has been taken in plotting one of the points, and only for $\theta = 86.25^{\circ}$ are the two points from the individual cells of which it is composed, plotted-dashed. It is seen that the lower energy point is too high and the higher energy point is too low compared with the curve, similar behaviour obtaining for the other zenith angles. This presumably arises because the boundary, above which particles were remeasured by the track simulator method, falls within these cells, resulting in a deficiency in the higher momentum cell. The error introduced in taking the mean of the two intensities will be small.

2.10. Discussion.

Invariably it was found in scanning that non-negligible discrepancies occurring in the calculated trajectory were outside the limits of toleration on track fitting in the trays and were largely determined by scattering in the magnets and uncertainties in the alignment and values of the constants, from which we conclude that the arrangement and efficiencies of the flash tubes are satisfactory. A comparison is made in table 2.4 of the present instruments with previous momentum spectrographs.

The agreement between the observed data and the predicted spectra is

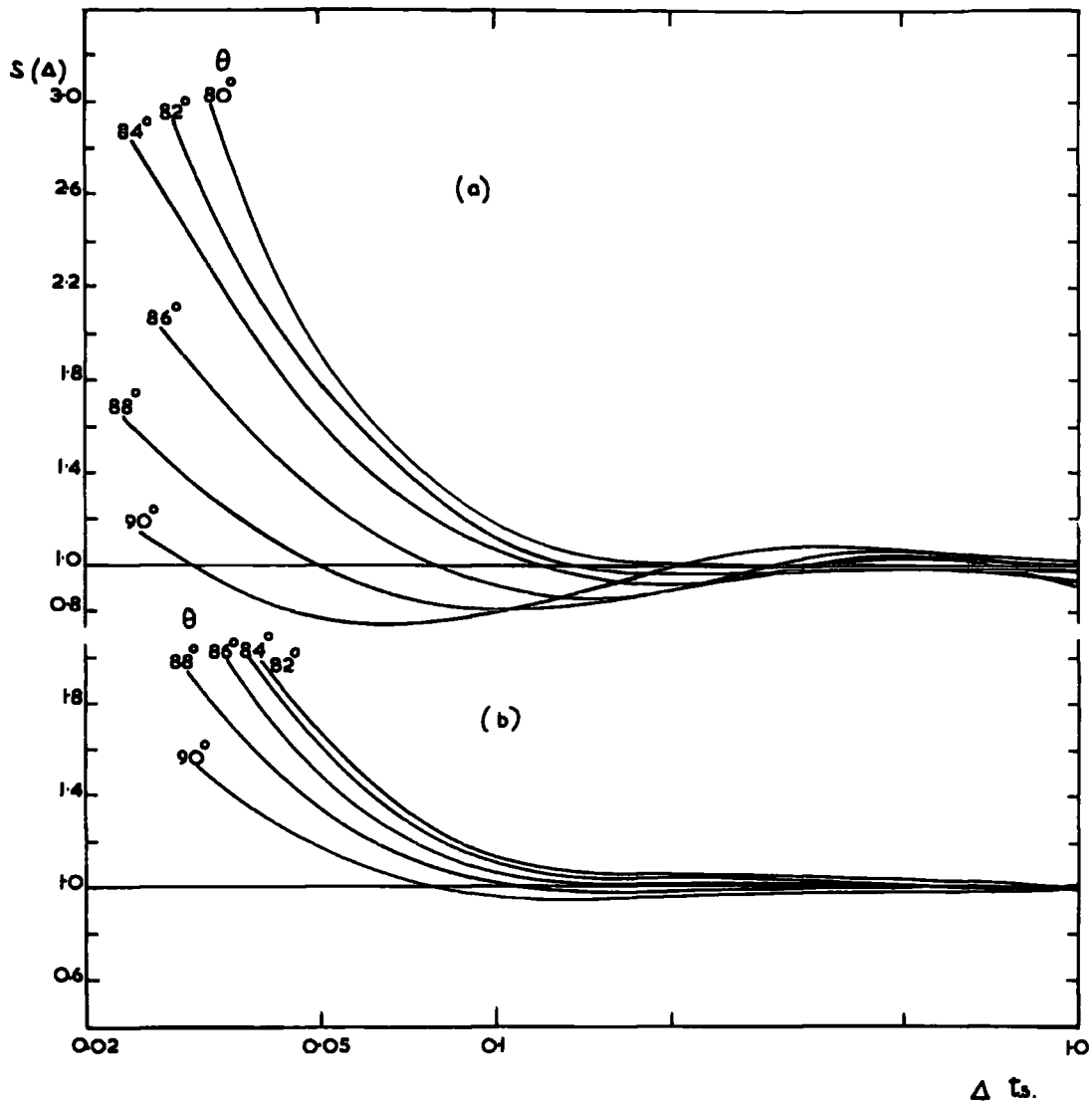

Fig.2.12 The scattering function S(Δ),(a) for the Mk.1 series;(b) for the Mk.2 series.

Table 2.4

Technique[+]	m.d.m.* GeV/c	Acceptance Area -cm^2 ster.	Authors
Air gap G.C.	50	0.7	Caro et al (1951)
Air gap spark chambers	30	0.39	Allkofer (1959)
Air gap, G.C., cloud chambers	260	7.9	Pine et al (1959)
Air gap, Emulsion on glass plates	300	Small	Allen and Apostolakis (1961)
Air gap, G.C., cloud chambers	350	0.93	Holmes et al (1961a)
Air gap, G.C., flash-tubes	650	8.0	Hayman and Wolfendale (1962b)
Solid F_e, flashtubes	Mk 1 300 Mk 2 1950	Mk 1 29.8** Mk 2 9.61**	present work

* "most probable" value

** Allowing for dead times and gaps in Geiger tube trays.

\+ 'Air gap', and 'solid iron' refer to the magnet used, G.C. ≡ geiger counters.

very good, indicating that the propagation model is good to this accuracy. By comparison with the vertical spectrum in fig. 2.10 the expected softening of the spectrum with zenith angle is seen and the relative increase of the intensity of high energy particles over the vertical flux is observed. The overall symmetry of the distributions, and concurrence of the spectra lead us to believe that no serious sources of error exist in the experiment and the data can be analysed with confidence from the view point of the muon charge ratio, the topic for consideration in the following chapters.

CHAPTER 3

Measurement of the Muon Charge Ratio

3.1 Introduction

The existence of a positive excess in the hard component of the cosmic radiation has been known since the first magnetic deflection studies on this component were carried out. The simplest measurable quantity is the muon charge ratio defined as

$$R_\mu(E_\mu) = \frac{\mu^+(E_\mu)}{\mu^-(E_\mu)}$$

where $\mu^+(E_\mu)dE_\mu$ and $\mu^-(E_\mu)dE_\mu$ are the sea level differential spectra of positive and negative muons. Early estimates of the excess of positive muons, which was still found to exist when the nucleonic component was rejected, were obtained by Blackett (1937), Leprince Ringuet and Crussard (1937) and Jones (1939). It was shown by Hughes (1940) that the excess existed in the incident radiation as distinct from being a possible instrumental effect e.g. preferential absorption of negative particles in traversing the spectrographs, and he determined μ^+/μ^- to be ~ 1.20, sensibly energy independent, but with large errors, in the region $E_\mu = 1 - 8$ GeV. Despite its early discovery it took many years for the variation of R_μ with muon energy even up to 20 GeV to be established, it eventually being determined by the statistically sound work of Owen and Wilson (1951) and Filosofo et. al. (1954). A notable extension of the energy range over which R_μ was measured was made by Hayman and Wolfendale (1962a) who showed that up to a few hundred GeV the charge excess still persisted, and was possibly increasing with energy.

The positive excess among the observed muons at sea level reflects the positive excess in the primary radiation, which consists largely of protons, and also mirrors the characteristics of the nucleon - air nucleus collisions in which the parents of the muons are produced, and in particular the multiplicity of produced particles in such collisions. The experimental position on R_μ after Hayman and Wolfendale, and the increasing interest in nucleon interactions at ultra-high energies, made a confirmation of their results, and if possible an extension of them, very desirable. Just such an extension is possible at large zenith angles if the momentum resolution is available, because of the greater flux of high energy particles and the greater energy at production being investigated at a given sea level energy.

3.2 Sources of Bias

Several methods have been adopted in the past for measuring the μ^+/μ^- ratio, the most general and direct being the magnetic deflection technique. Among the other possibilities - mostly at low energies - may be mentioned (i) the relative muon decay rates in different materials, Conversi (1949) Morewitz and Shamos (1953), and (ii) the deflection of the electrons from muon decay Nereson (1948).

Although the magnetic deflection technique is the simplest to identify the charge of the particle the results are, in general, subject to bias and ambiguities. These sources of bias are of three kinds, geometrical acceptance sources, time dependant instrumental sources and bias arising from methods of analysis. Since the spectrographs in the present work contained no selection devices for choosing the particles to be registered, bias due to the geometrical arrangement of the detecting trays can be

eliminated by accepting results from equal running times on each field direction. The former is true only if there are no time varying sources of instrumental bias, and these, if they exist, can be minimised by reversing the field frequently, in the present work the field being reversed daily. No serious source of bias from the methods of analysis is expected, the rejection of possible 'south-north' particles is believed to be more than adequate, such that contamination due to them will only occur at the very lowest momenta, which, for other reasons also, will not be considered in deriving the μ^+/μ^- ratio. Because R_μ is varying only slowly with energy small systematic errors in the determination of the energy of the particles will not be important. Serious errors may occur however in the region of the maximum detectable momentum due to scattering and errors in track location, because of the possibility of a particle being detected as of opposite sign, and the overspill of the much more numerous low energy particles due to scattering as determined by $S(\Delta)$ in §2.9.

3.3 The Basic Data

The observed numbers of positive and negative muons, divided by field direction, are given in table 3.1a for the Mk 1 series, a total of 10832 particles observed in 1508.56 hours; and for the Mk 2 series in table 3.1b, a total of 2167 particles observed in 2097.6 hours. In fig. 3.1 the calculated ratio for each field direction is shown for the two series and we see from the expected symmetry the absence of any serious sources of bias. The errors quoted correspond to one standard deviation, $R_\mu \pm \delta R_\mu$ where

$$\frac{\delta R_\mu}{R_\mu} = \sqrt{\frac{1}{\mu^+} + \frac{1}{\mu^-}} \qquad \ldots\ldots (3.1)$$

Table 3.1

Table 3.1a

Δ ts	$p_{\mu\ sl}$ GeV/c	H^+ μ^+	H^+ μ^-	H^+ R_μ^+	H^- μ^+	H^- μ^-	H^- R_μ^-
> 4.62	$p_\mu < 5$	492	77	6.389 ± .781	88	435	0.202 ± .024
1.54 < Δ ≤ 4.62	$5 \leq p_\mu < 15$	846	431	1.962 ± .116	487	754	0.646 ± .038
0.770 < Δ 1.54	$15 \leq p_\mu < 30$	793	439	1.806 ± .107	562	639	0.879 ± .051
0.462 < Δ 0.770	$30 \leq p_\mu < 50$	455	358	1.270 ± .090	433	412	1.051 ± .072
0.231 < Δ 0.462	$50 \leq p_\mu < 100$	475	408	1.164 ± .079	474	376	1.260 ± .087
0.105 < Δ 0.231	$100 \leq p_\mu < 220$	191	186	1.026 ± .106	246	181	1.138 ± .118
Δ ≤ 0.105	$p_\mu \geq 220$	174	140	1.242 ± .140	171	154	1.110 ± .123

Table 3.1b

Δ ts	$p_{\mu\ sl}$ GeV/c	H^+ μ^+	H^+ μ^-	H^+ R_μ^+	H^- μ^+	H^- μ^-	H^- R_μ^-
Δ > 12.7	$p_\mu < 5$	28	0	-	0	32	-
4.24 < Δ ≤ 12.7	$5 \leq p_\mu < 15$	152	25	6.080 ± 1.31	14	138	0.101 ± .028
2.12 < Δ ≤ 4.24	$15 \leq p_\mu < 30$	147	60	2.450 ± .372	73	113	0.646 ± .097
1.27 < Δ ≤ 2.12	$30 \leq p_\mu < 50$	130	65	2.000 ± .304	84	85	0.988 ± .151
.635 < Δ ≤ 1.27	$50 \leq p_\mu < 100$	134	79	1.696 ± .240	116	112	1.036 ± .137
.289 < Δ ≤ .635	$100 \leq p_\mu < 220$	90	82	1.097 ± .167	92	89	1.034 ± .154
.127 < Δ ≤ .289	$220 \leq p_\mu < 500$	49	29	1.690 ± .397	48	42	1.143 ± .240
0.064 < Δ ≤ .127	$500 \leq p_\mu < 1000$	8	12	0.563 ± .234	10	11	1.125 ± .387
Δ ≤ 0.064	$p_\mu \geq 1000$	1	4		8	5	

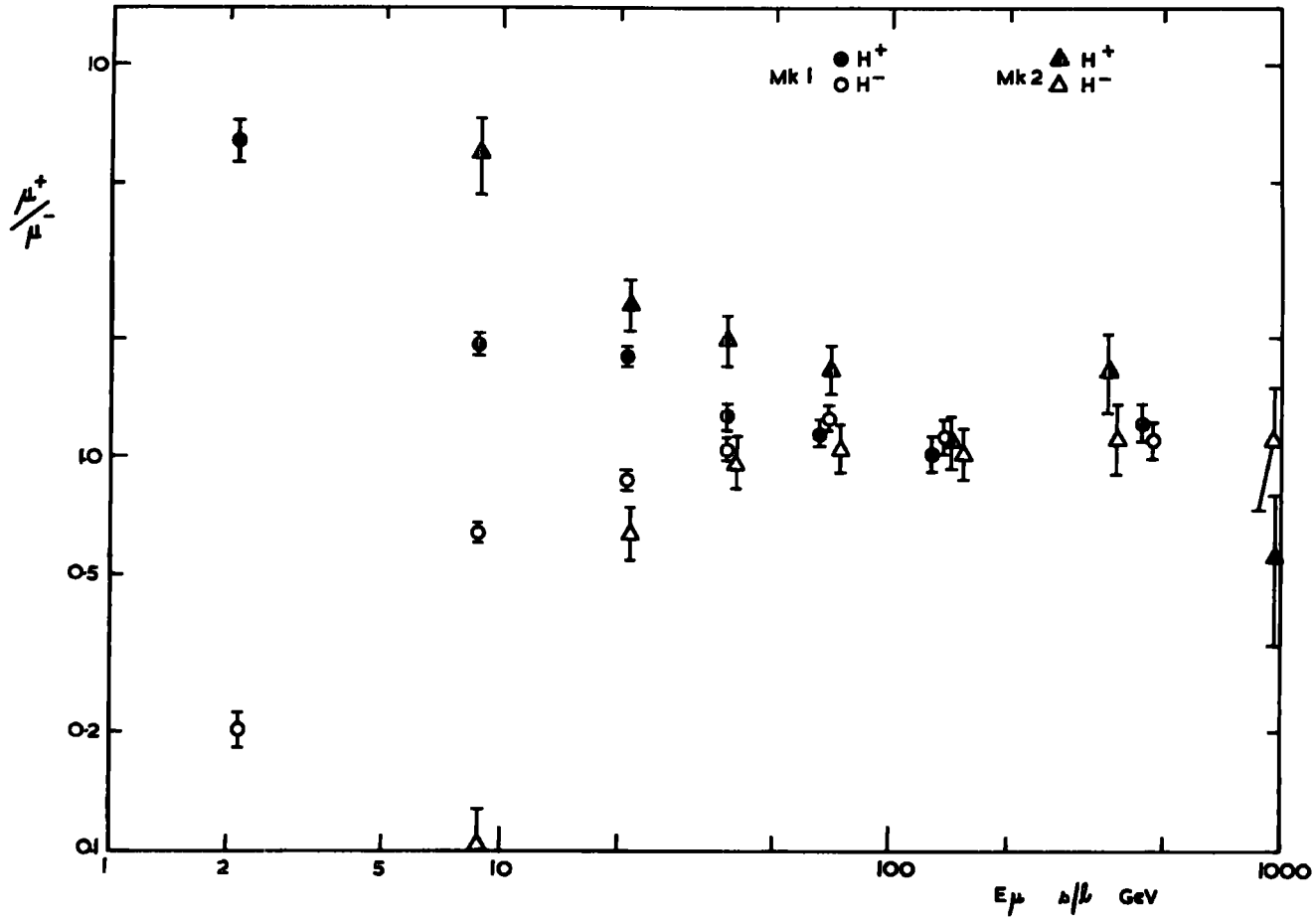

Fig.3.1 The charge ratio on the two field directions.

Another check was obtained by comparing the ratios $R^+ = \mu^+(H^+)/\mu^-(H^-)$ and $R^- = \mu^+(H^-)/\mu^-(H^+)$ which also agree very well with each other.

Since from the viewpoint of high energy interactions the quantity of interest is the charge excess among the muons at production, we must consider the corrections to be applied to the raw data to get back to this quantity. The observed data must first be corrected for noise and scattering, and for contamination, to derive the charge ratio in the incident flux. This quantity must then be corrected for the effects of geomagnetic deflection in the atmosphere, and then transferred to energy at production to find the effective charge ratio of the muons at production. We will denote by R_o, R_i and R_p the muon charge ratio as observed at sea level, as in the incident flux, and as at production respectively.

3.4 The Correction Factors

3.4.1 Contamination of the Muon Flux

Contamination of the muon beam by other charged particles may be corrected for as follows: if

$$\sigma = n^{\pm}/(\mu + n^{\pm})$$

where $n^{\pm}$ is the number of charged particles other than muons detected, the muon charge ratio is

$$R_i = R_o(1 - \sigma) - \sigma$$

Using a solid iron magnet this correction does not arise, but using air gap magnets in the vertical direction where the proton/muon ratio falls from ~ 6% to 0.5% from 0.7 - 10 GeV, Brooke and Wolfendale (1964a), the ratio π/μ is $\lesssim$ 0.2% up to 150 GeV, Brooke et. al. (1964b) - it provides a small correction at low energies.

3.4.2 Noise and Scattering

The correction due to noise arises from the fact that at momenta corresponding to deflections approaching the limits of resolution of the instrument, particles may be detected as being of opposite sign, the probability increasing with decreasing deflection. This has the effect of masking any charge excess among the observed particles. If scattering is important there is also the effect of the charge excess propagating from lower to higher energies which makes very difficult the determinations of the variation of R_μ with energy. For noise alone the charge ratio of the muons in the incident beam may be determined from that observed by applying a correction factor which depends on the location errors, muon momentum spectrum and energy dependance of the charge ratio in the incident flux The number of muons observed as being positive and of deflection $|\Delta|$ is

$$N_o^+(\Delta) = \int_{-\infty}^{o} \frac{N_i^-(\Delta')}{\sigma(\Delta')\sqrt{2\pi}} e^{-\frac{(\Delta'-\Delta)^2}{2\sigma^2(\Delta')}} d\Delta' + \int_{o}^{\infty} \frac{N_i^+(\Delta')}{\sigma(\Delta')\sqrt{2\pi}} e^{-\frac{(\Delta'-\Delta)^2}{2\sigma^2(\Delta')}} d\Delta'$$

$$= \int_{o}^{\infty} \frac{N_i^-(|\Delta'|)}{2\sqrt{2\pi}\,\sigma(\Delta')} e^{-\frac{(\Delta'+\Delta)^2}{2\sigma^2(\Delta')}} d\Delta' + \int_{o}^{\infty} \frac{N_i^+(|\Delta'|)}{2\sqrt{2\pi}\,\sigma(\Delta')} e^{-\frac{(\Delta'-\Delta)^2}{2\sigma^2(\Delta')}} d\Delta'$$

since $N_i^{\pm}(\Delta') = N_i^{\pm}(|\Delta'|)/2$

Similarly the number of muons observed as being negative and of deflection Δ is

$$N_o^-(\Delta) = \int_{o}^{\infty} \frac{N_i^-(|\Delta'|)}{2\sqrt{2\pi}\,\sigma(\Delta')} e^{-\frac{(\Delta'-\Delta)^2}{2\sigma^2(\Delta')}} d\Delta' + \int_{o}^{\infty} \frac{N_i^+(|\Delta'|)}{2\sqrt{2\pi}\,\sigma(\Delta')} e^{-\frac{(\Delta'+\Delta)^2}{2\sigma^2(\Delta')}} d\Delta'$$

and the observed ratio is

$$R_o = N_o^+(\Delta)/N_o(\Delta)$$

The inclusion of scattering in this treatment is very difficult because it depends on the functional form of $R_\mu(E_\mu)$, and since up to the m.d.m. the scattering effects are not very large it will not be included here, $\sigma(\Delta')$ is then taken as the noise component only $= \sigma_o$. At a given value of Δ the above equations should be integrated over the whole zenith angular range of interest, but since it is observed that at small values of Δ', $N(\Delta')d\Delta' \approx$ constant.$d\Delta'$ such a spectrum has been taken to apply over the whole angular range (i.e. $N(p)dp \sim p^{-2}\,dp$ dependance). With the further assumption that the charge ratio is not rapidly varying with energy, the above reduces to

$$R_o(\Delta) = \frac{N_o^+(\Delta)}{N_o^-(\Delta)} = \frac{(R_i + 1) + (R_i - 1)\ \mathrm{erf}\ (\Delta/\sigma_o\sqrt{2})}{(R_i + 1) - (R_i - 1)\ \mathrm{erf}\ (\Delta/\sigma_o\sqrt{2})}$$

where $R_i = N_i^+(\Delta)/N_i^-(\Delta)$ and $\mathrm{erf}(..) = \frac{2}{\sqrt{\pi}} \int_o^x e^{-t^2} dt$

We thus get the ratio in the incident flux,

$$R_i = \frac{(R_o + 1)\ \mathrm{erf}\ (q) + (R_o - 1)}{(R_o + 1)\ \mathrm{erf}\ (q) - (R_o - 1)} \qquad \ldots\ldots\ (3.2)$$

where $q = \frac{\Delta}{\sigma_o\sqrt{2}}$

For a $p^{-3}\,dp$ spectrum dependance, i.e. $N(\Delta')d\Delta' \propto \Delta' d\Delta'$ we get

$$R_i = \frac{(R_o + 1) + (R_o - 1)\ \phi'(q)}{(R_o + 1) - (R_o - 1)\ \phi'(q)}$$

where $$\phi'(q) = \frac{e^{-q^2}}{q\sqrt{2\pi}} + \mathrm{erf}(q)$$

We see that for these particular assumptions the correction depends on the ratio σ_o/Δ. Because it affects the numerator and denominator in a similar manner the correction is not as sensitive to the shape of the spectrum as

is the correction to the spectrum itself, and it has the opposite dependance on the exponent of the spectrum. In table 3.2 we show the effects of noise, for an observed ratio of $R_o = 1.1$, for the above two spectra.

Table 3.2

Δ/σ_o	0.2	0.4	0.6	0.8	1.0	1.5	2.0
R_o for p^{-2} spectrum	1.87	1.36	1.20	1.18	1.15	1.12	1.10
R_o for p^{-3} spectrum	1.49	1.25	1.17	1.15	1.12	1.10	1.10

While from energy conservation considerations the spectrum must eventually become more steep than p^{-2}, this is approximately its average slope in the regions of interest in the present work, and the observed charge ratios have been corrected as via (3.2) at the mean energies of the cells to give the charge ratio in the incident flux R_i in tables 3.3a and 3.3b.

3.4.3 Geomagnetic Deflection

If the axes of the detecting spectrograph does not coincide with the geomagnetic axes the charge excess in the incident flux at a given sea level energy is not simply related to the excess among muons at a given energy at production because of the opposite deflection of the two charges in traversing the atmosphere, and a correction must be applied to the incident charge ratio to find the charge ratio at production R_p. Because of the positive excess (~ 20%), a significant East-West assymetry is observed at energies much higher than where the geomagnetic deflection of primaries before entry into the atmosphere is important e.g. Quercia and Rispoli (1953, 1954) and Kamiya (1963), which has been shown by the latter author to be completely accounted for by considering the geomagnetic deflection of the muons.

Table 3.3 The Muon charge ratio

Table 3.3a

E_μ cut GeV	$\langle E_\mu \rangle$ GeV	$\langle E_\mu$ prod$\rangle$ GeV	$g(E_\mu)$	μ^+	μ^-	R_o	R_i	R_p
< 5	2.13	19.9	*	580	512	1.133 ± .069	1.133 ± .069	-
5-15	8.71	31.5	1.107	1334	1185	1.126 ± .045	1.126 ± .045	1.246 ± .050
15-30	21.0	46.8	1.057	1357	1081	1.255 ± .051	1.255 ± .051	1.327 ± .054
30-50	38.1	67.8	1.033	925	796	1.162 ± .056	1.162 ± .056	1.200 ± .058
50-100	68.8	103	1.017	986	840	1.174 ± .055	1.175 ± .055	1.196 ± .056
100-220	136	177	1.008	350	288	1.215 ± .097	1.256 + .118 − .116	1.266 + .118 − .116
>220	467	520	1.000	320	278	1.151 ± .094	1.541 + .451 − .357	1.541 + .451 − .357

Table 3.3b

E_μ cut GeV	$\langle E_\mu \rangle$ GeV	$\langle E_\mu$ prod$\rangle$ GeV	$g(E_\mu)$	μ^+	μ^-	R_o	R_i	R_p
< 5	3	29	*	28	32	0.875 ± .226	0.875 ± .226	-
5 - 15	8.8	43	1.185	166	163	1.018 ± .112	1.018 ± .112	1.206 ± .133
15-30	21.0	64	1.100	220	173	1.272 ± .129	1.272 ± .129	1.399 ± .142
30-50	38	87	1.063	214	150	1.427 ± .152	1.427 ± .152	1.517 ± .162
50-100	70	124	1.040	250	191	1.309 ± .126	1.309 ± .126	1.361 ± .131
100-220	139	204	1	182	171	1.064 ± .112	1.064 ± .112	1.064 ± .112
220-500	296	360	1	97	71	1.366 ± .214	1.366 ± .214	1.366 ± .214
>500	1090	1200	1	27	32	0.844 ± .221	0.774 ± .326 − .294	0.774 + .326 − .294

* Because the distribution in heights of production is not known the appropriate correction factor for geomagnetic deflection is not available.

The necessary geomagnetic correction factor to find the positive excess at production is composed of three factors, reflecting respectively the different energies at production, the different survival probabilities of muons and the decay probabilities of the parents of muons of the two charges. Since a charged particle experiences a force $F = ev \wedge H$ in a magnetic field H, we see in fig. 3.2(a) that the two charges are produced at different zenith angles, which means that for a given E_μ at sea level the survival probabilities, energy loss (and thus energy at production) and parent decay probabilities are different. Ignoring any energy dependance of the charge ratio at production and assuming all muons come from pion decay, we have, with subscripts i and p for incident and production

$$R_i(E_\mu) = \left(\frac{E_\mu^+}{E_\mu^-}\right)^{-\eta} \frac{S_\mu^+ D_\pi^+}{S_\mu^- D_\pi^-} R_p \qquad \ldots\ldots (3.3)$$

where E_μ^+, E_μ^- are the energies at production of positive and negative muons having an energy E_μ at sea level; S_μ^+, S_μ^- are the survival probabilities of the two charged states and D_π^+, D_π^- the decay probabilities of the parent pions; all these quantities depending in general on the zenith angle. η is the exponent of the differential pion production spectrum. The relevant geomagnetic data for Durham are given in table 3.4 and in fig. 3.2b.

Table 3.4

Geomagnetic* Data at Durham (1964)

Horizontal component	0.168 gauss
Angle of dip	70.0°
Angle of declination	9.5°W

* Refers to the local magnetic field.

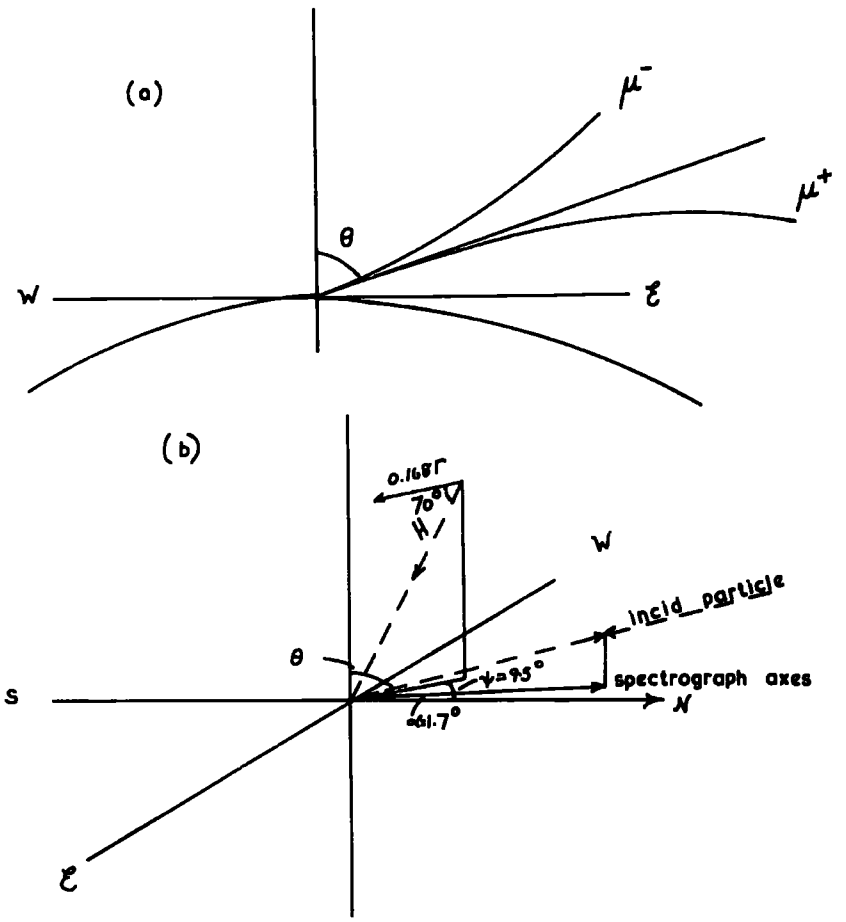

Fig.3.2 (a) the deflection of muons in the geomagnetic field. (b) The orientation of the spectrographs.

The geomagnetic cut off for primary protons is $E_o \approx 1.3$ GeV.

The spectrograph axes is at an angle 7.8^oE of the geomagnetic axes, (azimuth angle $\alpha = 1.7^oW$). The determination of E_μ^+, E_μ^-, S_μ^+, S_μ^- has been considered by Okuda (1963) and Kamiya (1964, private communication). Using the methods of these authors, based on the assumptions outlined below, the relevant production energies and survival probabilities have been found for various zenith angles θ.

Assumptions: (i) The primaries at the energies of interest are incident isotropically on the top of the atmosphere

(ii) The pion production spectrum may be approximated by the form $E_\pi^{-2.64}$, and the muons are produced at a unique depth of 120 g cm^{-2} in the atmosphere

(iii) The earth is a spherical surface of radius 6370 km. Starting from sea level with an energy E_μ the trajectories of the particles were extended back through the atmosphere in finite steps to the production level, taking into account the variation of ionisation loss with muon energy, the varying scale height of the atmosphere and the variation of the direction of the force with the direction of the particles motion, to find the production energies, survival probabilities and zenith angles at production. The values of these quantities for $\theta = 77.5^o$, 82.5^o, 87.5^o are given in table 3.5. Writing $R_p = k\, R_i$, $k = k(E_\mu, \theta)$ defined by (3.3) and taking

$$D_\pi^\pm = 1/1 + \frac{E_\mu^\pm}{rB_{\pi^\pm}} \quad \text{where } B_{\pi^\pm} = 1.827\ 10^{-4}\ H(\theta),$$

$H(\theta^\pm)$ the scale height of the atmosphere at the production level, the values of k are shown in table 3.6.

Table 3.5

The production energies, survival probabilities and zenith angles of positive and negative muons

$E_\mu s/\ell$ (GeV)		77.5°	82.5°	87.5°
3	E^+	14.6	22.9	56.6
	S^+	.141	.094	.075
	θ^+	78.21	83.42	88.54
	E^-	14.3	21.8	49.3
	S^-	.153	.104	.082
	θ^-	77.24	82.25	87.36
5	E^+	16.9	25.1	57.8
	S^+	.215	.144	.105
	θ^+	78.02	83.20	88.35
	E^-	16.7	24.3	52.1
	S^-	.227	.158	.115
	θ^-	77.33	82.32	87.33
10	E^+	22.5	30.7	62.6
	S^+	.350	.246	.171
	θ^+	77.82	82.96	88.12
	E^-	22.3	30.1	58.7
	S^-	.363	.258	.181
	θ^-	77.35	82.33	87.32
20	E^+	33.1	41.5	73.3
	S^+	.523	.395	.268
	θ^+	77.68	82.78	87.92
	E^-	33.0	41.2	70.7
	S^-	.530	.402	.281
	θ^-	77.39	82.36	87.33
30	E^+	43.5	52.1	84.1
	S^+	.610	.490	.345
	θ^+	77.62	82.75	87.82
	E^-	43.5	51.8	82.1
	S^-	.620	.500	.354
	θ^-	77.42	82.38	87.34
50	E^+	-	73.0	105.4
	S^+	-	.610	.448
	θ^+	-	82.63	87.72
	E^-	-	72.8	104.0
	S^-	-	.620	.450
	θ^-	-	82.41	87.38

Table 3.6

The function $k(E_\mu, \theta)$

θ \ E_μ(GeV)	3	5	10	20	30	50
77.5°	1.155	1.082	1.062	1.022	1.018	-
82.5°	1.261	1.189	1.098	1.034	1.030	1.022
87.5°	1.579	1.447	1.258	1.155	1.096	1.041

In order to apply this factor to the observed charge ratio it should be integrated over the incident spectrum, and over the energy range of each cell

$$R_o(\bar{E}_\mu) = \frac{\iint N_i(E_\mu, \theta)\, F(E_\mu, \theta)\, R_i(E_\mu, \theta)\, dE_\mu\, d\theta}{\iint N_i(E_\mu, \theta)\, F(E_\mu, \theta)\, dE_\mu\, d\theta}$$

$$= \frac{\iint N_o(E_\mu, \theta)\, R_p(E_\mu, \theta)/k(E_\mu, \theta)\, dE_\mu\, d\theta}{\iint N_o(E_\mu, \theta)\, dE_\mu\, d\theta}$$

Ignoring any dependance of R_p on θ, later shown to be very weak, and applying the mean value theorem to the integration over E_μ, we have the geomagnetic correction factor $g(\bar{E}_\mu)$

$$g(\bar{E}_\mu) = \frac{\int N_o(\bar{E}_\mu, \theta)\, d\theta}{\int N_o(\bar{E}_\mu, \theta)/k(\bar{E}_\mu, \theta)\, d\theta} \qquad \ldots\ldots (3.4)$$

The values of $g(E_\mu)$ appropriate to the energy cells chosen are given in tables 3.3a and 3.3b, where the final charge ratios at production, R_p, are also given. Because the assumption of a unique level of production is too crude, and R_p is more rapidly varying with energy, at very low energies the appropriate correction factor for $E_\mu \lesssim 5$ GeV is not available.

3.5 Energy at Production

In order to make direct comparison of the present charge ratio results with those obtained at other zenith angles, it is necessary to plot them as a function of energy at production. If the particles are produced at a depth x g cm^{-2}, their energy at production is given by

$$E_\mu(x,\theta) = E_\mu(t,\theta) + \int_x^{t(\theta)} \frac{dE_\mu(y)}{dy}\, dy \qquad \ldots\ldots (3.5)$$

For $E_\mu \gtrsim 1$ GeV $\quad \frac{dE}{dy} = \left(\frac{dE}{dy}\right)_{coll} + \left(\frac{dE}{dy}\right)_{other}$ where 'coll' denotes collision and 'other' denotes losses from pair production, bremsstrahlung and nuclear interactions. For air

$$\left(\frac{dE}{dy}\right)_{coll} = \cdot 0766 \left\{ 24.3 + \ln \frac{E_m}{m_\mu c^2} + \frac{1}{4}\left(\frac{E_m}{E_\mu + m_\mu c^2}\right)^2 \right\} \text{ MeV g}^{-1}\text{ cm}^2$$

where

$$E_m = \frac{E_\mu^2}{E_\mu + 1.13\,10^4} \text{ MeV}$$

Also

$$\left(\frac{dE}{dy}\right)_{other} = 10^{-7} E_\mu \left\{ 21.25 \frac{\ln \frac{E_\mu}{m_\mu} - 2.78}{\ln \frac{E_\mu}{m_\mu} - .485} + 1.8 \ln \frac{E_\mu}{m_\mu} + 6.84 \right\} \text{ MeV g}^{-1}\text{ cm}^2$$

which only becomes important for $E_\mu \gtrsim 30$ GeV, and up to energies higher than of interest can be approximated by a term

$b\, E_\mu$ where $b \sim 4.0\ 10^{-6}$ g^{-1} cm^2, Hayman et. al. (1963).

Using these formulae equation (3.5) can be solved by iteration, and the production energies for various θ are shown in fig. 3.3. Also shown in this figure is the energy at production of the particles observed averaged over the angular ranges in the two series, viz.

$$\langle E_{\mu\,prod} \rangle = \frac{\int N_o(E_\mu(E_{\mu\,prod}), \theta)\, E_{\mu\,prod}\, d\theta}{\int N_o(E_\mu(E_{\mu\,prod}), \theta)\, d\theta}$$

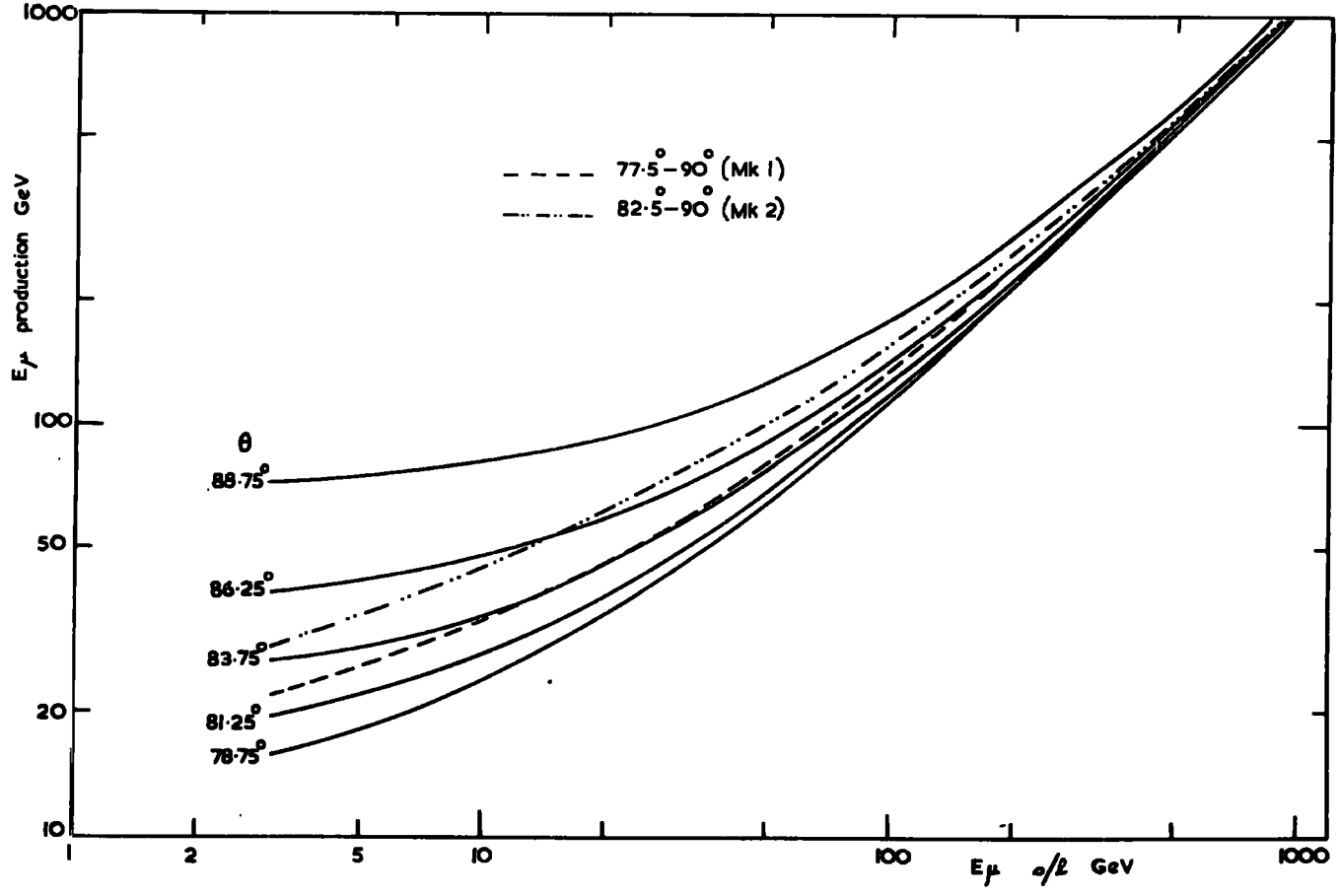

Fig.3.3 $E_{\mu prod}$ vs $E_{\mu sl}$ at large zenith angles.

the integration from 77.5 - 90° for Mk 1 and 82.5 - 90° for Mk 2. From this we see, for example, that an average particle observed with $E_\mu \approx 12$ GeV in the Mk 2 series has an energy at production of ~ 50 GeV. For the centre of the angular cell θ is 86°, where the intensity at 12 GeV is only a factor of ≈ 2 less than the intensity at 50 GeV at $\theta = 0°$, cf fig. 2.10; so for studying processes at production one is considerably better off at large angles than appears from a glance at the spectra; above a sea level energy of ~ 40 GeV in Mk 2 one is better off than at $\theta = 0°$. The appropriate mean production energies for the chosen cells are given in tables 3.3a and 3.3b.

3.6 The Final Results

The final charge ratio at production, from the two series, is shown as a function of energy at production in fig. 3.4. With regard to the Mk 1 series results we see that they are in good agreement with other work, see also fig. 4.2, showing very slight evidence for a minimum in the region 50-100 GeV and indicating an increasing ratio at high energies. The Mk 2 series, which was initiated mainly to investigate the behaviour at high energies, although based on a longer running period only contains about 1/5th of the number of particles measured in the Mk 1 series, and for energies below 200 GeV the data are statistically much weaker than the Mk 1 results. The Mk 2 data give no evidence for a minimum in the region 50-100 GeV, although in view of the large errors in this region the results cannot be regarded as inconsistent with the Mk 1 results.

Clearly the present results are inconclusive with regard to the existence of the minimum; further discussion of this point is given in Chapter 4.

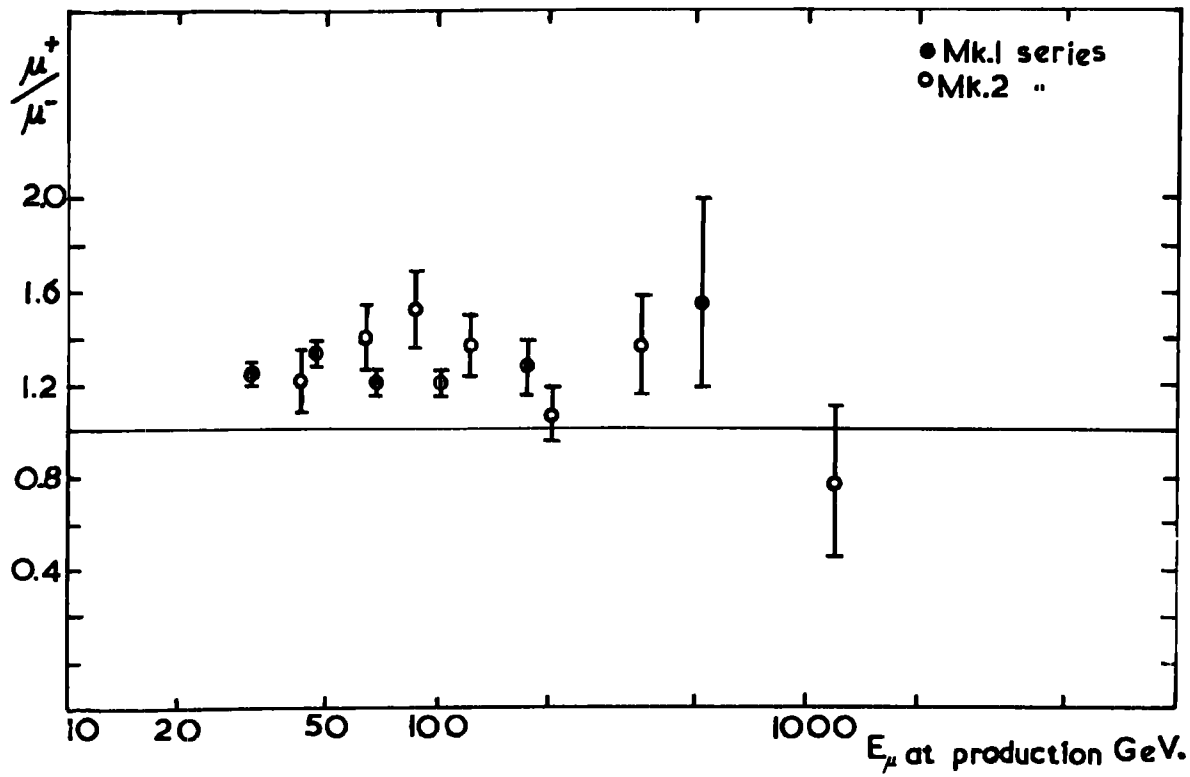

Fig.3.4 The corrected charge ratio as a function of energy at production as obtained in the two series.

The most noticeable feature is the negative excess found at the highest energies, i.e. $\mu^+/\mu^- = 0.774 \pm^{.326}_{.294}$ at $E_\mu \approx 1200$ GeV. Indeed for $E_\mu >$ 100 GeV in the Mk 2 series $\mu^+/\mu^- = 1.12 \pm 0.09$, possibly indicating a decreasing ratio at high energies but the overall results are not inconsistent with a value of 1.20 - 1.25 as suggested by an extrapolation of the ratio at $E_\mu \lesssim 100$ GeV, up to the highest energies measured, a conclusion which gains weight in the following chapter.

In the following chapter a survey of the charge ratio measurements will be made, to be followed in succeeding chapters by an interpretation of the experimental results.

CHAPTER 4.

A Review of Charge Ratio Measurements

4.1 The very low energy region

We will now review the present experimental data on the μ^+/μ^- ratio; previous reviews have been given by Puppi and Dallaporta (1952), Morewitz and Shamos (1953) and Fowler and Wolfendale (1961). The data have been divided into two groups, those measurements in the vertical direction having $E_\mu \leq$ 1 GeV at sea level, and the remainder. The former data are shown in fig. 4.1 as a function of sea level momentum. Most of the data have been discussed in the references above, and, for several reasons, notably, because of μe decay, many of these particles are produced locally in the atmosphere, the inequality and rapid variation of the pion nucleon cross-section at low energies, and a nuclear physics effect whereby a slight excess of neutrons occurs in the nucleonic component at low energies - Puppi and Dallaporta (1952) - the results are very distantly related to the primary nucleon - nucleus interaction, and their interpretation is rather involved. For these reasons the behaviour at these very low energies will not be considered further since it is not likely to throw much light on the original interactions.

4.2 The remaining data: a summary

The remaining data, $E_\mu >$ 1 GeV at $\theta = 0^\circ$ and all E_μ at larger zenith angles have been plotted as a function of energy at production, taken appropriate to the zenith angle assuming a unique production level of 120 g cm^{-2}, in fig. 4.2. The data of Pine et.al. (1959) and of Pak et.al. (1961) refer to an unstated mixture at $\theta = 0^\circ$ and 68°, the former angle has been attributed to them all in assigning E_μ at production.

All the published data will not have been corrected for the various

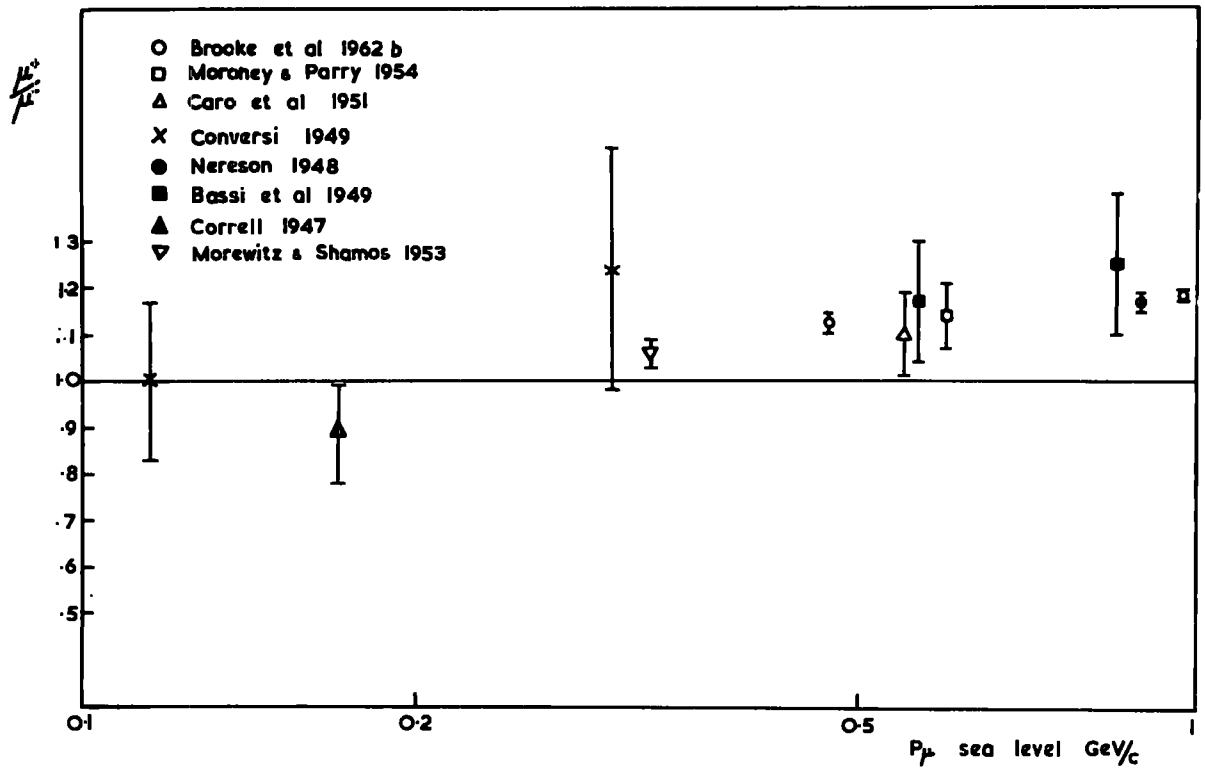

Fig.4.1 μ^+/μ^- measurements at $p_{\mu s l}<1$ GeV/c.

Fig. 4.2

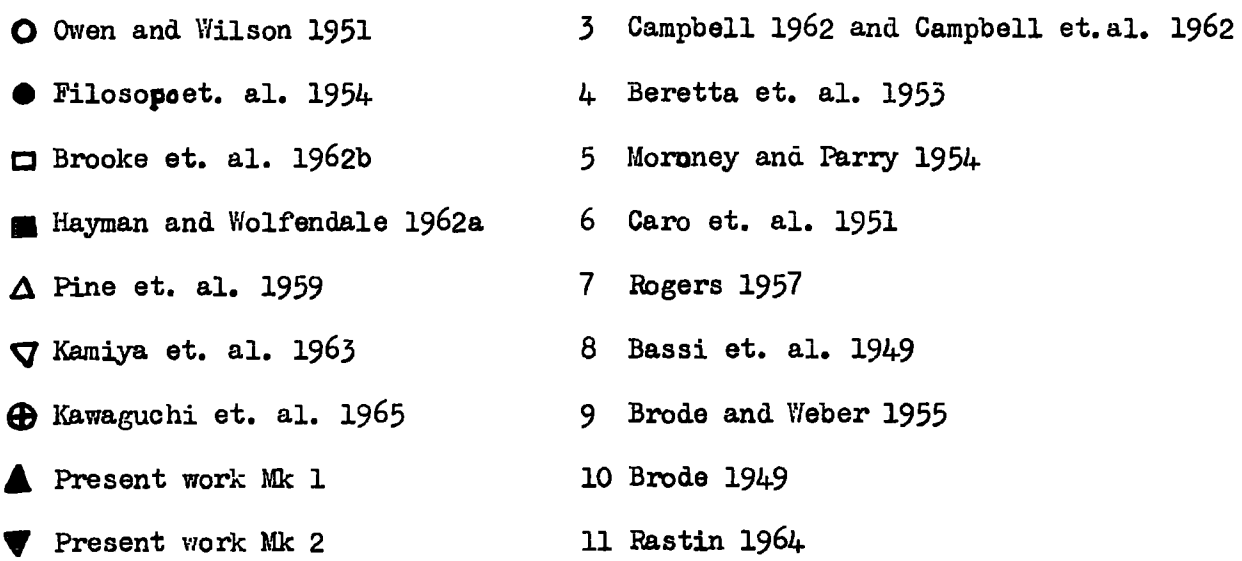
Owen and Wilson 1951
Filosopoet. al. 1954
Brooke et. al. 1962b
Hayman and Wolfendale 1962a
Pine et. al. 1959
Kamiya et. al. 1963
Kawaguchi et. al. 1965
Present work Mk 1
Present work Mk 2
1 Pak et. al. 1961
2 Holmes et. al. 1961b
3 Campbell 1962 and Campbell et.al. 1962
4 Beretta et. al. 1953
5 Moroney and Parry 1954
6 Caro et. al. 1951
7 Rogers 1957
8 Bassi et. al. 1949
9 Brode and Weber 1955
10 Brode 1949
11 Rastin 1964
12 Rastin et. al. 1965
13 Aurela 1965

effects listed in Chapter 3, but, except at very high energies, statistically sound work in all the energy ranges, corrected in detail, is available. At energies $\lesssim$ 20 GeV there is the work of Owen and Wilson (1951) using an airgap magnetic spectrograph, the authors having performed an auxillary interaction experiment to correct for proton contamination, and corrected at high momenta for contamination by charges of opposite sign. The determination of μ^+/μ^- with the greatest accuracy is the work of the Padua group - Filosofo et.al. (1954) - which eliminates both the above mentioned corrections as these authors looked at a fixed, narrow momentum cell of muons at various depths underground, corresponding to narrow energy intervals at sea level. Some work at $E_\mu \lesssim$ 20 GeV at various depths in the atmosphere e.g. Alikhanian et.al.(1957), Allkofer and Trumper (1964) which requires correction for proton contamination has not been included since the data seems well enough established in this region. Also excluded are two points of Groetzinger and McClure (1950) at 24° and 58° of considerable statistical accuracy which give charge ratios significantly lower than the results of all other workers in this energy region. The agreement of most of the other works with the two high accuracy works cited above suggests no serious systematic biases, the case of greatest discrepancy, Brode (1949), having been shown by Owen and Wilson (1951) to be due to overcorrecting and is very probably not inconsistent with the other data.

Over the last six years extensive data in the region $20 \lesssim E_\mu \lesssim 100$ GeV has become available, notably Pine et.al.(1959), Hayman and Wolfendale (1962a) Kamiya et.al.(1963) and the present work, all of which has been corrected in detail. The agreement between all this work is not as good

as at low energies, in particular some authors find evidence for a minimum in the region 50-100 GeV, and this will be discussed later in the chapter. Some recent results from the Durham vertical spectrograph (Aurela (1965)., private communication) of which only three points have been plotted in fig. 4.2 have uncertainties in the energy determination, and the full results are given in table 4.1; they show little sign of a significant minimum.

At energies $\gtrsim$ 100 GeV, due to the considerable statistical errors on all the available data one cannot say that there is disagreement between the various results. Despite the very great spread, only one point out of the 18 with $E_\mu > 100$ GeV has a ratio less than unity, and then not significantly.

4.3. Best estimate of the μ^+/μ^- ratio

In order to get a better picture of the energy dependance of the μ^+/μ^- ratio the data in fig. 4.2 have been combined into energy cells at production. To see if there is any dependance on zenith angle they have been further divided into two groups, $\theta < 75^\circ$ and $\theta > 75^\circ$, the former cell consisting almost entirely of measurements made near the vertical. As a consistency condition it was demanded that all accepted points lie within three standard deviations from the mean in a cell, and as a result three points at low energies have been excluded from the summary, a point at 6.1 GeV due to Caro et. al. (1951), at 3.7 GeV due to Rodgers (1957) and the one at 3.7 GeV due to Brode (1955), all of which are very high. The points within each cell were combined by weighting each according to the inverse square on the quoted errors.

$$\langle R \rangle = \frac{\sum_i R_i/S_i^2}{\sum_i 1/S_i} \quad \text{and the error on } \langle R \rangle, \langle S \rangle = \left(\sum_i 1/S_i^2 \right)^{-\frac{1}{2}}$$

Table 4.1

The μ^+/μ^- results of Aurela (1965) at $\theta = 0^\circ$

E_μ sl GeV	μ^+/μ^-
12	1.240 ± 0.036
23	1.262 ± 0.031
$31 \pm^{8}_{10}$	1.279 ± 0.038
$47 \pm^{17}_{15}$	1.208 ± 0.069
$66 \pm^{26}_{24}$	1.269 ± 0.085
$102 \pm^{53}_{50}$	1.280 ± 0.116

A point in the lowest energy cell for $\theta < 75^{\circ}$ by Filosofo et.al. (1954), (E_{μ} = 2.90GeV, μ^+/μ^- = 1.212 $\pm$.001) has been plotted separately, indicated by F, because the quoted error on it is very much smaller than on the other points in the cell. The chosen cells and resulting means for the two zenith angular ranges are shown in table 4.2 and the resulting points in fig. 4.3.

From the results we notice

(i) There is very little dependance on zenith angle

(ii) While the low energy points are best established near the vertical the high energy region is almost totally dependant on studies at large zenith angles.

(iii) There is very little evidence for a sharp minimum in the ratio.

This latter fact might arise from the rather arbitrary energy cells chosen - the upper limit being doubled every time. However even if a cell 50 - 85 GeV is chosen, a point μ^+/μ^- = 1.175 $\pm$ 0.026 at 64.1 GeV is obtained, shown dashed in fig. 4.3., which, because of ambiguity in the behaviour of the charge ratio at higher energies does not enable us to determine conclusively the existence or non-existence of a minimum.

The overall impression is that the charge ratio remains remarkably constant over a very wide energy region $\sim$3 - 500 GeV. In the following chapters the interpretation of these observations will be considered in detail.

Table 4.2

The Muon Charge ratio as a function of zenith angle.

	$75^\circ < \theta < 90^\circ$			$\theta < 75^\circ$			
$E_{\mu\ prod}$ GeV	No. of points	$\langle E_{\mu\ prod} \rangle$	R_H	No. of points	$\langle E_{\mu\ prod} \rangle$	R_v	R_H/R_v
< 3				9*	2.72	$1.170 \pm .009$	
$3 \leq E < 5$				10	3.90	$1.215 \pm .007$	
$5 \leq E < 10$				21	5.78	$1.264 \pm .003$	
$10 \leq E < 20$	1	18.5	1.235 ± 0.120	22	12.4	$1.250 \pm .006$	$0.988 \pm .096$
$20 \leq E < 40$	9	29.1	$1.270 \pm .023$	21	26.4	$1.260 \pm .009$	$1.008 \pm .020$
$40 \leq E < 80$	8	55.0	$1.227 \pm .026$	8	54.9	$1.193 \pm .037$	$1.028 \pm .038$
$80 \leq E < 160$	6	102	$1.217 \pm .034$	7	101	$1.249 \pm .069$	$0.974 \pm .060$
$E > 160$	7	213	$1.192 \pm .060$	3	244	$1.417 \pm .187$	$0.841 \pm .119$
$160 \leq E < 320$	4	182	$1.186 \pm .065$				
$E > 320$	3	620	$1.227 \pm .160$				

* A point in this cell by Filosofo et.al. ($E_{\mu\ prod} = 2.90$ GeV, $R = 1.212 \pm 0.001$) has been plotted separately because the quoted error on it is very much smaller than on any other point in the cell.

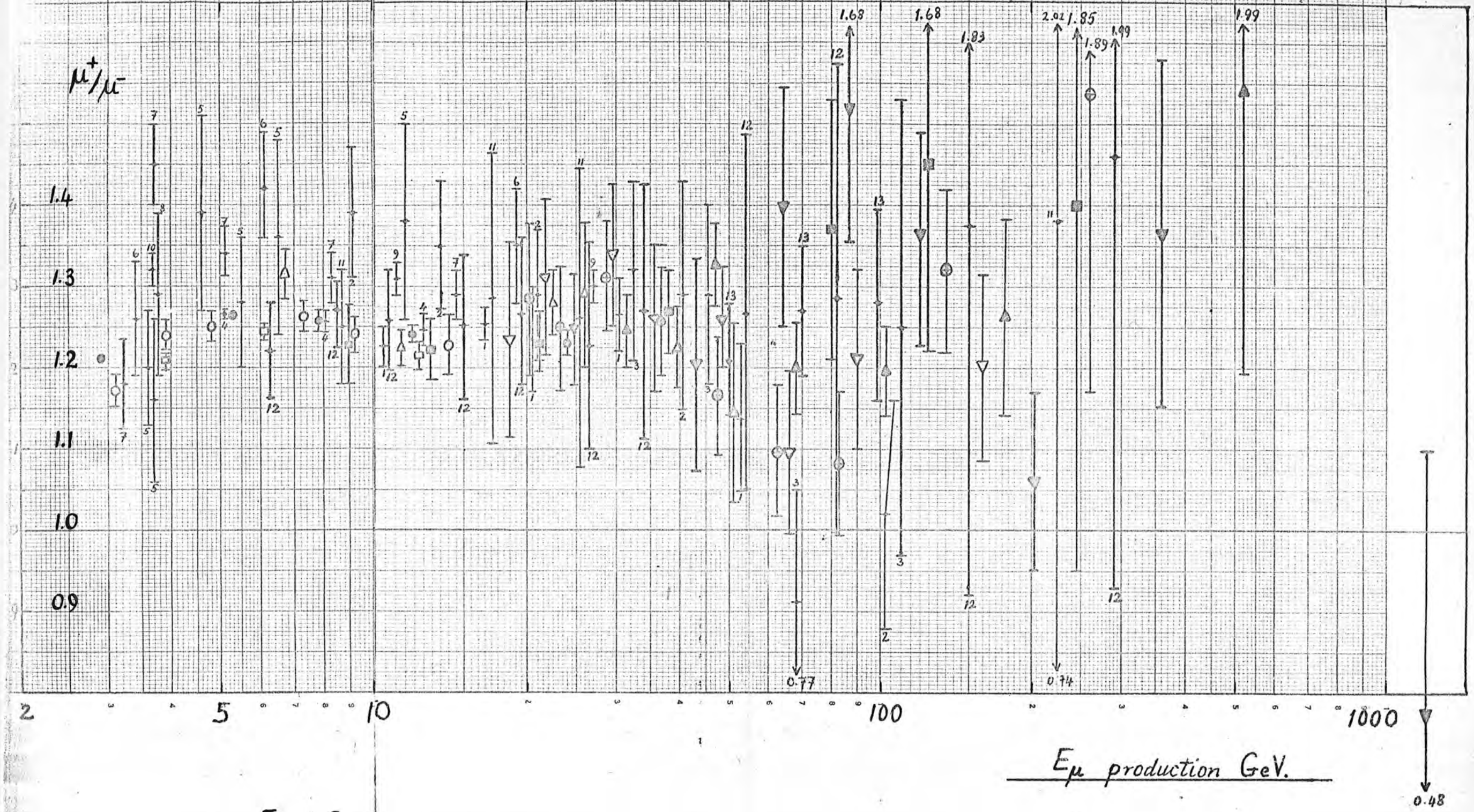
μ^+/μ^-
1.4
1.3
1.2
1.1
1.0
0.9
1.68
1.68
1.83
2.02
1.85
1.89
1.99
1.99
0.77
0.74
0.48
2
5
10
100
1000
E_μ production GeV.

FIG. 4.2

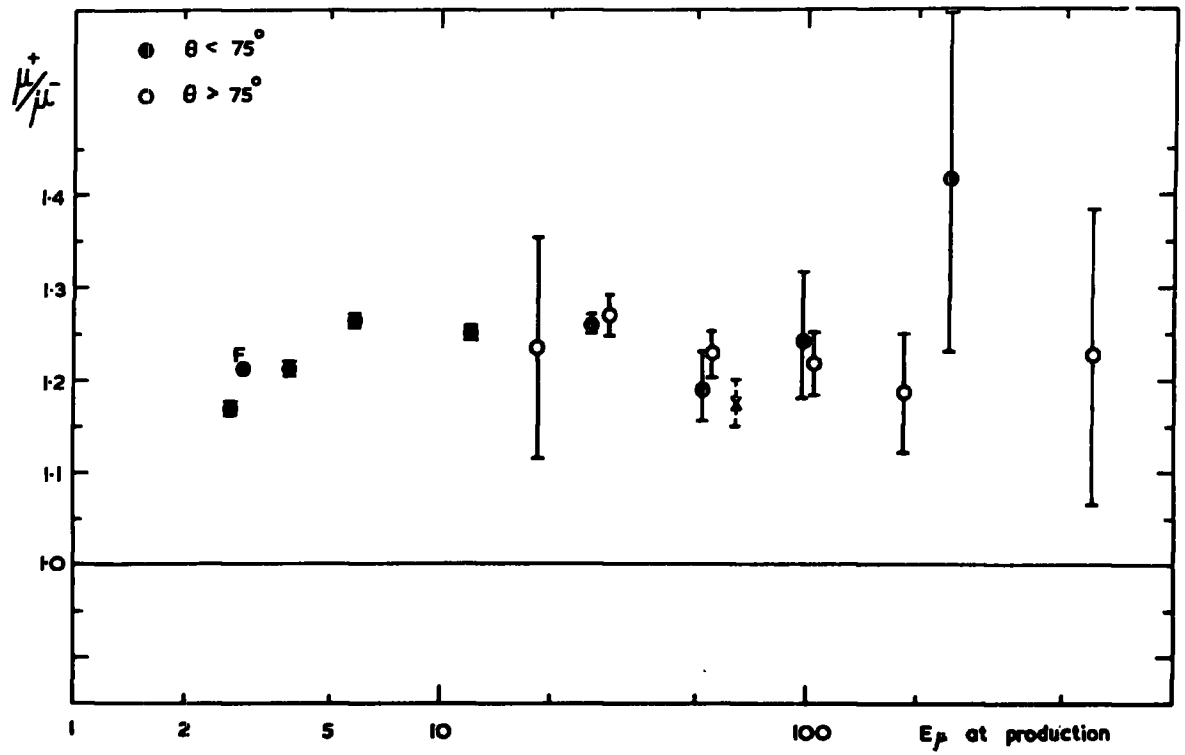

Fig.4.3 A survey of all experimental data on the μ^+/μ^- ratio divided by zenith angle.

CHAPTER 5.

The Interpretation of the μ^+/μ^- ratio

5.1 Introduction

The importance of the μ^+/μ^- ratio over other sea level cosmic ray observations for the interpretation of high energy interactions arises from the fact that it strongly reflects the behaviour of the first generation events, and at high energies the observed sea level muons are almost all derived from first generation nucleon collisions. If one uses various interaction models to predict the muon charge excess, rather than use the observed excess to find out something about the interactions, a greater insight into the mechanisms responsible can be obtained, and better correlation with observations on nucleon interactions at lower energies (i.e. the accelerator region) found. The latter approach, however, is also useful and has been adopted by, among others, Pal and Peters (1964), Volkova and Zatsepin (1965), and Melkman et.al. (1965).

The interpretation of the observed charge excess requires a knowledge of three separate factors, (i) the properties of the primary radiation, i.e. its charge and particle composition and energy spectrum; (ii) the parameters which characterise the propagation in the atmosphere of both the primary and the hard secondary component, and (iii) the dynamical properties of the collision between the primaries and the air nuclei in the region $E_o = 3\ 10^{10} - 3\ 10^{14}$ eV. In the following sections the general approach will be outlined and our knowledge of the three above mentioned features reviewed.

5.2 The present approach

From the theoretical point of view it is easiest to consider the muon

positive excess $\delta(E_\mu)$ defined as

$$\delta(E_\mu) = \frac{\mu^+(E_\mu) - \mu^-(E_\mu)}{\mu^+(E_\mu) + \mu^-(E_\mu)}$$

which is related to the charge ratio R (E_μ) by

$$R(E_\mu) = \frac{1 + \delta(E_\mu)}{1 - \delta(E_\mu)}$$

Some authors work in terms of a quantity $\eta(E_\mu) = 2\,\delta(E_\mu)$. The most rigorous theoretical approach to the problem is an exact solution of the diffusion equations in the atmosphere e.g. Fowler and Wolfendale (1961), including the dynamical properties of the interactions in the production spectra of the various components. This is rather tedious if the dynamical properties are not well known, or easily formulated, as is the case in practice and is unprofitable if one wishes to investigate the consequences of various models of interaction. Fortunately, sufficiently valid approximations may be made such that a less rigorous treatment may be adopted.

We will denote by $N(E_o, x)\,dE_o$ the nucleon differential spectrum at a depth x g cm^{-2} in the atmosphere; $\sigma_{n,p}(E_o, n_\pi, k_\pi)\,dk_\pi$ the differential cross-section for a nucleon of energy E_o to produce a total of n_π pions in a collision with an air nucleus, with an inelasticity k_π, i.e.

$$\sum E_\pi = k_\pi E_o \;;$$

$N_\pi(E_o, k_\pi, n_\pi, E_\pi)\,dE_\pi$ the differential energy spectrum of pions produced in such a collision;

$n_\mu(E_\pi, E'_\mu)\,dE'_\mu$ the energy spectrum of muons from pion decay, where $E'_\mu = E_\mu'(E_\mu, x)$ is the energy of a muon produced at x which arrives at sea level with an energy E_μ,

$\delta_o\ (E_o,x)$ the charge excess in the nucleon flux at a depth x, i.e.

$$\delta_o(E_o,x) = \frac{N_p(E_o,x) - N_n(E_o,x)}{N_p(E_o,x) + N_n(E_o,x)} \quad ;$$

$\Delta\ (E_\pi,\ n_\pi)$ the charge excess of a pion having an energy E_π, produced in a collision in which a total of n_π pions were produced i.e.

$$\Delta\ (E_\pi,\ n_\pi) = \frac{\pi^+(E_\pi) - \pi^-(E_\pi)}{\pi^+(E_\pi) + \pi^-(E_\pi) + \pi^o(E_\pi)} \quad ;$$

$P_\pi(E_\pi,x)$ the probability that a pion of energy E_π, produced at a depth x, will decay rather than interact;

$S_\mu(x,t,E_\mu)$ the probability that a muon produced at a depth x will arrive at sea level, depth t, $\equiv t(\theta)$, with energy E_μ.

Then if we assume that all the observed muons come from pion decay, the proton and neutron cross-section are equal, and ignore the energy dissipated in the production of particles other than pions, we can write the muon charge excess at sea level as

$$\delta(E_\mu) = \frac{\sum \int N(E_o,x)\sigma(E_o)N_\pi(E_\pi)n_\mu(E_\mu')P_\pi(E_\pi,x)S_\mu(E_\mu,x)\delta_o(E_o,x)\Delta(E_\pi,n_\pi)\,dx\,dE_o\,dk_\pi\,dE_\pi\,dE_\mu'}{\sum \int N(E_o,x)\sigma(E_o)N_{\pi^\pm}(E_\pi)n_\mu(E_\mu')P_\pi(E_\pi,x)S_\mu(E_\mu,x)\,dx\,dE_o\,dk_\pi\,dE_\pi\,dE_\mu'}$$

We have $dE_\mu' = \frac{dE_\mu'}{dE_\mu}\,dE_\mu \simeq dE_\mu$, $N_{\pi^\pm}(E_\pi) = \frac{2}{3}N_\pi(E_\pi)$. Also

$$N(E_o,x)\,dE_o = N(E_o,0)\,e^{-x/\Lambda_o}\,dE_o$$

where Λ_o is the attenuation length of nucleons, assumed energy independent. Also if we may assume $\delta_o(E_o,x)$ independent of E_o, $\equiv \delta_o(x)$ - this will be discussed later, the above expression may be written in the form

$$\delta(E_\mu) = \frac{\int_0^t dx\, e^{-x/\Lambda_o}\delta_o(x)P_\pi(\langle E_\pi\rangle,x)S_\mu(E_\mu,x)\sum_{n=1}^{\infty}\int_0^1 dk_\pi\int_{E_\pi}^{\infty}dE_o\int_{E_{\pi\,min}}^{E_{\pi\,max}}dE_\pi\,N(E_o,0)\,\sigma_n(E_o)\,N_\pi(E_\pi)\,n_\mu(E_\mu')\,\Delta}{\frac{2}{3}\int_0^t dx\, e^{-x/\Lambda_o}P_\pi(\langle E_\pi\rangle,x)S_\mu(E_\mu,x)\sum_{n=1}^{\infty}\int_0^1 dk_\pi\int_{E_\pi}^{\infty}dE_o\int_{E_{\pi\,min}}^{E_{\pi\,max}}dE_\pi\,N(E_o,0)\,\sigma_n(E_o)\,N_\pi(E_\pi)\,n_\mu(E_\mu')}$$

where, as an approximation, in P_π the mean value of E_π contributing to E_μ

has been taken for ease of calculation, not a very severe assumption. We see that in all the terms to the right of the summation signs the dependance on x only enters through the dependance of E'_μ on x, and then in the same way in the numerator and denominator. Since the other terms involving x include exponentials we will for convenience evaluate the terms to the right of the summation signs at some appropriate x where most of the muons are produced. With these approximations we can write

$$\delta(E_\mu) = D(E_\mu, \theta)\,\delta_1(E_\mu) \qquad \ldots(5.2)$$

where $\delta_1(E_\mu)$ is the charge excess of muons coming from primary nucleon collisions for a pure proton beam, and $D(E_\mu,\theta)$ is a 'dilution' factor which reflects the composition of the primary radiation, and the relative contribution of muons from first generation collisions to those from all generations, at sea level. Once $D(E_\mu,\theta)$ has been obtained the problem reduces to determining $\delta_1(E_\mu)$ for the dynamical model under consideration

5.3 The dilution factor $D(E_\mu,\theta)$

From (5.1) we have

$$D(E_\mu,\theta) = \frac{\int_0^{t(\theta)} e^{-x/\Lambda_0}\,\delta_0(x)\,P_\pi(E_\pi,x)\,S_\mu(E_\mu,x)\,dx}{\int_0^{t(\theta)} e^{-x/\Lambda_0}\,P_\pi(E_\pi,x)\,S_\mu(E_\mu,x)\,dx} \qquad (5.3)$$

When $\theta \neq 0$ $x \longrightarrow x(s)$ and $dx \longrightarrow ds$ where ds is an element of path length.

The charge excess in the nucleon beam $\delta_0(x)$, in fact, depends on the characteristics of the interactions. Mindful that the air nuclei are charge symmetric (i.e. they have equal numbers of protons and neutrons), then if the probability of charge exchange in a nucleon air nucleus collision is 0.5 the charge excess of nucleons, other than primaries which have not interacted, is zero, and as a result

$$\delta_0(x) = \frac{\delta_0(0)\,e^{-x/\lambda_0}}{e^{-x/\Lambda_0}} = \delta_0(0)\,e^{-x(1/\lambda_0 - 1/\Lambda_0)} \qquad (5.4)$$

where λ_0 is the interaction length of nucleons. If some interactions are characterised by a mechanism where the charge exchange probability is not 0.5, e.g. if charge retention occurs this result would not be valid, but the evidence suggests that the relative cross-sections for mechanisms of this type is small, though just such mechanisms might be responsible for the major part of the observed high energy muons. Also in such mechanisms it is likely that the energy lost by the nucleon in a collision will be comparable to that lost in the normal collisions. If such cross-sections are neglected, $\delta_0(x)$ will be energy independant, (5.4), and this is assumed. If we further neglect the variation of energy loss with energy we can write

$$E_\mu'(x) = E_\mu + \alpha(t - x), \alpha = \partial E_\mu / \partial x \quad ;$$

and further we can ignore the narrow spectrum of muons from pion decay in the integrals and write, suppressing the dash on E'

$$E_\pi(x) = E_\mu(x)/r \text{ where } r = \frac{M_\mu}{M_\pi} = 0.76.$$

At high energies, depending on the zenith angle, since $\alpha \approx$ 2MeV $g^{-1}cm^2$, the energy loss can be neglected, and $S_\mu(E_\mu, x)$ constant, whence we get the assymptotic form of $D(E_\mu, \theta)$

$$D(E_\mu, \theta) \rightarrow \delta_0(\theta) \frac{\int_0^t e^{-x/\lambda_0} P_\pi(E_\mu, x)\, dx}{\int_0^t e^{-x/\Lambda_0} P_\pi(E_\mu, x)\, dx}$$

which, to a good approximation, reduces to, Duthie et al (1962),

$$\frac{\delta_0(0)}{(\lambda_0/\Lambda_0)} \frac{1 - bE_\mu/rB_\pi(1-b)\ln(1-b)}{1 - aE_\mu/rB_\pi(1-a)\ln(1-a)}$$

with $a = 1 - \lambda_\pi/\lambda_0$, $b = 1 - \lambda_\pi/\Lambda_0$, λ_π the pion interaction length, and $B_\pi = B_\pi(\theta) = \frac{m_\pi c^2}{c\tau_\pi} H(\theta)$ where $H(\theta)$ is the scale height of the atmosphere; $B_\pi(0) = 117$ GeV.

Taking $\lambda_0 = 80$ g cm^{-2}, $\Lambda_0 = 120$ g cm^{-2} and at high energies $\lambda_\pi = 125$ g cm^{-2},

Brooke et al (1964b), we get

$$\theta = 0^\circ \qquad D(E_\mu) = \frac{\delta_0 \lambda_0}{\Lambda_0} \frac{1 + E_\mu/90.5}{1 + E_\mu/110} \xrightarrow[E_\mu \to \infty]{} 0.815\,\delta_0$$

$$\theta = 80^\circ \qquad D(E_\mu) = \frac{\delta_0 \lambda_0}{\Lambda_0} \frac{1 + E_\mu/450}{1 + E_\mu/549} \xrightarrow[E_\mu \to \infty]{} 0.815\,\delta_0$$

At low energies the energy loss becomes important, especially at large θ, and must be included. The expression for the survival probability is, Rossi(1952),

$$S_\mu(E_\mu, x) = \left\{ \frac{x/t}{1 + \alpha(t-x)/E_\mu} \right\}^{\frac{B_\mu(x)}{E_\mu + \alpha t}}$$

where $B_\mu = \frac{m_\mu c^2}{c\,\tau_\mu} H_\pi(\theta)$, and α is assumed constant. For the pion decay probability the approximate form

$$P_\pi(E_\pi, x) = \frac{1}{1 + E_\pi(x)/B_\pi(x,\theta)}$$

has been used. Including the dependance of path length on x, $s(x)$, and with H (0) as given by Rossi (1952), and α = 2.2 MeV $g^{-1}cm^2$ these expressions have been inserted in (5.3), and $D(E_\mu,\theta)$ numerically evaluated for $\theta = 0^\circ$ and 80°. $D(E_\mu,\theta)/\delta_0$ is shown in fig. 5.1, as is the assymptotic expression derived above for high energies.

From the intensities of the various primary nuclei above 2.4 GeV/c per nucleon, Waddington (1960), we can find δ_0, with the result that $\delta_0 = 0.74$, i.e. 87% protons and 13% neutrons, - an upper limit of 5% to the flux of antiprotons in the relevant range of primary energy has been set by Brooke and Wolfendale (1964b). This has been taken to hold over a very wide energy region, however, most of the evidence indicates that this composition holds up to energies $\sim 10^{14}$eV, Malhotra et al(1965), but the apparent steepening of the primary nucleon spectrum at $E_0 \gtrsim 10^{15}$ eV, and the increasing frequency of multiple cored air showers, McCusker (1963), possibly heralds a change in composition at these energies. The above

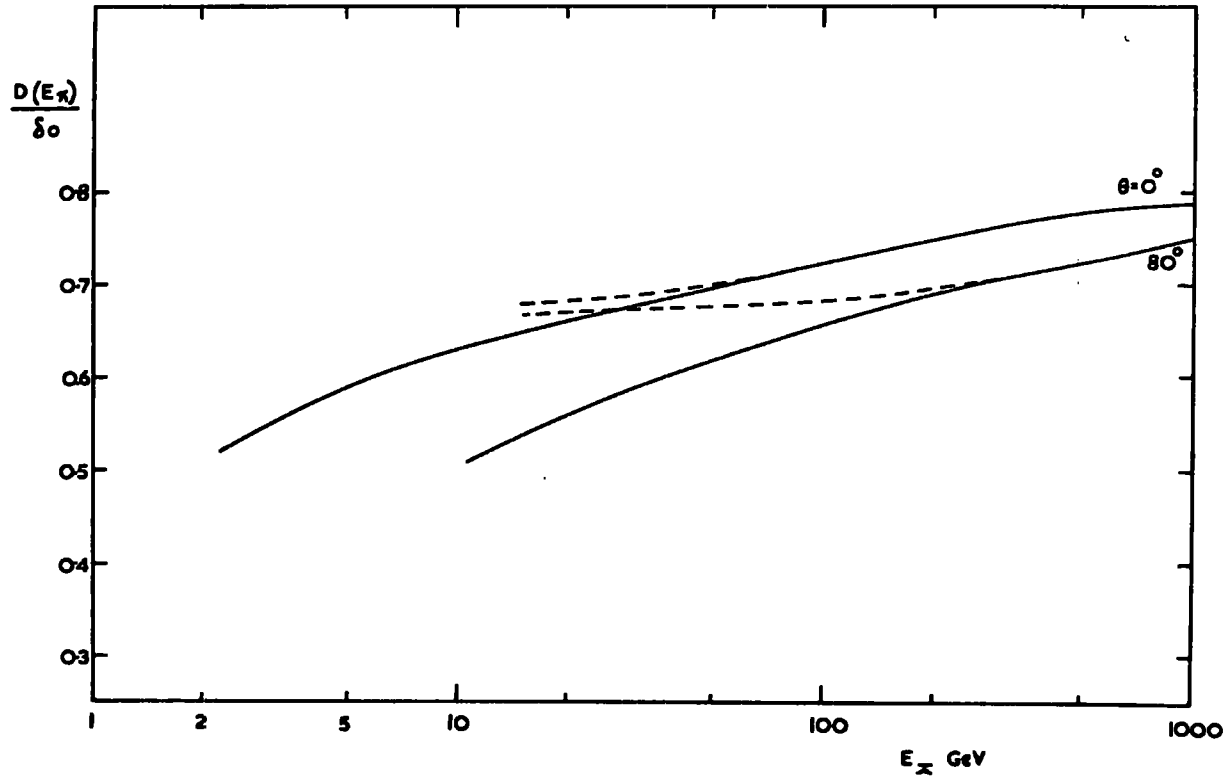

Fig.5.1 The dilution factor as a function of E_{π}.

constant value will be assumed throughout the present work.

5.4 $\delta_I(E_\mu)$ from simple considerations.

The following general assumptions will be made throughout unless otherwise stated.

(i) The primary nucleon spectrum may be represented by a single power law $N(E_o)\ dE_o = E_o^{-\gamma} dE_o$ to a normalising constant, on which the charge excess does not depend.

(ii) The inelastic collision cross-section for protons and neutrons are the same, and are independant of energy, the latter assumption is indicated on theoretical grounds and seems reasonable from a survey of nucleon cross-sections up to 30 GeV, Morrison (1963), Pinkau (1964). A slight rise in σ_{inel} may occur with E_o as the elastic channel becomes less favourable at high energies. The evidence from cosmic ray work in favour of σ rising appreciably with energy is tenuous, and the majority of workers do not see indications of a rapid rise, the experimental data, however, is rather scarce and often difficult to interpret.

We can now see the behaviour of the charge excess from the simplest reasonable assumptions on the characteristics of proton air nucleus collisions. If we consider that pions are the only particles produced which contribute to the muon flux, and that all the interactions at a given energy are characterised by a unique inelasticity and multiplicity of pions, we can write

$$\sigma(E_o,\ n_\pi\ ,\ k_\pi) = \sigma_o\ \delta(k_\pi - \langle k_\pi \rangle)\ \delta(n_\pi - \langle n_\pi \rangle)$$

Further, we assume that the pions are produced in two sharp cones in the c.m.s. i.e. an angular distribution

$$f(\omega^*) = \tfrac{1}{2}\delta(1 - |\omega^*|), \quad \omega^* \equiv \cos\theta^*$$

and that all the available energy in the laboratory system is equidistributed amongst those pions in the forward cone i.e.

$$E_\pi \frac{\langle n_\pi \rangle}{2} = k_\pi E_0 \qquad \ldots.(5.5)$$

The assumption of a forward-backward angular distribution is not restrictive as it has been shown by Yeivin (1956) that the computed excess is very insensitive to $f(\omega)$. We then have

$$N_\pi(E_\pi) = \frac{\langle n_\pi \rangle}{2} \delta(E_\pi - \langle E_\pi \rangle)$$

As to the pion charge excess at production if one assumes a probability of charge exchange of the incident nucleon = 0.5 in collision with an air nucleus we get $\langle \pi^+ - \pi^- \rangle = \frac{1}{2}$, and if we assume this excess charge is uniformly distributed over the produced pions

$$\Delta(E_\pi, n_\pi) \equiv \Delta(n_\pi) = 1/2\langle n_\pi \rangle$$

In fact the conservation of isotopic spin modifies this relation and we get

$$\Delta(n_\pi) = \varphi(n_\pi)/2n_\pi \qquad \ldots\ldots(5.6)$$

The function $\varphi(n_\pi)$ which tends to unity as $n_\pi \to \infty$, is tabulated in table 5.1 and its derivation is discussed in the appendix.* Ignoring the spectrum of muons from pion decay, i.e. setting $E_\pi = E_\mu/r$, and inserting the above assumptions into the expression for $\delta_1(E_\mu)$ - (5.1), we get simply

$$\delta_1(E_\mu) = \frac{\varphi(\langle n_\pi \rangle)}{2\langle n_\pi \rangle \cdot \frac{2}{3}} = \frac{\varphi(\langle n_\pi \rangle)}{2\langle n_{\pi^2} \rangle} \qquad \ldots.(5.7)$$

$$R_1(E_\mu) = \frac{2\langle n_{\pi^2} \rangle + \varphi(\langle n_\pi \rangle)}{2\langle n_{\pi^2} \rangle - \varphi(\langle n_\pi \rangle)}$$

Taking k_π independent of E_0 and $\langle n_\pi \rangle = BE_0^\alpha = B^{\frac{1}{1-\alpha}} \left\{ \frac{\langle E_\pi \rangle}{2\langle k_\pi \rangle} \right\}^{\alpha/1-\alpha}$ and $\alpha = \frac{1}{4}$, which as will be indicated later is a reasonable value, we get, at high energies where $D(E_\mu)$ becomes constant,

---

* The author is very grateful to Dr. L. Cohen who kindly provided his computations from which $\varphi(n_\pi)$ could be derived.

Table 5.1

The Isotopic Spin weighting function

n_π	$\varphi(n_\pi)$
1	.75
2	.75
3	.833
4	.856
5	.883
6	.898
7	.911
8	.920
9	.929
10	.934

$$\delta(E_\mu) \sim E_\mu^{-\frac{1}{3}}$$

in constract to the constant behaviour observed, $R(E_\mu)$ from the above assumptions corrected for dilution, with $\langle k_\pi \rangle = 0.3$, B = 2.7, is shown in fig. 5.2 for both the cases of $\varphi(n_\pi)$ included, and set = 1. Since it is believed that $\langle n_\pi \rangle$ does not behave significantly different from an $E_0^{\frac{1}{4}}$ behaviour, and as will be shown later, $\delta(E_\mu)$ does not depend very severely on k_π, we see that this simple approach fails to account for the experimental results.

5.5 Previous theoretical work

Among many early, apparently successful, attempts to account for the muon charge ratio we may mention Lewis et.al (1948), Caldirola and Loinger (1950), Cini and Wataghin (1950) and Yeivin (1955). All of this work was performed when the knowledge on interactions at machine energies was not available, and it is easy now, in view of our present information, to see the assumed features which resulted in agreement with the experimental data. From a theory of multiple production by analogy with the theory of electrodynamics, Lewis et al (1948) found $\delta(E_\pi) \sim E_\pi^{-\frac{1}{2}}$ a much more rapid fall off than observed. Caldirola and Loinger (1950) solved the diffusion equations with a simple production model, which required, even for a decreasing charge ratio above 3 GeV, a multiplicity of $\langle n_{\pi^\pm} \rangle \approx 2$ at $E_\pi \approx 15$ GeV. We now know that such a pion energy would be characterised by a multiplicity $\langle n_{\pi^\pm} \rangle \approx 6$. A similar argument holds for the results of the detailed analysis given by Cini and Wataghin (1950) who included a pion spectrum in each interaction. Several early authors used the Heitler-Janossy theory of plural production, which is not now accepted, and which causes the charge excess amongst the produced pions to be preferentially distributed among those in the high energy tail of the pion spectrum, which because of the rapidly

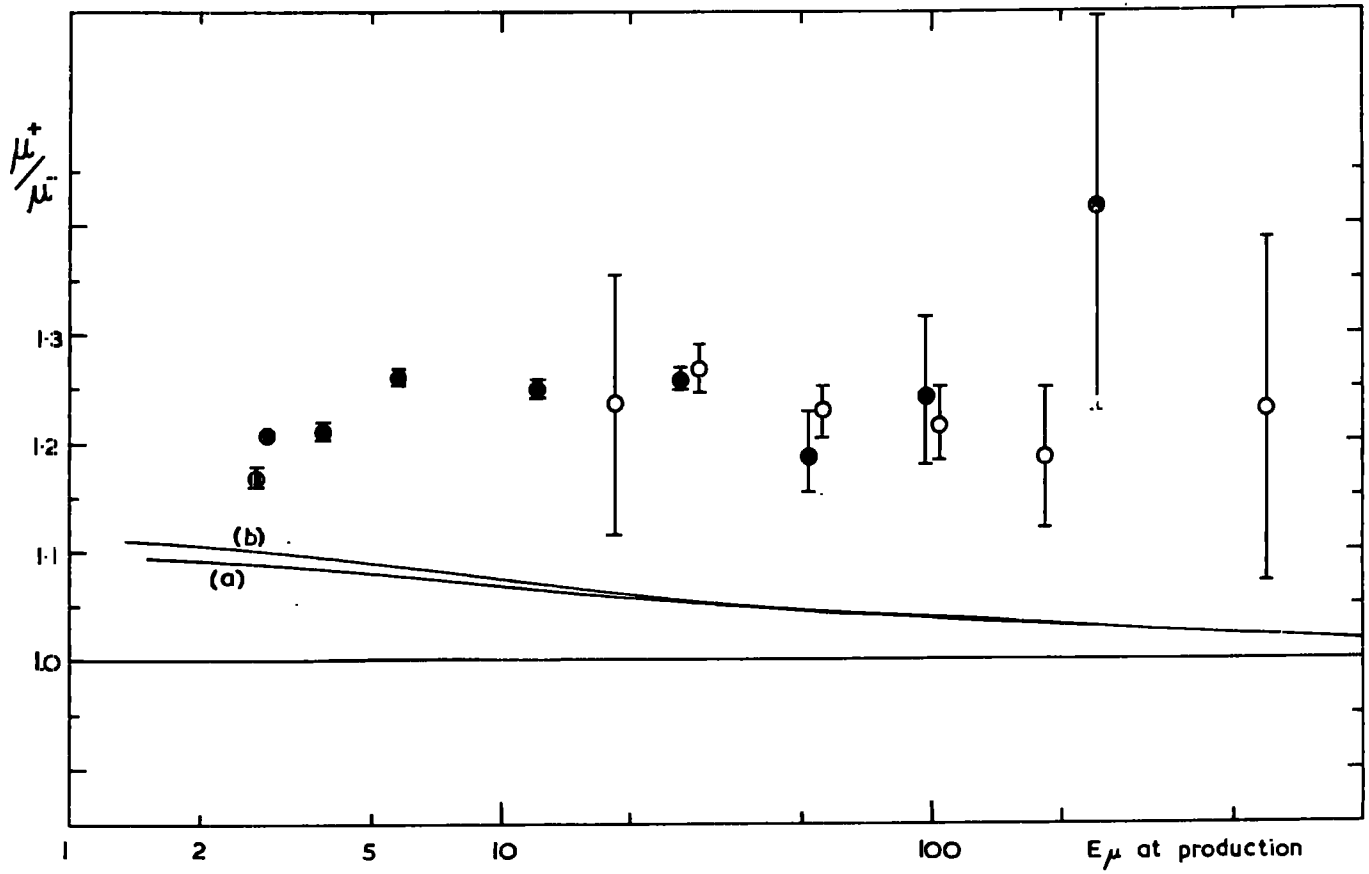

Fig. 5.2 The μ^+/μ^- ratio from simple pionisation (a) including and (b) excluding the isospin weighting function.

falling primary spectrum would give rise to an appreciable charge excess at sea level.

The first detailed study of the positive excess based on the theory of multiple production, in the light of results then being obtained with accelerators, was the work of Yeivin (1955). He showed that the variation of the muon charge ratio could be characterised by a single parameter β, of which it is a rapidly varying function, where

$$\beta = \frac{\gamma - \alpha}{1 - \alpha}$$

where α and γ are the indices of the multiplicity dependance on primary energy, and the primary differential spectrum respectively. On normalising his results to the experimental data at E_μ = 1 GeV he found $\beta = 2.3$ as a best fit. However if we take values for α and γ suggested by our present knowledge viz $\alpha \approx \frac{1}{4}$, $\gamma \approx 2.6$ we find $\beta = 3.1$ which gives a very much lower and rapidly falling excess; even for $\alpha = 0$ $\beta = \gamma$ which is certainly not less than 2.4 we still get a ratio which falls off rapidly at high energies. While all the above work seemed adequate at the time on the basis of the knowledge of high energy interactions and the muon charge ratio then obtaining, we see now that even at low energies they do not satisfactorily account for the observations, and they are all essentially equivalent to the approach leading to (5.7). In order to proceed beyond this, greater detail of the interactions must be included in the calculations, and to this end the properties of high energy interactions will be reviewed in the following section, and it will be followed by a summary of our information on the primary nucleon spectrum and the propagation in the atmosphere.

5.6 High Energy interactions

5.6.1 General

Working from our knowledge of nuclear interactions at machine energies the most striking features of interactions at higher energies is the weak dependance of the various parameters on primary energy. At these energies most of the investigations so far have been conducted by the method of jets in emulsions, supplemented by γ-cascade studies, and in the most recent years by ionisation calorimeters. In the method of jets some selection criteria must be chosen, and when one also considers that some unexpected features, such as asymmetries, may occur, the determination of energies is never a very confident procedure, and since the primary spectrum is rapidly falling errors in the energy determination can lead to erroneous dependances of the parameters on energy being deduced, Mursin (1965). However, when jet results are combined with the more reliable accelerator, and ionisation calorimeter results, and indications from E.A.S. studies, a sensible picture of high energy interactions up to $E_o \sim 10^{14}$ eV emerges.

Apart from the constancy of cross-sections, already noted, the dominant features of these interactions are the constancy of at least three quantities (i) the mean inelasticity (ii) the particle composition of produced secondaries and (iii) the mean transverse momentum. The most rapidly varying property is the c.m.s. angular distribution, a factor important in analysing the type of mechanism responsible for particle production, but one to which our calculations on the charge excess are insensitive. The mean multiplicity depends to some extent on the primary energy.

5.6.2 Inelasticity

While it is characterised by a distribution extending from 0 to 1, studies from accelerator energies up to the attenuation of E.A.S. indicate

that the mean inelasticity is constant, having a value $\sim 0.4 - 0.5$ for nucleon light nucleus collisions; Brooke et al (1964a) deduced a value for the inelasticity going into pion production $\langle k_\pi \rangle = 0.35$. This means that in the majority of collisions the most energetic particle leaving the collision is a nucleon, possibly in an excited state.

5.6.3. Particle composition.

It has been known now for a long time that at low energies the majority of produced particles are pions and most of the evidence available indicates that such a behaviour extends up to high energies, and, as at accelerator energies, kaons seem to be the next most favoured particle at these energies. Since kaons are quite efficient at producing muons their contribution is important in the present context and detailed evidence for the K/π ratio will shortly be discussed. No direct evidence is yet available for the frequent production of nucleon-antinucleon pairs, nor for copious hyperon production; indirect evidence against abundant production of hyperons is the fact that a muon positive excess could only occur if one made the unlikely assumption that the positive charge was distributed solely among the secondary baryons, Kotov and Rozental (1962), and also it was shown by Bowler et al (1962), that a hyperon model for muon production was not necessary to account for the observed γ ray spectrum.

The evidence for the K/π ratio at production has been reviewed by Osborne (1964) and Osborne and Wolfendale (1964). Some information on the K/π ratio in the region $E_o = 6\ 10^2 - 10^5$ GeV may be obtained from the present work, by way of a comparison of the muon spectrum at large zenith angles with that at the vertical. In figs.5.3 and 5.4 there is plotted

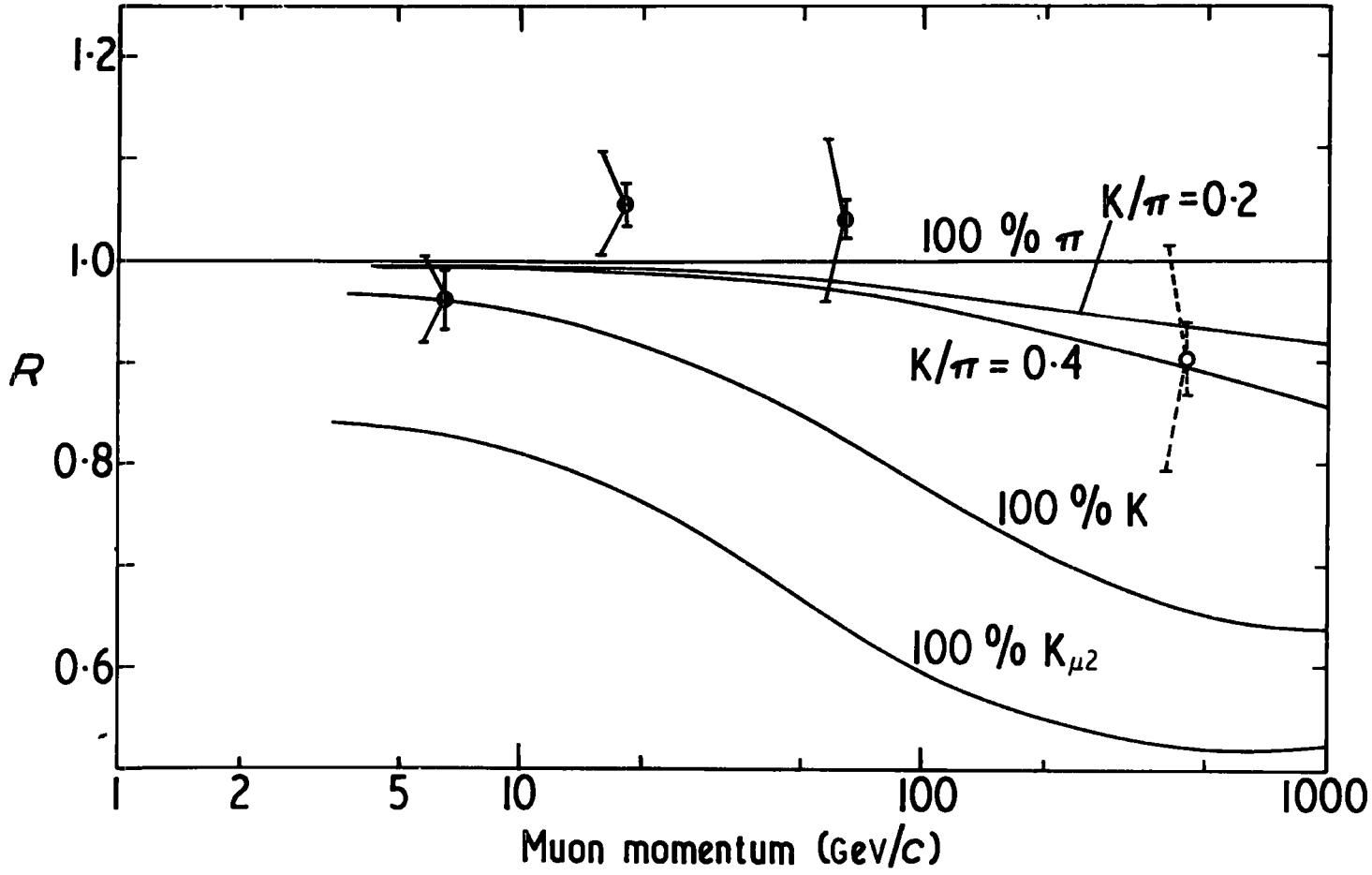

Fig.5.3 A comparison of the observed intensity with that expected for various K/π ratios at production for the Mk.1 series.

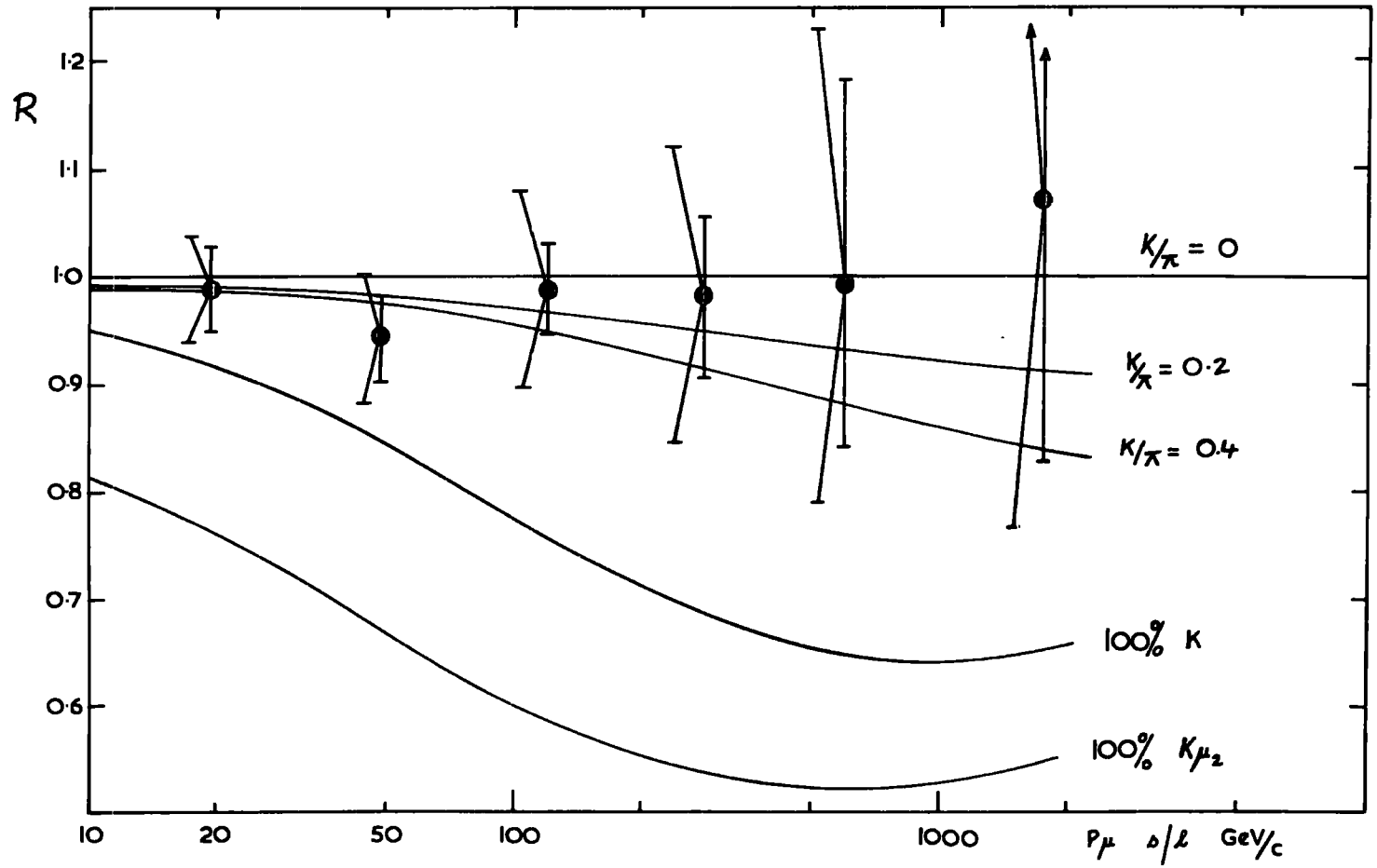

Fig. 5.4 A comparison of the observed intensities with those expected for various K/π ratios at production, for the EK.2 series.

the ratio of the number of muons predicted in the present experiment for the cases where K/π = 0.2, 0.4, ∞ at production to the numbers expected if pions alone were the source of muons. In determining the numbers predicted for a certain fraction of kaons contributing, all the kaon modes giving rise to muons directly and indirectly have been considered as has been the energy spectrum of pions and muons from kaon decay. The case of 100% kaons where only the K_{μ_2} mode is considered has also been plotted in the figures. The experimental points in these figures are the ratio of the observed numbers to the numbers predicted for all pions as parents as calculated via (2.15). The predicted ratios are uncertain, especially at high energies because of the uncertainties in the vertical muon sea level spectrum. This uncertainty has been incorporated in the error flags on the points, the inclined flags representing the errors when allowance for this is included. The reduced sensitivity when all kaon modes are included over the case when the K_{μ_2} mode alone is considered, and the uncertainty in the initial datum, i.e. the vertical spectrum, limit our ability to draw firm conclusions from the results, but both experiments indicate that we can set an upper limit to the K/π ratio, namely

$$(K/\pi)_{all} \lesssim 0.4$$

This value is in good agreement with other indirect investigations of the frequency of kaon production in the works cited above. These authors, from an analysis of the data on the polarisation of muons at sea level, and from a comparison of the spectrum of electromagnetic cascades in the atmosphere with the measured muon spectrum, subject to some assumptions, infer the behaviour of the K/π ratio at primary energies $E_0 \lesssim 300$ GeV and $E_0 \gtrsim 2\ 10^4$ GeV. It

should be noted that if the mean energy of kaons is greater than that of pions these estimates will be an overestimate. The various estimates of the K/π ratio are summarised in fig. 5.5.

We see that there is not much evidence that the fraction of charged particles other than pions produced, so called X particles, is very different from the value quoted by Perkins (1961), viz

$$\frac{N_{X^\pm}}{N_{X^\pm} + N_{\pi^\pm}} = 0.18 \pm 0.05$$

up to $E_o \approx 10^{14}$ eV, this quoted value depending on the assumption that all observed γ rays in emulsions come from π^o decay and $\pi^o = \pi^\pm/2$. It should be emphasised that this result applies to the final state at a time after the interaction long compared with the characteristic time of strong decays, a fact which must be borne in mind when formulating theories for nucleon interactions, since this feature was thought to exclude the statistical model of Fermi.

5.6.4 The transverse momentum and energy distributions

The importance of the transverse momentum $P_\perp$ of particles produced in an interaction is that it is a Lorentz invariant quantity, and thus provides us with one of the few c.m.s. parameters directly observable in the laboratory system, and it is closely related to the energy of particles in the c.m.s. The mean value of $P_\perp$ for secondaries, in the region $E_o \gtrsim 20$ GeV, where constraints from energy-momentum conservation are not important, is $\langle p_\perp \rangle \approx$ 400 MeV/c, its constancy reflecting the increasing angular anisotropy in the c.m.s. $P_\perp$ is characterised by a distribution of the Boltzmann shape with a tail which seldom extends beyond 1.5 GeV/c. Two features more recently detected are (i) a dependance of $\langle p_\perp \rangle$ on the mass of the particle, $\langle p_\perp \rangle$

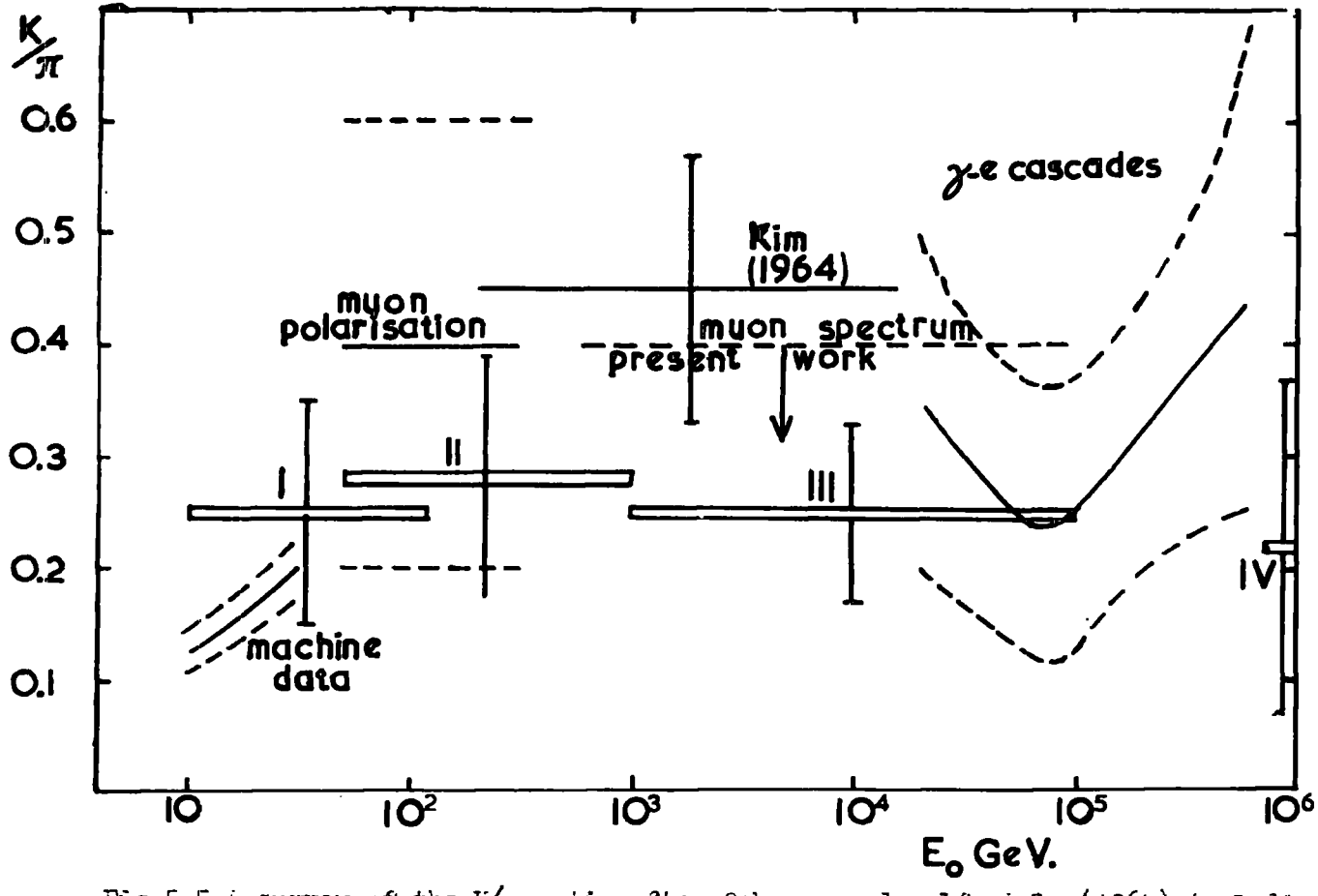

Fig.5.5 A survey of the K/π ratio, after Osborne and Wolfendale (1964), including the present work. I-IV, Heinz (1961), γe cascades reconsidered by Pattison (1965, p.c.).

increasing with increasing mass, the dependance being approximately linear, Pinkau (1964), and (ii) a slight suggestion that $\langle p_\perp \rangle$ is increasing at high energies, $\sim 10^{14}$ eV. Some dependance of $P_\perp$ on the angle of emission θ^* is also observed, it being smaller at the extreme angles.

For a given inelasticity the energy spectrum of the secondary particles extends almost up to kE_o. Again the difficulties in measuring E_o enter for the determination of the secondary energies, the high energy tail of the spectrum can only be investigated by looking at γrays from π^o decay and interactions produced by the secondary particles, or by looking at particles in the backward cone in the c.m.s. The pion energy spectrum has a peak at a few pion masses, and then decreases rapidly. On the basis of results at accelerator energies Cocconi et al (1961) derived a phenomenological model for nucleon interactions, which has recently been shown by Hugget (1965), to have many features in common with the two centre models. These authors concluded that the spectrum could be represented to good accuracy by an exponential dependance

$$N(E_\pi)\, dE_\pi = \frac{n_\pi}{2T} e^{-E_\pi/T}\, dE_\pi \,, \quad T = T(E_o) \approx \langle E_\pi \rangle .$$

Here it is assumed that half of the produced pions carry all the energy above 1 GeV, which is almost all the available energy $k_\pi E_o$. This expression is quite a good fit to the available data at accelerator energies and to the spectrum of π^os as deduced from spectra from jets, Boult et al (1964), provided $E_\pi \gtrsim 1$ GeV and $E_b \gtrsim 20$ GeV. By combining the space angular distribution and the Boltzman transverse momentum distribution Aly et al (1964) derived a distribution which gives a very good fit at accelerator energies, a differential momenta spectrum of the form

$$N(p_\pi)\,dp_\pi \propto \frac{1 + c\,p_\pi^{-b}}{p_\pi^{14}}\; e^{-a p_\pi^{-b}}\, dp_\pi$$

While neither of these expressions is an exact fit to the most recent experimental data they represent the energy dependance in the high energy tail to sufficient accuracy.

The nucleon spectrum is peaked towards high values, having a shape similar to a reversed Boltzmann distribution. Of the energy spectrum of the other particles not much can be said, but some information has become available recently on kaons, which indicates that kaons are produced with a higher mean energy than pions, no doubt related to the higher transverse momentum of kaons already noted. From the work of Brandt et al (1963) on K^o production in $\pi^- p$ collisions at 10 GeV, we find an averaging over all events $p_K^* / p_\pi^* = 1.48$. In an analysis of jets ($N_h \leq 3$), $E_o \simeq 10^{12}$ eV, Kim (1964) studying the extreme backward cone in the c.m.s., $\theta \geqslant 175^o$, finds $p_K^* / p_\pi^* = 1.72$, where the particles were identified by grain density, scattering, and range measurements. From a much more detailed experiment on p-p and p-light nucleus collisions at 18.8 and 23.1 GeV by Dekkers et al (1964) two features appear (i) the energy spectra of K^+ and K^- are quite different, the K^+ spectrum being much flatter and (ii) the K^- spectrum is very similar to the pion spectrum only falling off more rapidly. The flat K^+ energy spectrum also appears in the work of Diddens et al (1964), on p-p collisions at 19 and 24 GeV. Since K^+ are more frequently produced than K^- the mean energy of kaons is greater than that of pions.

5.6.5 Multiplicity of secondary particles

At a given primary energy there is a considerable fluctuation in multiplicity from one event to another, and the mean multiplicity is a slowly varying function of energy. From general arguments relating to a statistical

model for particle production one expects the multiplicity to depend on E_o as $E_o^{\frac{1}{4}}$. At the highest energies all the data comes from jets in emulsions, and some selection criteria must be adopted to separate out approximate nucleon nucleon collisions, and to separate the original nucleons from all the secondaries. After this it would seem that $\langle n_\pi \rangle \approx 2.7\ E_o^{\frac{1}{4}}$ is a reasonable fit to the data for nucleon light nucleus collisions passing through the well established data at $E_o \leq 30$ GeV. At present there is considerable controversy as to the energy dependance of $\langle n_\pi \rangle$, some maintaining that it rises as $\ln E_o$, and others that it rises faster than $E_o^{\frac{1}{4}}$. Many of the proposed dependences only become distinguishable at high energies and arguments in favour of both a $\ln E_o$ and an $E_o^{\frac{1}{4}}$ dependance can be adduced from E.A.S, studies. McCusker and Peak (1964) from an analysis of jets at $3\ 10^{12}$ eV, $N_h \leq 2$, deduce a value for charged secondaries, $\langle n_s \rangle = 10.8 \pm 0.8$ where the energy refers to the median Castagnoli energy of the sample, which supports a logarithmic dependance; but in this respect one must be mindful of the work of Mursin (1965) already cited, which shows the tendency of $\langle n_s \rangle$ to apparently saturate when errors in the determination of E_o are not considered. Malhotra et al (1965) find $\langle n_s \rangle \approx 33 \pm 5$ at $E_o \sim 10^4$GeV. There is a general class of models for high energy interactions, the peripheral models, where the interaction is mediated by a single or repeated exchange of quanta, from which a logarithmic dependance follows, Koba and Krzywicki (1963), Frautschi (1963) and a similar dependance has been derived by Krisch (1964) from a simple field theoretical model. Despite this however, the highest energy air showers, and the study of γ rays from π^o decay, assuming charge independance, on the whole favour an $E_o^{\frac{1}{4}}$ multiplicity dependance.

The sources of bias in all the cosmic ray measurements are very great,

in particular the N_h selection in jets. As Feinberg remarked at the Jaipur conference the selection of $N_h = 1, 2$ may be biassing towards untypical events where the momentum transfers in the collision are smaller than usual which might explain the saturation in multiplicity deduced by Malhotra, (1963), from a survey of experimental jets, since he used the criterion $N_h \leq 2$.

It should be emphasised that almost all the above discussion referred to nucleon-nucleon or nucleon-light nucleus collisions. Information on pion collisions is much scarcer, but their features do not appear to be much different except that the inelasticity in such collisions seems to be much nearer to unity and many of the results on apparently large inelasticities may be attributed to pion collisions.

5.6.6 High Energy Theories

One of the earliest theories of particle production was the statistical theory due to Fermi, in which the collision, and particle production parts were separated; and although the angular isotropy and the frequent production of particles other than pions were not observed, interest in it has emerged again after recent success in describing elastic scattering, Fast and Hagedorn (1963), and the possibility of including quarks in the formation stage Koba (1965). Various modifications of the statistical model were tried, eventually leading to the 'two centre' and fireball models, which, in the absence of a rigorous model, give a good overall pictorial view of the interaction. Here the interaction may be viewed as in fig. 5.6 where the case of the production of two fireballs and two excited nucleons is shown.

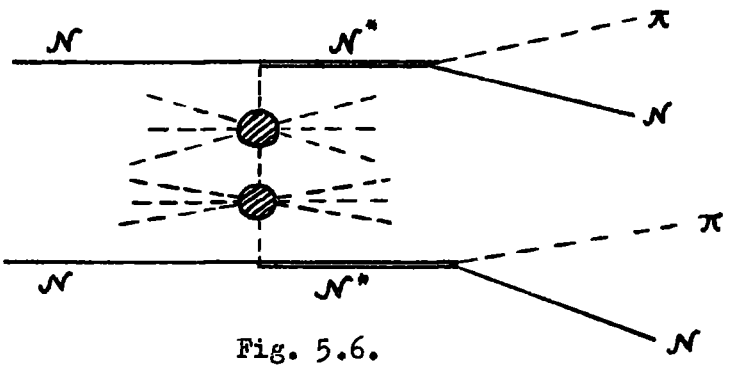

Fig. 5.6.

In any particular collision all of these vertices need not be present. Such a picture is convenient for visualising the production processes but the dynamical reality of the fireballs should not be taken too seriously. The relevance of more rigorous theoretical models to the present work will be discussed later as appropriate.

5.7 The Primary spectrum and atmospheric propagation

5.7.1 The primary spectrum

We are interested in the spectrum of primary nucleons in the region contributing to sea level muons in $2 < E_\mu \lesssim 2\ 10^3$ GeV, which, on assuming $\langle k_\pi \rangle = 0.3$, $\langle n_\pi \rangle = 2.7\ E_0^{\frac{1}{4}}$ corresponds to primary energies $3\ 10^{10} \lesssim E_0 \lesssim 3\ 10^{14}$ eV/nucleon. Because of the low fluxes and uncertainties in energy measurements the establishment of the primary spectrum is difficult; but despite this, several workers are in fair agreement, at least on the exponent of the spectrum, if not on the absolute intensities.

Boradzei et al (1964) using an ionisation calorimeter at mountain altitude conclude that in the region 10^{10} - $5\ 10^{11}$ eV the spectrum has an integral exponent of 1.6, and in the region $5\ 10^{11}$ - 10^{15} eV is of the form

$$N\ (>E_0) = 500 \left(\frac{Eo}{10^{12}}\right)^{-1.7} \left[-0.15 + 2.75\left(\frac{Eo}{10^{12}}\right)^{-0.2} - 1.6\left(\frac{Eo}{10^{12}}\right)^{-0.4}\right] \text{nucleons m}^{-2}\ \text{hr}^{-1}\ \text{sterad}^{-1}$$

Zatsepin et al (1963), from a study of air showers conclude that in the region $2\ 10^{10}$ - $6\ 10^{14}$ eV, $\gamma - 1 \approx 1.62 \pm 0.05$; a similar value $\gamma - 1 \approx 1.63$ also being

found by Miyake (1963) from an analysis of γ cascade data. Brooke et al, (1964a), derived the primary nucleon spectrum indirectly by correlating sea level measurements on the muon and proton components assuming a model for the energy distribution of produced particles in a collision. In this way they derived a spectrum in the energy region 10^{10} - 3 10^{13} eV of the form

$$N(>E_o) = 0.87 \pm \begin{matrix} 0.52 \\ 0.30 \end{matrix} E_o^{-1.58} \text{ nucleons cm}^{-2}\text{sec}^{-1}\text{sterad}^{-1}$$

It appears that over a wide energy range 5 10^9 - 10^{15} eV the integral spectrum has an index γ - 1 very near 1.60. In some small energy region around 10^{15} eV there is a transition to a steeper spectrum resulting in an exponent γ - 1 $\approx$ 2.2. As we are here interested in E_o up to ~ 3 10^{14} eV a differential spectrum with index γ = 2.58 will be assumed throughout. Recent work of Malhotra et al (1965) is also in very good agreement with an index of 1.6 over the region of interest. Very recently results have been reported by Grigorov et al (1965a) on a direct measurement of primary fluxes using an ionisation calorimeter in an earth orbitting satellite, which gives fluxes very much lower than those derived by the authors mentioned above, and values of γ-1 = 1.75 at $E_o \leqslant 10^{11}$ eV, 1.85 for $10^{11} \leqslant E_o \leqslant 10^{12}$ and 1.95 in E_o = 10^{12} - 10^{14} eV. Thus it is seen that this spectrum is appreciably steeper than the works quoted above and nearer the value of γ - 1 = 1.9 in E_o = 10^{11} - 10^{13} eV earlier derived by Grigorov (1963), from ionisation calorimeter measurements. While the satellite method is a very direct approach to determining the primary spectrum the results, as yet, should be considered preliminary, but must be kept in mind.

5.7.2 Propagation in the atmosphere

The absorption length of nucleons in the atmosphere, Λ_o, can be derived from a comparison of the measured sea level proton spectrum, Brooke and Wolfendale (1964a), with the primary nucleon spectrum in the corresponding energy region. A value of the nucleon interaction length λ_o can be found from various measurements on nucleon cross-sections at accelerator energies and neutron cross-sections at cosmic ray energies. A correlation between these two quantities by means of the determined value of total inelasticity in nucleon air nucleus collisions is possible from the relation

$$\lambda_o = \Lambda_o (1 - \eta^\gamma)$$

where $\eta = 1 - k$ is the coefficient of elasticity. By this means fair agreement on the value $\lambda_o \simeq 80$ g cm^{-2} and $\Lambda_o \simeq 120$ g cm^{-2}, independant of energy, is found.

The data on λ_π and Λ_π are much less certain but at $E_\pi \gtrsim 80$ GeV Brooke et al (1964b), suggest that pion collisions are catastrophic, whence $\lambda_\pi = \Lambda_\pi$ equal to ≈ 120 g cm^{-2}, At lower energies they find $\Lambda_\pi = 150$ g cm^{-2}. A value of $\lambda_\pi \approx 120$ g cm^{-2} also follows from the measured ratio of $\sigma_{pp} / \sigma_{\pi p}$ at accelerator energies, Morrison, (1963).

The presence of pions in the nuclear active component in the atmosphere, which on interaction may contribute to the muon flux must not be overlooked. Several measurements at great depths in the atmosphere indicate that the $\pi^\pm / p$ ratio rises from $\sim 10\%$ at 1 GeV to $\sim 50\%$ at 20 GeV and thereafter remains constant at least up to ~ 500 GeV, Brooke et al (1964b), Grigorov et al (1965b) and Subramanian (1962). However it has been argued by Pal and Peters (1964) that the pion flux at 200 g cm^{-2} is small and the resulting muon flux is not much affected by pion production by pions.

CHAPTER 6

μ^+/μ^- From a Quasi Statistical Model

6.1 Fluctuations in mutliplicity

If we consider pions to be the only particles produced in high energy collisions, the fluctuations, from one event to another, in the mutliplicity of charged pions will have a pronounced effect on the muon positive excess. An idea of the fluctuations in the number of produced secondaries over a fixed band of E_o can be obtained from fig. 6.1a, after Kobayashi et. al. (1964b), where δn_s, the mean variance in n_s, is plotted versus $\langle n_s \rangle$ for I.C.E.F. jets with $N_h \leq 5$, $n_s \geq 6$. The importance of fluctuations for the charge excess arises from the fact, that, if the inelasticity is not positively correlated with the multiplicity in an event, low multiplicity events give rise to pions having a relatively large charge excess, and an energy larger than is usual for the primary energy responsible, this latter fact being much accentuated by the falling primary spectrum.

The correlation between inelasticity and multiplicity is very much an unknown quantity; in pp collisions at 24 GeV, Dodd et. al. (1961), observe a slight positive correlation, fig. 6.1b, while Wolter (1964), also finds some tenuous evidence for a positive correlation at $E_o \approx 3$ TeV based on a small sample of nucleon jets with all N_h values. Imaeda and Kazuno (1964), from an analysis of I.C.E.F. primary, and neutral secondary jets with $N_h \leq 5$, estimate the inelasticity for fireball production, and, as can be seen from fig. 6.1b find little correlation. We will assume here that n_π and k_π are independent which means that we can write

$$\sigma(E_o, n_\pi, k_\pi)\, dk_\pi = \sigma(E_o, n) f(k_\pi)\, dk_\pi$$

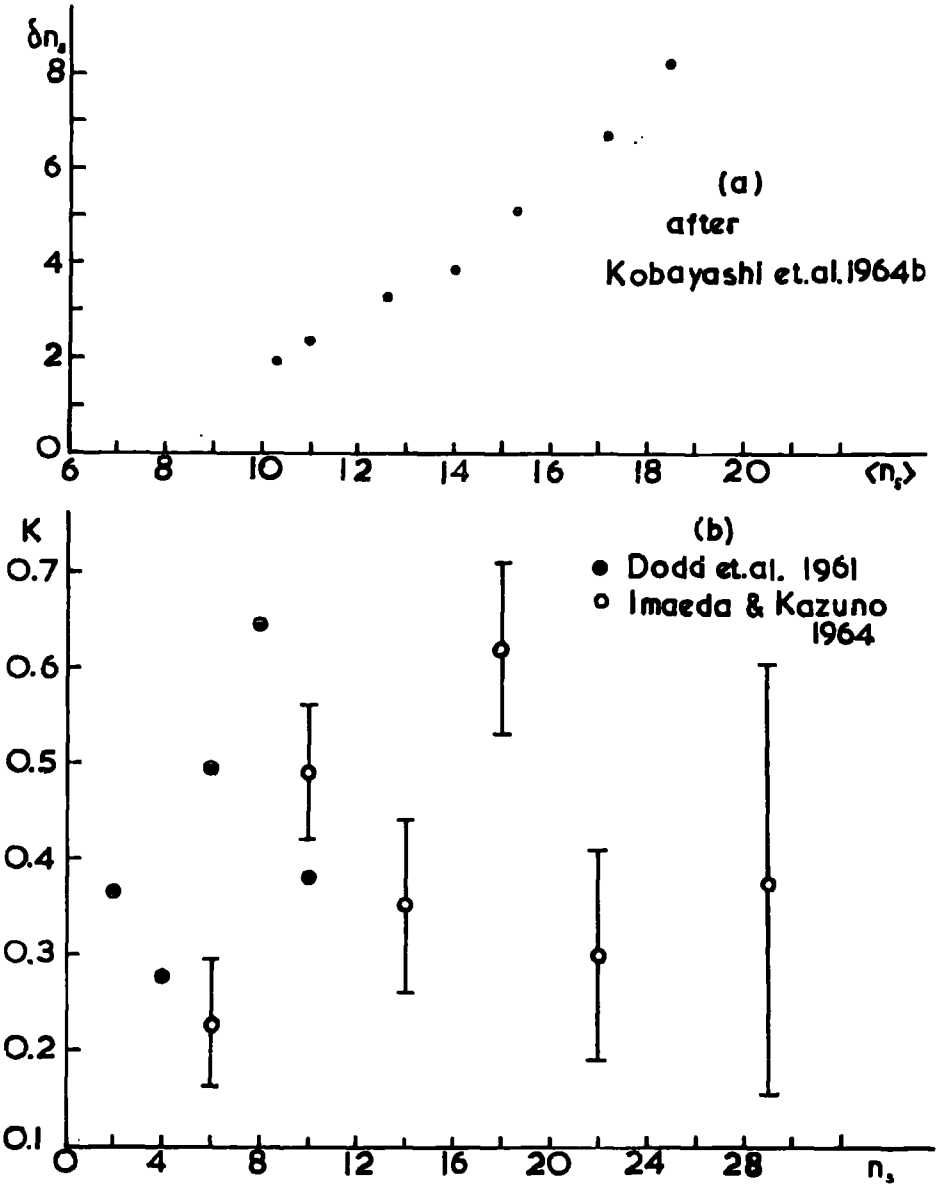

Fig.6.1 (a) The variance in n_s vs $\langle n_s \rangle$ for ICEF jets.
(b) Correlation between inelasticity and multiplicity.

From some early work on multiplicities in jets, Hayman (1962), derived a multiplicity distribution of the form

$$\sigma_n(E_o) = \tfrac{1}{2}\left(n \ln j\right)^{-1} \text{for } \frac{2\langle n\rangle \ln j}{j^2-1} \leq n \leq \frac{2j^2\langle n\rangle \ln j}{j^2-1}$$

where j, $(=j(E_o))$, is a parameter indicating the degree of fluctuations. With $\langle n\rangle = BE_o^{\alpha}$ and j = 2. Hayman indeed showed that a significant effect on the charge ratio resulted. This distribution is not, however, the best fit to the experimental data.

It is instructive to see the effect of a Poissonian distribution in multiplicity on the charge ratio. Many theoretical models lead to such a multiplicity distribution e.g. the multiperipheral model Koba and Krzywicki (1963), a quasi statistical model due to Krzywicki (1963) and the field theory model of Krisch (1964), etc.

$$\sigma(E_o, n) = \frac{\langle n\rangle^n}{n!} e^{-\langle n\rangle}$$

The simple forms for the other functions have been assumed i.e. constant k_π and equal energy among the pions in the forward cone.

$$\frac{n}{2} E_\pi = k_\pi E_o$$

- when a multiplicity of one occurs it is assumed that it goes forward half of the time. With $N(E_o)dE_o = E_o^{-\gamma}dE_o$ and $\langle n\rangle = BE_o^{\alpha}$ the calculation has been performed for two cases (i) where a unique energy of a muon from pion decay is assumed, $E_\mu = rE_\pi$, whence

$$\delta_1(E_\mu) = \frac{3}{4}\,\frac{2^{\alpha-\gamma+1} B q^{\alpha-\gamma} e^{-B(2q)^{\alpha}} \varphi(1) + \sum_{n=2}^{\infty} B^n q^{n\alpha-\gamma} n^{n\alpha-\gamma} e^{-B(nq)^{\alpha}} \varphi(n)/(n-1)!}{2^{\alpha-\gamma+1} B q^{\alpha-\gamma} e^{-B(2q)^{\alpha}} + \sum_{n=2}^{\infty} B^n q^{n\alpha-\gamma} n^{n\alpha-\gamma+1} e^{-B(nq)^{\alpha}}/(n-1)!}$$

where $q = E_\mu/2rk_\pi$;

and (ii) where the spectrum of muons from pion decay is included. In this case

$$n_\mu(E_\mu, E_\pi)dE_\mu = \frac{m_\pi dE_\mu}{2p_\pi p^*_\mu} \approx \frac{dE_\mu}{(1-r^2)E_\pi} \quad ;$$

and

$$\delta_1(E_\mu) = \frac{3}{4} \frac{2^{\alpha-\gamma+1} B\varphi(1) I(1) + \sum_{n=2}^{\infty} B^n n^{n\alpha-\gamma} \varphi(n) I(n)/(n-1)!}{2^{\alpha-\gamma+1} B I(1) + \sum_{n=2}^{\infty} B^n n^{n\alpha-\gamma+1} I(n)/(n-1)!}$$

where

$$I(1) = \int_{E_\mu/2k_\pi}^{E_\mu/2r^2k_\pi} x^{\alpha-\gamma-1} e^{-B(2x)^\alpha} dx \,, \qquad I(n) = \int_{E_\mu/2k_\pi}^{E_\mu/2r^2k_\pi} x^{n\alpha-\gamma-1} e^{-B(nx)^\alpha} dx \,, \quad n>1$$

This latter expression for $\delta_1(E_\mu)$ turns out to be not more than 1% greater than the expression ignoring $\pi\mu$ decay spread, showing that this feature has no effect on the charge excess and it will henceforth be ignored. For values of $\gamma = 2.58$, $B = 2.7$, $\alpha = 0.25$, $k_\pi = 0.31$ the resulting $R(E_\mu)$ on applying the dilution factor is shown in fig. 6.2 where it is seen that the fluctuations only have an effect at the energies where cases of $n_{\pi^\pm} = 1,2$ arise, because only for these cases is $\Delta(n_\pi)$ appreciably different from unity. If k_π is positively correlated with n_π the above expressions become independant of γ, and the charge excess resulting is negligibly different from the case where no fluctuations in n_π were included; this is as expected since low multiplicity pions also have a lower energy than if produced in the k_π = constant case.

Using the above methods the sensitivity of $\delta_1(E_\mu)$ to the parameters γ, α and $\langle k_\pi \rangle$, denoted generally by t, has been investigated and in fig. 6.3 there is plotted $\delta/\langle\delta\rangle$, where $\langle\delta\rangle$ is the value of $\delta_1(E_\mu)$ at E_μ = 20 GeV

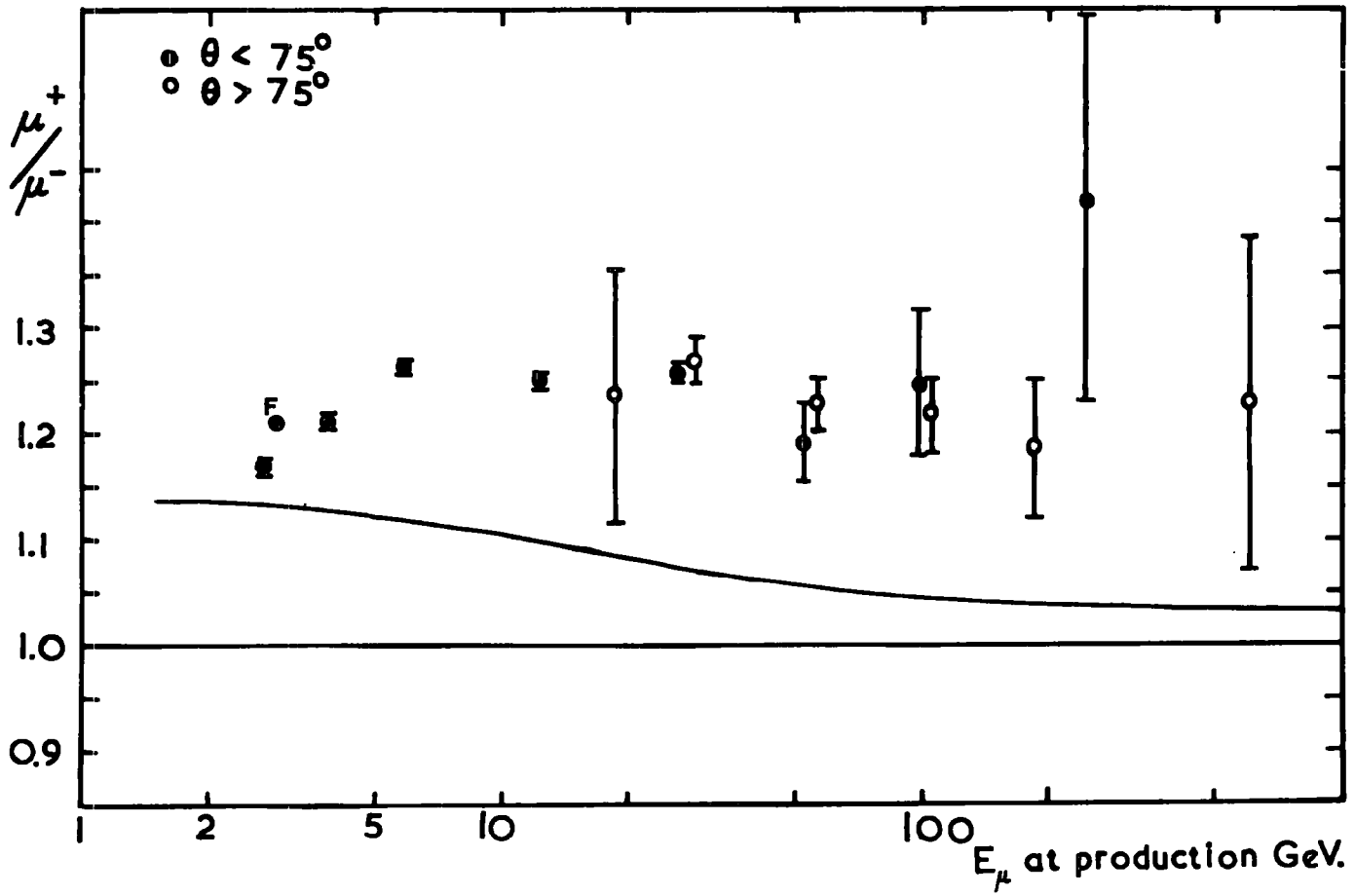

Fig.6.2 The computed charge ratio from pionisation with Poissonian fluctations in multiplicity.

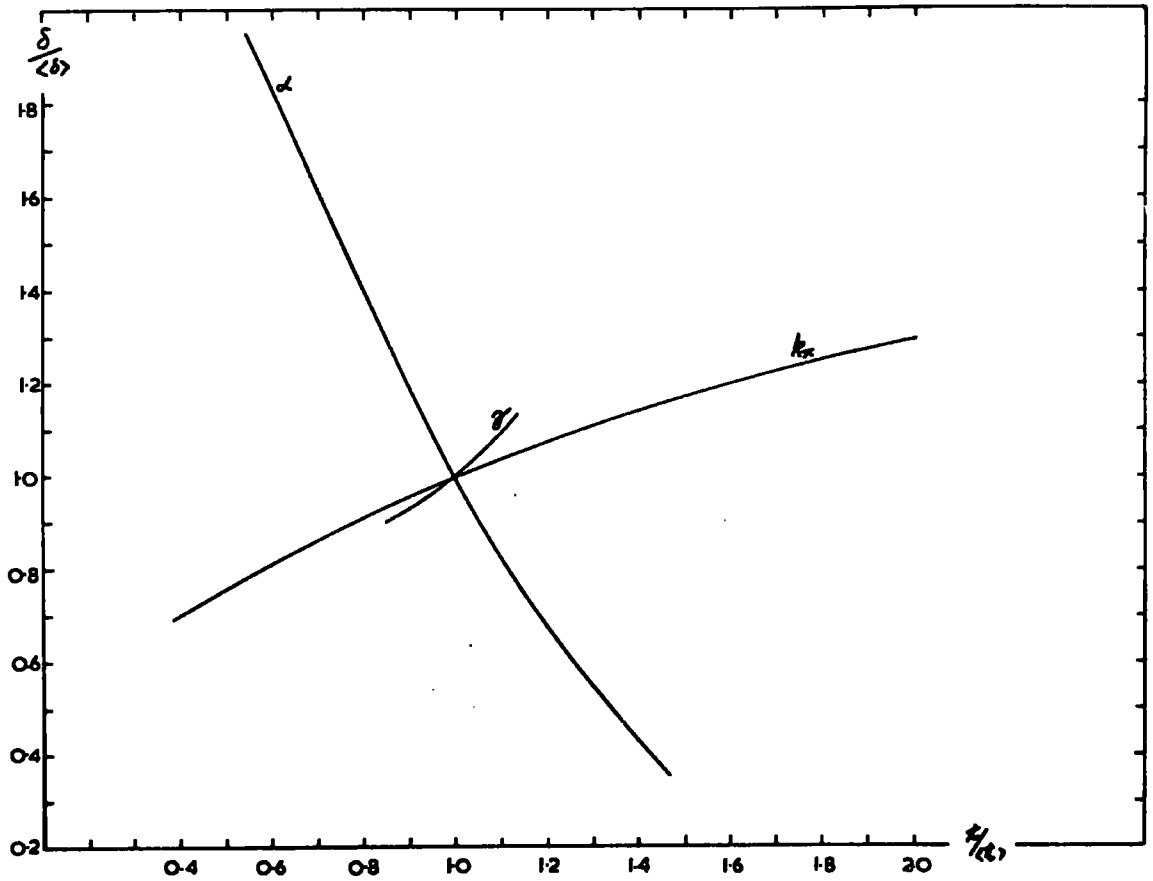

Fig. 6.3 The sensitivity of the computed excess to the parameters α, γ, and k_π.

for the values of the parameters as given above. In varying each of the parameters the remaining two have been held at the values given above. The variation with α is not very meaningful far away from the mean since B was held constant, = 2.7 throughout. Although, as we shall see shortly, despite the theories, the Poisson distribution is not a good fit to the experimentally observed multiplicity distribution at high energies, the above analysis indicates the effects of fluctuations.

A multiplicity distribution of the form

$$\sigma_n(E_o) = \frac{(1-p)^2}{p} np^n \quad , \quad p = \frac{<n>-1}{<n>+1}$$

has been considered by Bowler (1963, private communication) which is a good fit to the data at high energies, but not at low and intermediate energies.

The available data on n_π, or more usually on n_s, the number of charged shower particles in an event, is scarce, and difficult to evaluate because of undoubted sources of bias occuring in its compilation. However the existence of fluctuations, even at accelerator energies, to a degree greater than could be accounted for on purely statistical grounds is indicated. As has already been noted, Fowler and Perkins (1964), Kobayashi et. al. (1964b) the width of the distribution increases with primary energy, and it has been pointed out by the latter authors that this widening distribution in n_s can be related to the observed distribution in momentum transfers in the interactions, which is determined by the dynamics of the production mechanism, the diffuse distribution suggesting a superposition of several production mechanisms. The useful available data on n_s distributions are as follows, Dodd et. al. (1961) p p collisions at 24 GeV

in a hydrogen bubble chamber, Subramanian (1962), cosmic ray nucleon interactions at ~ 30 GeV in a cloud chamber and total absorption spectrometer, cosmic ray nucleon-light nucleus collisions at $E_o \approx 300$ GeV by Dobrotin (1963, private communication) in a cloud chamber and ionisation calorimeter, and jets with $N_h \leq 5$ in emulsions $E_o \sim 10^4$ GeV, Fowler and Perkins (1964) and ICEF collaboration (1964), $E_o \approx 1.5\ 10^4$ GeV. In the ionisation calorimeter work there is possibly a bias against low n_s events, while in the jets a bias towards large n_{π^o}, and thus presumably towards low n_s, is possible though this will not be serious for volume scanning. A more important effect for the distribution from jets is the selection criterion on N_h, the number of black prongs in the event. In fig. 6.4a there are shown the observed distributions in n_s for the different selection criteria $N_h < 2$, $N_h = 2\text{-}7$ and $N_h > 7$ for 28 GeV nucleon collisions in emulsion. In fig. 6.4b the effect of N_h selection on n_s for nucleon jets at ≈ 250 GeV, Lohrmann et. al. (1961), and Barkow et. al. (1961) at $E_o \approx 3.5$ TeV is shown. Over this very wide energy region we see that any correlation between n_s and N_h is very weak for $N_h \leq 5$, and this is in sharp contrast with the rapid rise in n_s with increasing N_h for $N_h > 5$. One also sees that, if as severe a criterion as $N_h = 0$ was demanded for nucleon-nucleon collisions, the fluctuations in n_s would still be appreciable. From this we see that it is not unreasonable to assume that $N_h \leq 5$ events correspond to nucleon nucleon or nucleon light nucleus collisions. To derive the distribution of created charged particles from the n_s data the fast nucleons must be excluded. This problem has been considered by Malhotra (1963), who deduces that n_p rises from 0.6 at low energies to ~ 1 at $E_o \gtrsim 50$ GeV, so in the present work the distribution in $(n_s\text{-}1)$ will be

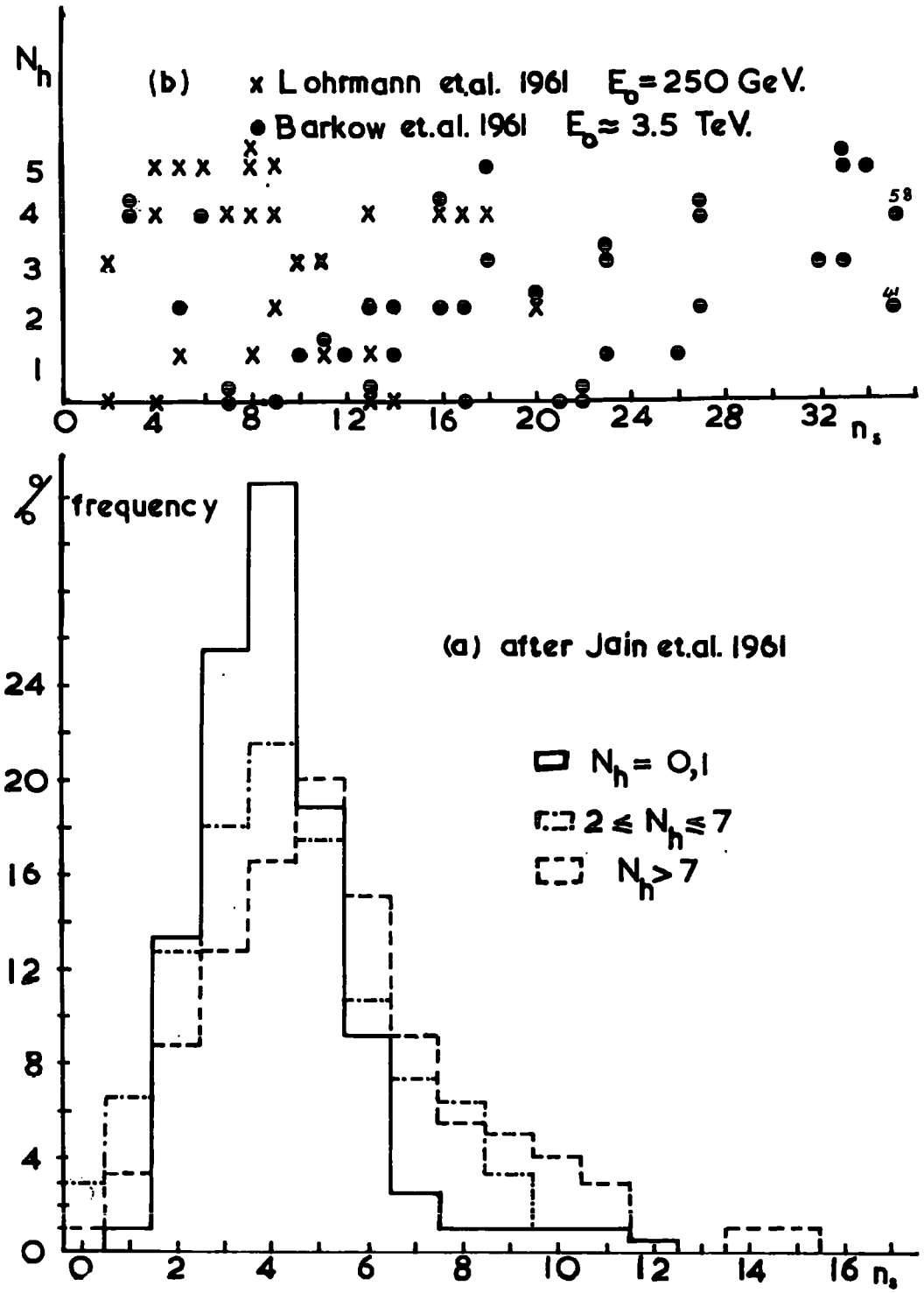

Fig. 6.4 Correlation between N_h and n_s in jets.

assumed to be the distribution of created charged particles, which will be assumed to be pions, this latter assumption is reasonable at low multiplicities where the importance lies.

In fig. 6.5 a-e there are shown the observed distributions in (n_s-1), where the varying shape of the distribution with increasing energy is evident. Several attempts were made to fit curves to the data, and those in the figures represent the Polya distribution

$$\sigma(E_o,n) = \frac{\langle n\rangle^n}{n!}\left\{1+\zeta\langle n\rangle\right\}^{-(n+1/\zeta)}\prod_{j=1}^{n-1}(1+j\zeta)\cdots\cdots \quad (6.1)$$

where $n = \frac{3}{2}(n_s-1)$ and $\langle n\rangle = 2.7E_o^{\frac{1}{4}}$. ζ is a parameter indicating the extent of the fluctuations, and has been taken as a function of E_o.

$\zeta \equiv \zeta(E_o) = 0.4\ (1 - e^{\frac{-E_o}{5.55\ 10^3}})$ with E_o in GeV. $\zeta = 0$ corresponds to the Poisson distribution and $\zeta = 1$ to Furrys distribution. It can be seen that such a distribution, taken as the most convenient overall fit to the data, underestimates the frequency of the important cases $n_{\pi^\pm} = 1,2$. The charge excess will be calculated from this distribution and the very low multiplicity events considered later.

6.2 Fluctuations in inelasticity

The inelasticity for pion production $k_\pi = \sum E_\pi/E_o$ is characterised by wide fluctuations over the whole available range. Since the mean inelasticity seems independent of primary energy the failure to take account of the finite $k_{total} - k_\pi$ difference, ≈ 0.12, Brooke et. al. (1964a), may be taken care of by altering the absolute intensity of the primary nucleon flux, on which the charge excess does not depend. Among investigations of the inelasticity parameter we may cite the work of Dodd et. al. (1961),

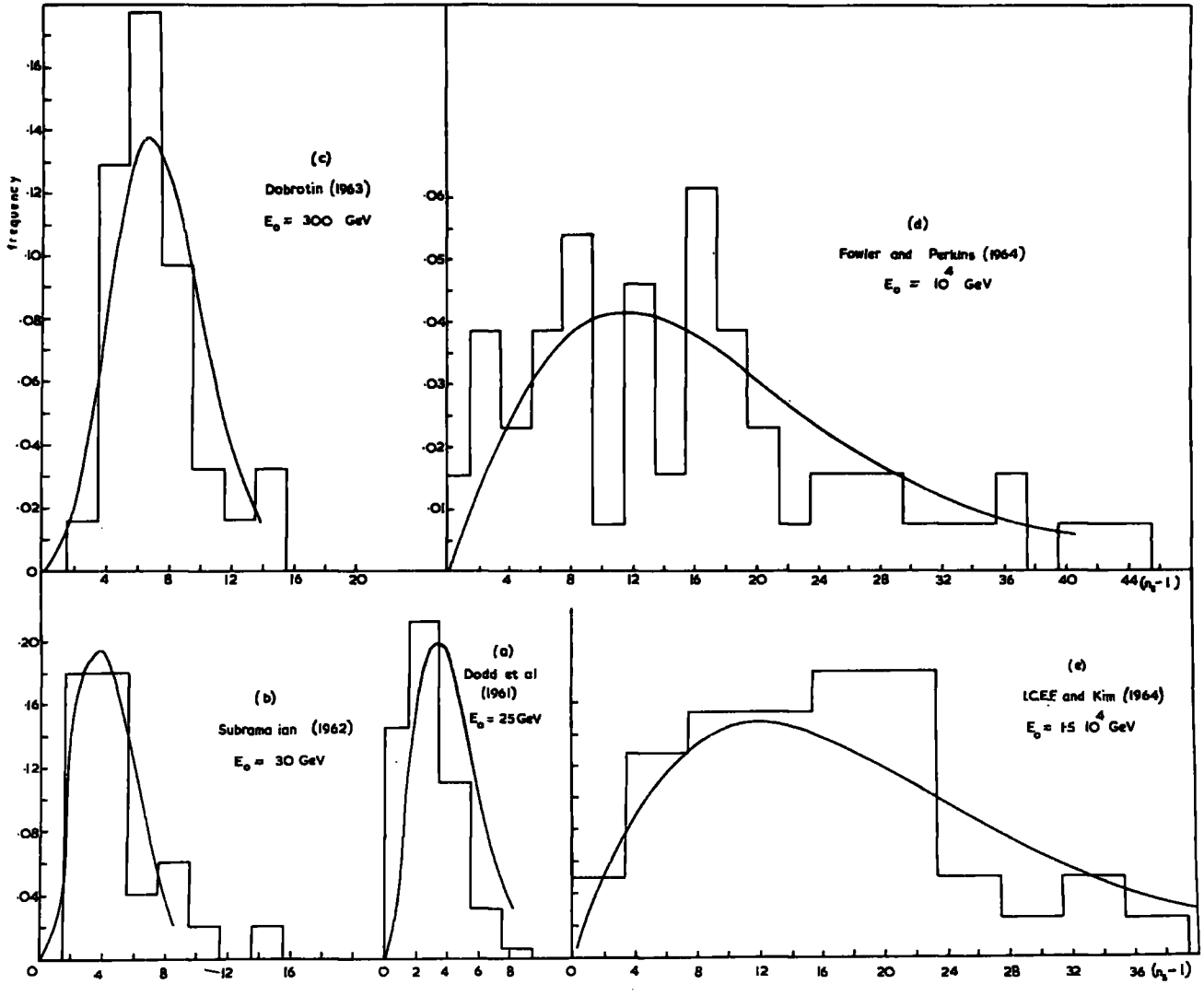

Fig. 6.3 The observed distributions in (n_s-1), solid curve=Polya distribution.

who looked at the elasticity of backward moving protons in the c.m.s. in p p collisions at 24 GeV. Compared with other work their distribution shows a dearth of low elasticity events, this bias against high inelasticity probably arising from their selection criteria. Allowing for a tail in their distribution it is well fitted by the expression due to Brooke et. al., (1964a), viz

$$f(k_\pi)dk_\pi = -(1+\beta)^2 (1 - k_\pi)^\beta \ln (1 - k_\pi)dk_\pi \qquad \ldots\ldots (6.2)$$

$$\text{where } \langle k_\pi \rangle = 1 - \left(\frac{\beta+1}{\beta+2}\right)^2$$

This expression is also a good fit to the data of Guseva et. al., (1961) for the inelasticity distribution in nucleon light nucleus collisions at $E_o \approx 300$ GeV. At higher energies, where up until now the measurements are confined to emulsions, the energy determination is often suspect with a resulting uncertainty in k. This may account for the fact that the distribution in k_t, (in the c.m.s.), in high energy jets, ($E_o \approx 10$ TeV, $N_h \leq 5$), derived by Imaeda and Kazuno, (1964), is rather more flat than in the cases noted above, though the mean value, $\langle k_t \rangle = 0.42$, is in good agreement. Some work has been done on the fraction of energy going into the π^o component and the results of Lal et. al., (1965), at $E_o = 20$-100 GeV are in good agreement with $k_\pi = 3k_{\pi^o}$ and these authors give a distribution which is similar to the one above, (6.2), only more cumbersome. Among other interesting features of the inelasticity parameter there are the reports on two different experiments, Babayan et. al. (1963a,b) which indicate that at $E_o \sim 10^{12} - 10^{13}$ eV values of k_{π^o} greater than 0.65 occur with a frequency of 10-15%. Independent confirmation of such behaviour is desirable, and the results will be mentioned later.

6.3 Pion energy spectrum

Experimental data on the energy spectrum of pions in individual interactions is almost non-existent, but the expression due to Cocconi et. al. (1961), henceforth to be known is the C.K.P. spectrum, seems a reasonable fit to the data averaged over all interactions at a given primary energy, viz.

$$\langle N(E_\pi)\rangle\, dE_\pi = \frac{\langle n\rangle}{2T}\, e^{-E_\pi/T}\, dE_\pi$$

$$T = 2k_\pi E_0/\langle n\rangle \approx 2k_\pi \frac{E_0^{1+\alpha}}{B}$$

This spectrum is a consequence of folding in the distribution in n_π and k_π, and an energy spectrum in an individual interaction characterised by n_π and k_π, i.e.

$$\langle N(E_\pi)\rangle dE_\pi = dE_\pi \sum_{n_\pi} \int_0^1 \sigma(E_0, n_\pi) f(k_\pi) N_\pi(E_\pi, E_0, k_\pi)\, dk_\pi \qquad \ldots\ldots (6.3)$$

Taking for $\sigma(E_0,n)$ the Poisson distribution and for the inelasticity distribution the expression (6.2) we will look at the consequences of taking various energy spectra of pions in individual interactions.

(a) equal energy distribution among pions in the forward cone, i.e.

$$N(E_\pi) = \frac{n}{2}\, \delta\left(E_\pi - \frac{2k_\pi E_0}{n}\right)$$

which gives, on insertion into (6.3),

$$\langle N(E_\pi)\rangle\, dE_\pi = \sum_{n=1}^{\infty} \sigma(E_0, n)\, \frac{n}{2}\, f\left(\frac{nE_\pi}{2E_0}\right) \frac{n}{2E_0}\, dE_\pi$$

$$= -\frac{(1+\beta)^2}{4E_0}\, dE_\pi \sum_{n=1}^{\infty} \frac{n^2\langle n\rangle^n}{n!} e^{-\langle n\rangle} \left\{1 - \frac{nE_\pi}{2E_0}\right\}^\beta \ln\left(1 - \frac{nE_\pi}{2E_0}\right)$$

This is compared with the C.K.P. spectrum in fig. 6.6 curves (a), for $\langle k_\pi \rangle = 0.31$ ($\beta = 4$), $\langle n \rangle = 2.7\, E_o^{\frac{1}{4}}$, at $E_o = 30$ GeV and $E_o = 10^3$ GeV. It can be seen that it does not agree with the C.K.P. distribution, seriously underestimating the frequency of large pion energies.

(b) taking the C.K.P. energy spectrum in each interaction

$$N(E_\pi)\,dE_\pi = \frac{n^2}{4 k_\pi E_o}\, e^{-\frac{nE_\pi}{2k_\pi E_o}}\, dE_\pi$$

then

$$\langle N(E_\pi)\rangle\, dE_\pi = -\frac{(1+\beta)^2}{4E_o}\, dE_\pi \sum_{n=1}^{\infty} \frac{n\langle n\rangle^n e^{-\langle n\rangle}}{(n-1)!}\, F(E_o, E_\pi, n)$$

where

$$F(E_o, E_\pi, n) = \int_0^1 (1-x)^\beta \ln(1-x)\, e^{-\frac{nE_\pi}{2E_o x}}\, dx/x$$

This has also been compared with the C.K.P. expression for $E_o = 30$ GeV in fig. 6.6, curve (b), where it is seen to overestimate the frequency of high energy pions.

We thus seek an energy spectrum in each interaction which, when combined with the fluctuations in multiplicity and inelasticity will yield the C.K.P. spectrum as an average over all interactions at a given primary energy. If we try a spectrum of the form

$$N(E_\pi)dE_\pi = C\,\frac{n}{2}\, E_\pi\, (k_\pi E_o - E_\pi)^\nu$$

we can determine C and ν from the number and energy conservation conditions, viz.

$$\int_0^{k_\pi E_o} N(E_\pi)\, dE_\pi = \frac{n}{2}\,, \qquad \int_0^{k_\pi E_o} E_\pi\, N(E_\pi)\, dE_\pi = k_\pi E_o$$

From these it follows that

$$\nu = n-3 \quad \text{and} \quad C = \frac{(n-1)(n-2)}{(k_\pi E_o)^{n-1}}$$

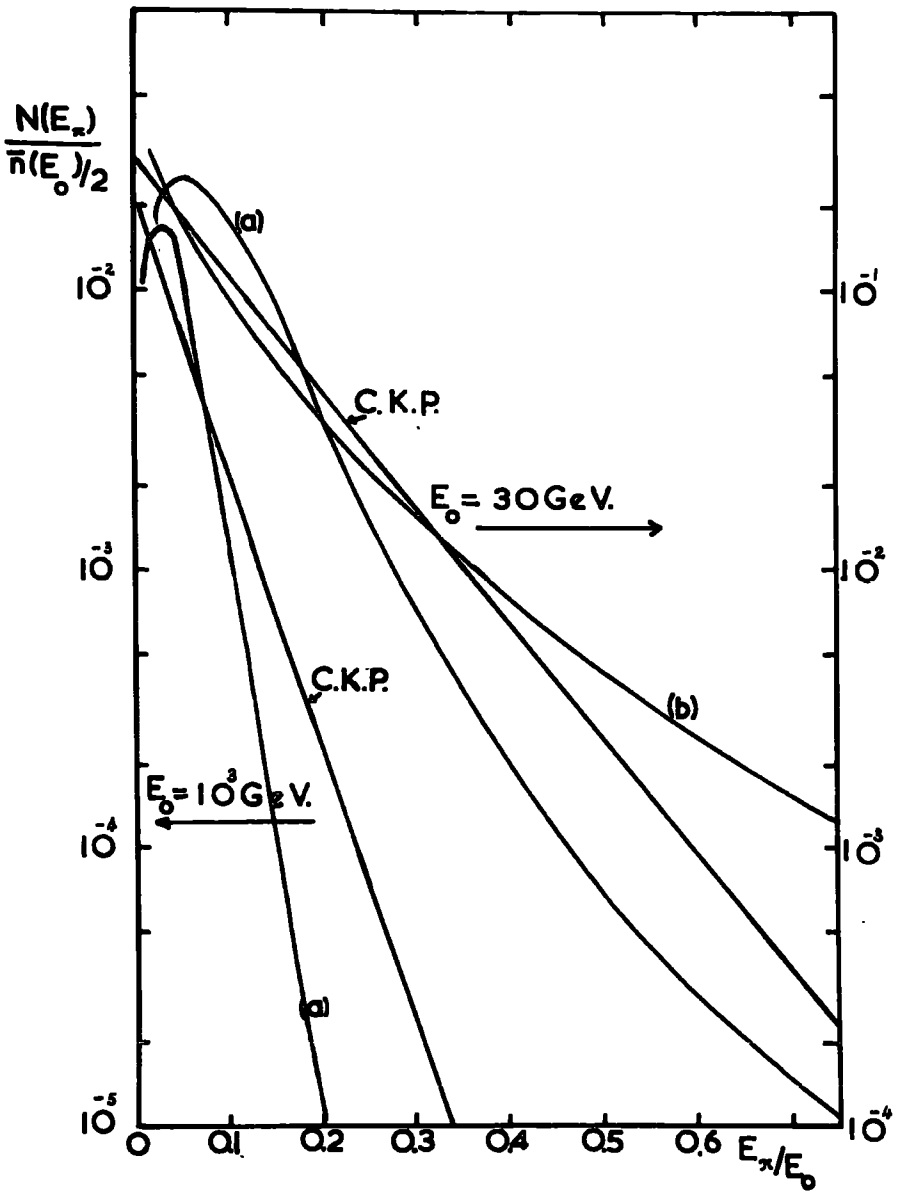

Fig. 6.6 Comparison of various pion energy spectra with the C.K.P. expression.

This will only hold for $n \geq 3$. For $n = 1$ we will assume that in half the cases the pion goes forward in the c.m.s., and for $n = 2$, that one pion carries all the available energy. Then we can write

$$\begin{aligned} n = 1 \qquad & N(E_\pi) = \delta(E_\pi - k_\pi E_o) \text{ with frequency } \frac{\sigma(E_o,1)}{2} \\ n = 2 \qquad & N(E_\pi) = \delta(E_\pi - k_\pi E_o) \\ n = 3 \qquad & N(E_\pi)dE_\pi = \frac{n(n-1)(n-2)}{2(k_\pi E_o)^{n-1}} E_\pi (k_\pi E_o - E_\pi)^{n-3} dE_\pi \end{aligned} \qquad \ldots\ldots (6.4)$$

Then on folding in the multiplicity and inelasticity spectra we get

$$\langle N(E_\pi)\rangle dE_\pi = -\frac{(1+\beta)^2}{4E_o} dE_\pi \left\{ 2\langle n\rangle(\langle n\rangle+1)e^{-\langle n\rangle}\left(1-\frac{E_\pi}{E_o}\right)^\beta \ln\left(1-\frac{E_\pi}{E_o}\right) + 2\frac{E_\pi}{E_o}\sum_{n=3}^{\infty}\frac{\langle n\rangle^n e^{-\langle n\rangle}}{(n-3)!} F(E_o, E_\pi, n)\right\}$$

where

$$F(E_o, E_\pi, n) = \int_{E_\pi/E_o}^{1} (1-x)^\beta \ln(1-x)\left(x - \frac{E_\pi}{E_o}\right)^{n-3} dx/x^{n-1}$$

This expression has been compared with the C.K.P. spectrum at $E_o = 30$ and 10^3 GeV in fig. 6.7, curves (a). The agreement at 30 GeV is quite good, this expression being slightly less than the C.K.P. expression, which is not serious since the C.K.P. spectrum appears to overestimate slightly the frequency of high energy pions. At $E_o = 10^3$ GeV the agreement is almost exact which must be regarded as rather fortuitous considering the arbitrary origin of the expression adopted.

6.4 The charge ratio from pionisation

Adopting this energy spectrum, (6.4), we will combine it with our best estimate of the multiplicity distribution (6.1), and the inelasticity distribution (6.2), to derive the best estimate of the charge excess from this simple pionisation model. We have, ignoring $\pi\mu$ decay spread

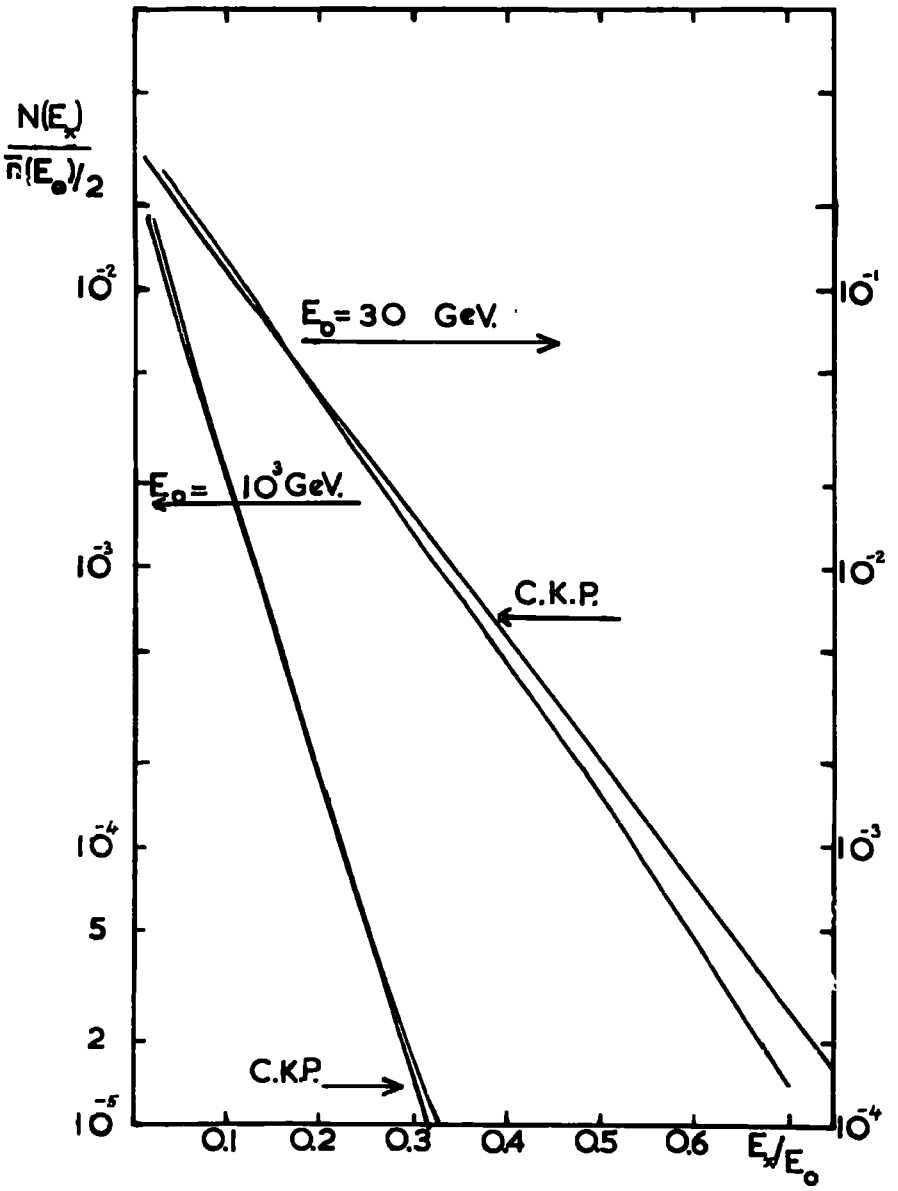

Fig. 6.7 A comparison of the adopted pion energy spectrum with the C.K.P. expression.

$$\delta_1(E_\mu) = -\frac{3}{2}\frac{\sum_{n=1}^{\infty}\int_{E_\mu/\gamma}^{\infty}\int_{E_\mu/\gamma E_0}^{1} N(E_0)\,\sigma(E_0,n)\,f(k_\pi)\,N\left(\frac{E_\mu}{\gamma},E_0,n\right)\Delta(n)\,dk_\pi\,dE_0}{\sum_{n=1}^{\infty}\int\int N(E_0)\,\sigma(E_0,n)\,f(k_\pi)\,N\left(\frac{E_\mu}{\gamma},E_0,n\right)dk_\pi\,dE_0}$$

which reduces to

$$\delta_1(E_\mu) = \frac{3}{4}\frac{B\left(\frac{E_\mu}{\gamma}\right)^{\alpha-\gamma}\varphi(1)I_1(E_\mu) + B^2\left(\frac{E_\mu}{\gamma}\right)^{2\alpha-\gamma}\frac{\varphi(2)}{2}I_2(E_\mu) + \frac{E_\mu}{\gamma}\sum_{n=3}^{\infty}\frac{B^n}{(n-3)!}\frac{\varphi(n)}{n}I_3(E_\mu,n)}{B\left(\frac{E_\mu}{\gamma}\right)^{\alpha-\gamma}I_1(E_\mu) + B^2\left(\frac{E_\mu}{\gamma}\right)^{2\alpha-\gamma}I_2(E_\mu) + \frac{E_\mu}{\gamma}\sum_{n=3}^{\infty}\frac{B^n}{(n-3)!}I_3(E_\mu,n)}$$

where

$$I_1(E_\mu) = \int_0^1 x^{\gamma-\alpha-1}\left[1+\zeta B\left(\frac{E_\mu}{\gamma x}\right)^{\alpha}\right]^{-(1+1/\zeta)}(1-x)^{\beta}\ln(1-x)\,dx, \quad \zeta = g\left(1-e^{-\frac{hE_\mu}{\gamma x}}\right)$$

$$I_2(E_\mu) = \int_0^1 x^{\gamma-2\alpha-1}\left[1+\zeta B\left(\frac{E_\mu}{\gamma x}\right)^{\alpha}\right]^{-(2+1/\zeta)}(1+\zeta)(1-x)^{\beta}\ln(1-x)\,dx \quad \zeta = g\left(1-e^{-\frac{hE_\mu}{\gamma x}}\right)$$

$$I_3(E_\mu,n) = \int_{E_\mu/\gamma}^{\infty}\int_{E_\mu/\gamma E_0}^{1}\left\{\prod_{i=1}^{n-1}(1+j\zeta(E_0))\right\}E_0^{n\alpha-\gamma-2}\left(1+\zeta B E_0^{\alpha}\right)^{-(n+1/\zeta)}(1-k)^{\beta}\ln(1-k)\left(k-\frac{E_\pi}{E_0}\right)^{n-3}\frac{dk}{k^{n-1}}\,dE_0, \quad \zeta = g\left(1-e^{-hE_0}\right)$$

With $\alpha = 0.25$, $\beta = 4$, ($\langle k_\pi \rangle = 0.31$), $\gamma = 2.58$, $B = 2.7$, $g = 0.4$, $h = 1/5.55\ 10^3$ this has been computed, the dilution factor applied, and converted into muon charge ratio, the final result being plotted in fig. 6.8, curve (a) The denominator in (6.5) above represents, to within a constant factor, the pion production spectrum. The above calculation was also performed for the simple constant E_π and constant k_π case, and it was found that the inclusion of the inelasticity and energy spectra has very little effect on the computed excess, and this just reflects the insensitivity to $\pi\mu$ decay spread already noted, and the insensitivity to angular distribution noted by Yeivin (1956). This is due to the fact that the charge excess is uniformly distributed over the produced pions and the energy spectrum enters in the same way in both the numerator and denominator.

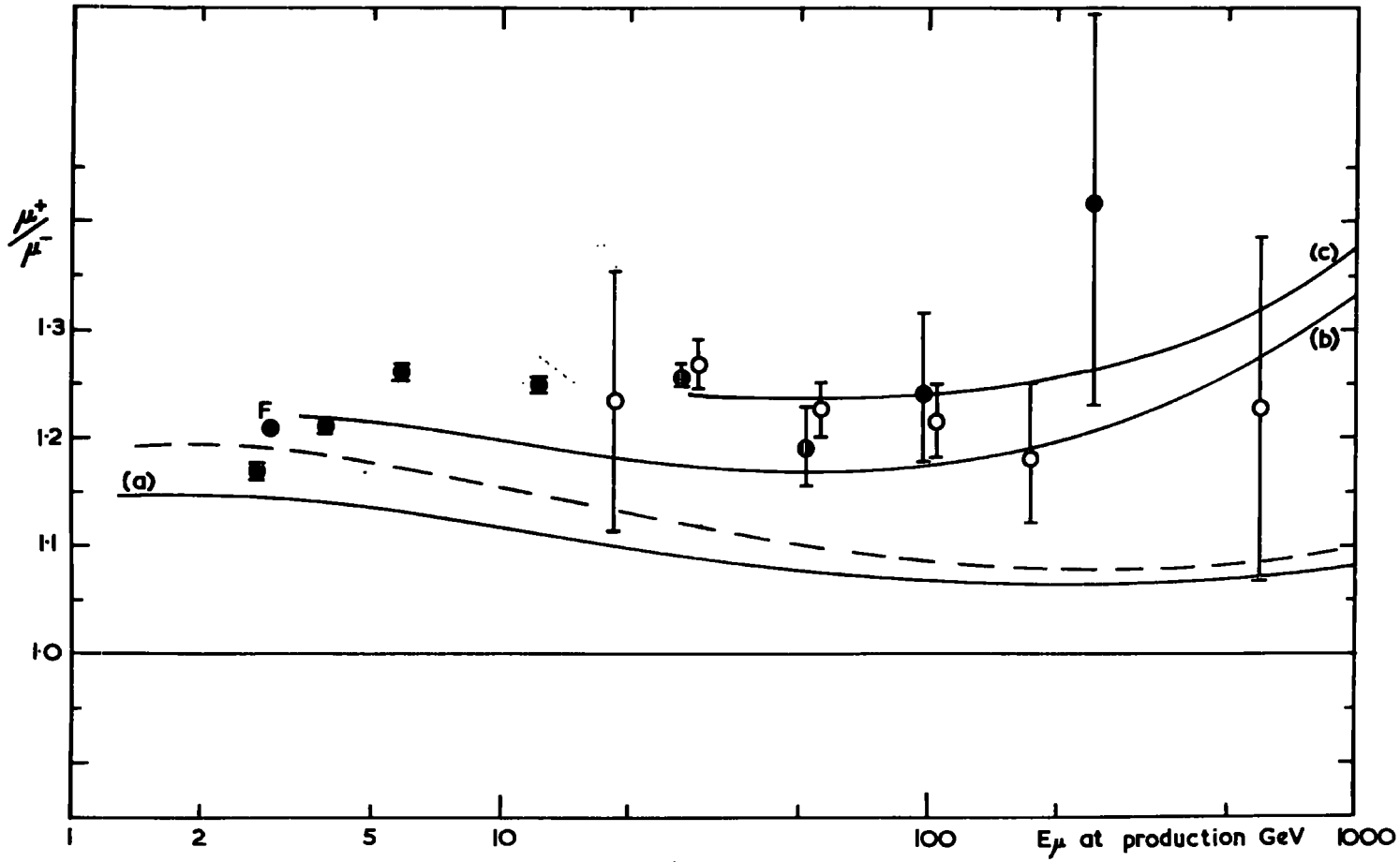

Fig.6.8 The calculated charge ratio; (a)-pion:sation,dashed curve:upper limit;(b) as (a) with $K/\pi = 0.2, K^+/K^- = 4$; (c) as (b) with $K/\pi = 0.5$.

As an upper limit on the computed ratio we can take the most favourable values of the parameters consistent with experimental data, $\langle k_\pi \rangle \to 0.41$, $\gamma \to 2.8$ $\alpha \to 0.24$. We have from fig. 6.3 at $E_\mu \approx 20$ GeV

$$\frac{\partial \delta}{\partial \alpha} \approx -2\frac{\langle \delta \rangle}{\langle \alpha \rangle}, \quad \frac{\partial \delta}{\partial \gamma} \approx \frac{\langle \delta \rangle}{\langle \gamma \rangle}, \quad \frac{\partial \delta}{\partial k_\pi} \approx 0.4\frac{\langle \delta \rangle}{\langle k_\pi \rangle}$$

and these will presumably not be extremely energy dependent. In this way with $d\alpha = -0.01$, $d\gamma = 0.22$, $dk_\pi = 0.1$ the upper limit to the muon charge ratio from the present considerations has been evaluated and is shown as the dashed curve in fig. 6.8. If the nucleon nucleon cross-section increases with E_0 then a further increase in this computed ratio will occur, but even allowing for this the insufficiency of the assumptions considered so far is evident.

An extreme fluctuation model, based on the results of Babayan et. al. (1963), already mentioned, has been developed by Grigorov and Shestoperov (1963, 1964), and these authors obtain a constant charge ratio up to energies $\sim 10^3$ GeV, but the experimental foundations for the model are as yet too uncertain.

6.5 The inclusion of kaons

It is necessary next to consider the production of particles other than pions in these collisions, and we will here treat the case of kaon production, the evidence for such has already been reviewed in the last chapter. The effect of kaons may be appreciable if their charge excess at production, is different from that of pions, and while they are less efficient in producing muons at a given energy those modes which give rise to muons directly will play a very significant role at high energies

because of pion interaction. From a recent summary by Nikolic (1965) it appears that the K^+-nucleon and K^--nucleon cross-sections are tending to equality at high energies.

We will consider the effect of kaon production on the charge excess under the following assumptions (i) the ratio of all kaons to all pions at a given energy at production is independent of energy i.e. the energy spectra of kaons and pions are assumed to have the same shape; we will write $\xi = (K/\pi)_{all}$ at production. (ii) The production spectra $F_{K^+}(E_K)$ and $F_{K^0}(E_K)$ are identical as are the spectra $F_{K^-}(E_K)$ and $F_{\bar{K}_0}(E_K)$, and $\nu = K^+/K^-$ is independent of energy and the nature of the incident nucleon.

Kaons can give rise to muons by virtue of several decay modes, many of which are mediated by a pion. For ease of calculation only the three most important kaon modes will be considered, the $K_{\mu 2}$, $K_{\pi 2}$ and K_1^0 modes

$$K^{\pm}_{\mu 2} \rightarrow \mu^{\pm} + \nu$$

$$K^{\pm}_{\pi 2} \rightarrow \pi^{\pm} + \pi^0$$

$$K^0_1 \rightarrow \pi^+ + \pi^-$$

We will write

$$S_\mu = \frac{M_{K_{\mu 2}}(E_\mu)}{M_\pi(E_\mu)} \quad , \quad S_\pi = \frac{M_{K_{\pi 2}}(E_\mu)}{M_\pi(E_\mu)} \quad , \quad S_0 = \frac{M_{K_1^0}(E_\mu)}{M_\pi(E_\mu)}$$

where $M_\pi(E_\mu)dE_\mu$ is the production spectrum of muons from pion decay, $M_{K_{\mu 2}}(E_\mu)dE_\mu$ the production spectrum of muons from kaons decaying in the $K_{\mu 2}$ mode for $\xi = 1$, etc. In general $S = S(E_\mu, \theta)$. Noting that for the K_1^0 mode equal numbers of π^+ and π^- are produced we can write at production, a θ dependance implied,

$$\mu^{+}(E_\mu) = (S_\mu + S_\pi)\frac{\xi}{1+\xi}\frac{\nu}{1+\nu} + S_0\frac{\xi}{1+\xi}\frac{1}{2} + \frac{1}{1+\xi}\frac{1+\delta_\pi(E_\mu)}{2}$$

$$\mu^{-}(E_\mu) = (S_\mu + S_\pi)\frac{\xi}{1+\xi}\frac{1}{1+\nu} + S_0\frac{\xi}{1+\xi}\frac{1}{2} + \frac{1}{1+\xi}\frac{1-\delta_\pi(E_\mu)}{2}$$

where it is assumed that the muons from pionisation have the same charge excess as has been calculated in §6.4 above, $\delta_\pi(E_\mu)$ previously being written simply as $\delta(E_\mu)$, $\delta_\pi(E_\mu) = D(E_\mu, \theta)\,\delta_i(E_\mu)$; as stated above ξ and ν are being assumed independent of the energy of the incident nucleon and of kaon energy.

The functions S_μ, S_π and S_0 will now be calculated. For simplicity it will be assumed that the production spectra of both pions and kaons may be written as a pure power law. Then, for $\xi = 1$

$$F_K(E_K)dE_K = F_\pi(E_\pi)dE_\pi = E^{-\gamma}dE$$

Such a step is not fully justified since to obtain the observed muon sea-level spectrum - which follows quite well from a pion production spectrum of constant exponent - from a mixture of pions and kaons, the kaon spectrum must become progressively steeper with energy if the index of the pion spectrum is constant because of the greater decay probability of the kaon modes producing muons directly. Assuming $\Lambda_\pi \approx \Lambda_0$ we have, following Barrett et. al. (1952) and ignoring $\pi\mu$ decay spread

$$M_\pi(E_\mu) = \frac{2}{3}\frac{(E_\mu/r)^{-\gamma}}{r}\frac{1}{1+\frac{E_\mu}{r B_\pi(\theta)}}$$

with

$$B_\pi(\theta) = \frac{m_\pi c^2}{c\,\tau_\pi} H_\pi(\theta) = 1.827\,10^{-4} H_\pi(\theta)\,, \quad r = \frac{m_\mu}{m_\pi} = 0.76$$

For the production spectra of muons and pions from kaon decay the energy spectrum of the produced particles must be folded in with the production spectrum of kaons. For the $K_{\mu 2}$ mode

$$N(E_\mu)\,dE_\mu = \frac{dE_\mu}{E_K(1 - 1/21.58)} = 1.049\,E_K^{-1}\,dE_\mu$$

and

$$M_{K_{\mu 2}}(E_\mu)\,dE_\mu = \frac{f_{K_{\mu 2}}}{2}\,1.049\,dE_\mu \int_{E_\mu}^{21.58\,E_\mu} E_K^{-\eta}\,\frac{dE_K}{E_K}\,\frac{1}{1 + E_K/B_{K^\pm}} = 1.049\,\frac{f_{K_{\mu 2}}}{2}\,I_{K_{\mu 2}}\,dE_\mu$$

where

$$B_{K^\pm}(\theta) = \frac{m_K c^2}{c\tau_K}\,H_x(\theta) = 1.341\,10^{-3}\,H_x(\theta), \quad I_{K_{\mu 2}} = \int_{.0463}^{1} \frac{t^{\eta-1}\,dt}{1 + \frac{E_\mu}{t\,B_{K^\pm}}}$$

and $f_{K_{\mu 2}}/2$ is the branching ratio for the $K_{\mu 2}$ mode into a charged kaon. In a similar manner, allowing for the spectrum of pions from $K_{\pi 2}$ and K_1^0 decay we can write

$$M_{K_{\pi 2}}(E_\mu) = \frac{f_{K_{\pi 2}}}{2}\,1.2\,\frac{(E_\mu/r)^{-\eta}}{r}\,\frac{I_{K_{\pi 2}}}{1 + \frac{E_\mu}{r\,B_\pi(\theta)}}, \quad M_{K_1^0}(E_\mu) = \frac{f_{K_1^0}}{2}\,2.42\,\frac{(E_\mu/r)^{-\eta}}{r}\,\frac{I_{K_1^0}}{1 + \frac{E_\mu}{r\,B_\pi(\theta)}}$$

where

$$I_{K_{\pi 2}} = \int_{.087}^{.918} \frac{t^{\eta-1}\,dt}{1 + \frac{E_\mu}{r t\,B_{K^\pm}}}, \quad I_{K_1^0} = \int_{.089}^{.914} \frac{t^{\eta-1}\,dt}{1 + \frac{E_\mu}{r t\,B_{K_1^0}}}, \quad B_{K_1^0} = \frac{m_K c^2}{c\tau_{K_1^0}}\,H_x(\theta) = 1.844\,10^{-1} H_x(\theta)$$

Thus

$$S_\mu = \frac{3}{4}\,f_{K_{\mu 2}}\,\frac{1.049\,I_{K_{\mu 2}}}{r^{\eta-1}}\left(1 + \frac{E_\mu}{r\,B_\pi(\theta)}\right), \quad S_\pi = \frac{3}{4}\,f_{K_{\pi 2}}\,1.2\,I_{K_{\pi 2}}, \quad S_0 = \frac{3}{4}\,f_{K_1^0}\,2.42\,I_{K_1^0}$$

$f_{K_{\mu 2}} = 0.58$, $f_{K_{\pi 2}} = 0.26$, $f_{K_1^0} = 0.35$.

These factors have been evaluated for $\eta = 2.7$ at $\theta = 0^\circ$, 78.75° and 88.75° and are shown in fig. 6.9. Using these values the charge ratio at production at $\theta = 0^\circ$ has been evaluated for the case of $\xi = 0.2$ and 0.5, and $\nu = 4$ and the results are shown as curves (b) and (c) in fig. 6.8.

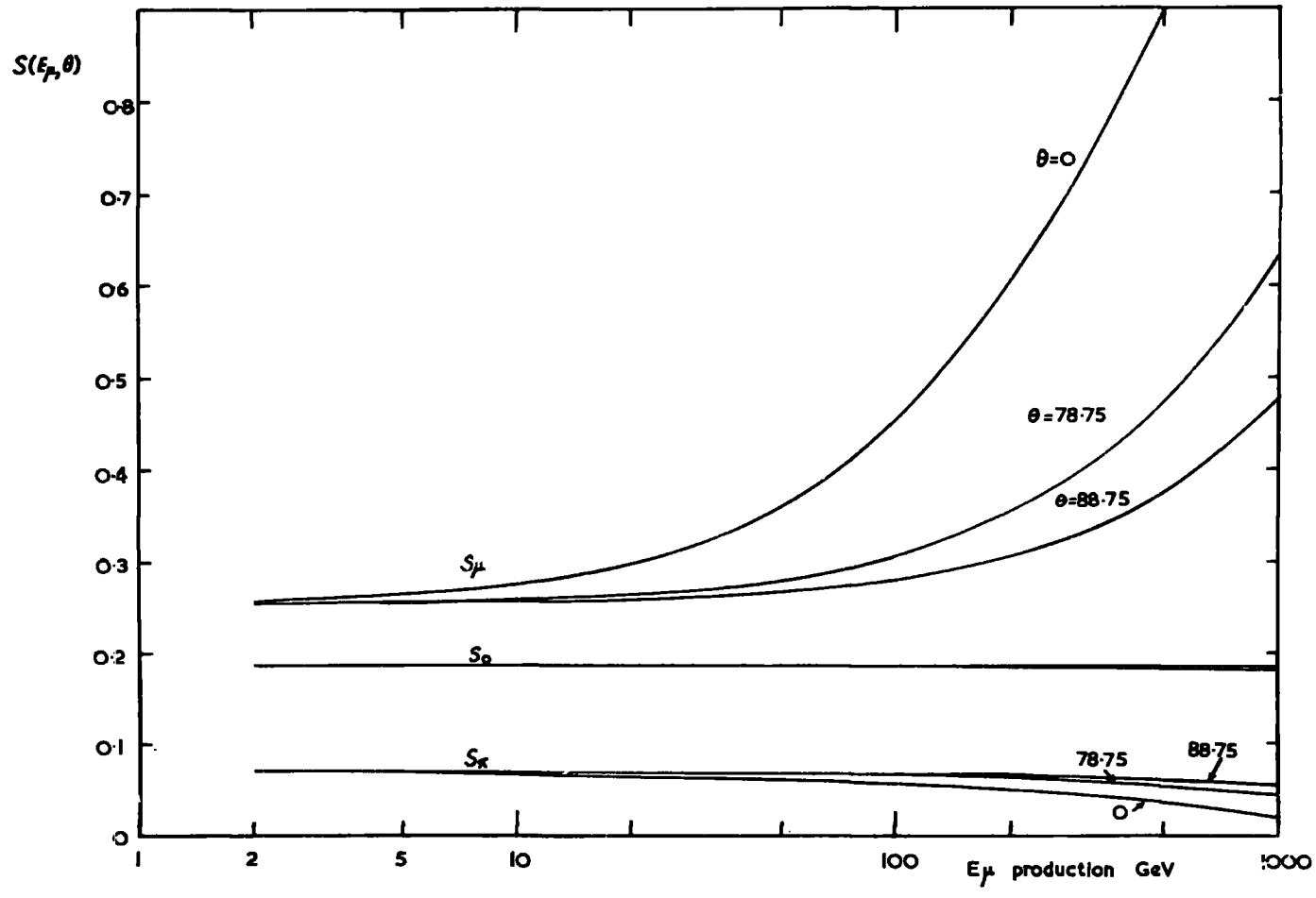

Fig. 6.3 The functions S_μ, S_π, and S_0 for $K/\pi = 1$.

The several assumptions made in the calculations on the effects of kaons are more serious than any made in the earlier calculations on pionisation. The fact that similar kaon and pion production spectra have been taken will result in a greater contribution from kaons at the higher energies, so the calculated ratio in this region will be a slight overestimate. The effect of neglecting the other kaon modes will be most serious at low energies but will not be very significant since, apart from the small branching ratios, several of them give rise to equal numbers of π^+ and π^-, tending to dilute the excess while others lead to preferential π^+ and μ^+, so the two factors operate in opposite directions. The serious assumptions are that the spectra of K^+ and K^- are parallel and especially that the charge excess is uniformly distributed over the produced kaons, i.e. ν independent of kaon energy, the value of $\nu = 4$ adopted is approximately the mean value observed at accelerator energies. From the review of the K/π ratio in the previous chapter it is difficult to derive a confident figure for this ratio except at accelerator energies, where it rises from 0.1 up to $\sim$ 0.2 at 30 GeV, as already emphasised the various other estimates depend on the assumption that the various spectra at production are parallel. However it seems certain that K/π is not greater than 0.5 over the range of interest and is probably nearer 0.3. The curve for $\zeta = 0.2$ will be an underestimate at high energies if as indicated by Dekkers et. al. (1964) the charge excess is more concentrated on the high energy particles. Part of the cause for the charge excess among the kaons is probably the phenomenon of associated production, since a K^- can only occur in a K^+K^- pair

$$N\,N \rightarrow N\,N\,K^+\,K^-$$

whereas positive kaons may occur in association with a hyperon

$$N\,N \rightarrow N\,K^{+}\,Y$$

but in view of the apparent correlation between charge excess and kaon energy some other features of the interaction may also be involved.

6.6 Zenith angle effects

The measured charge ratio may depend on the zenith angle by virtue of two effects. Firstly there is the dilution factor $D(E_\mu, \theta)$ which reflects the relative roles of muons from collisions of primary nucleons and from all collisions of nucleons. The effect of this is negligible as can be seen from fig. 6.10 where the relative ratio of R_μ at 80° and 0° is shown for the pionisation model discussed in §6.4. Secondly if there is a contribution to the charge excess from kaons having a large charge excess at production, the relative strength of muons from pion decay in diluting this excess will be greater at large zenith angles than at the vertical because of the higher energy at which pion interaction begins to compete with pion decay at these angles. The ratios of the two computed muon charge ratios at 80° and 0° for the assumptions on kaons plus pionisation discussed in §6.5 for $\xi = 0.2, 0.5, 1.0$ are shown in fig. 6.10. Also shown in this figure are the experimental data, $R_\mu(\theta > 75^\circ)/R_\mu(\theta < 75^\circ)$ derived via the survey in fig. 4.2. It is clear that there is some sensitivity at very high energies and indeed, unless the K/π ratio is very large, since the ratio of the ratios at a given value of ξ is not unique, the results are consistent with our observations in

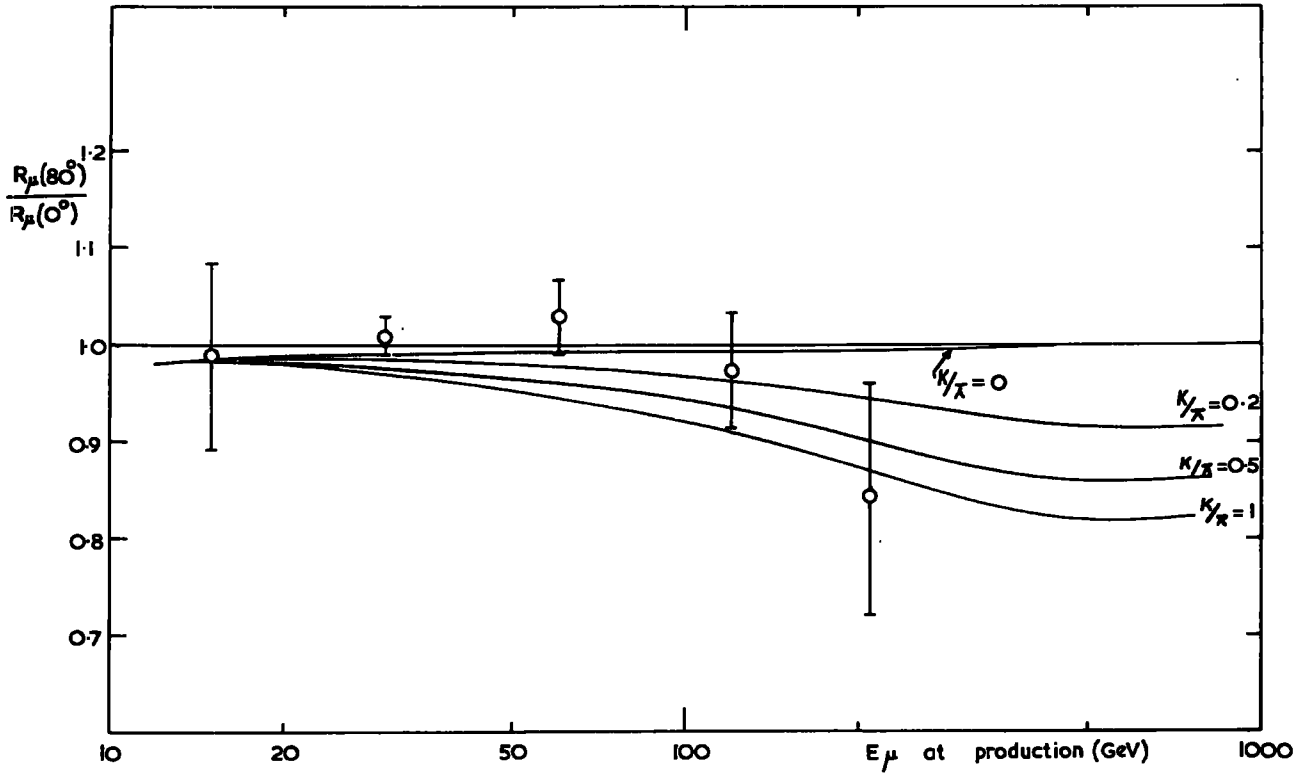

Fig.6.10 The charge ratio at 80° relative to that at the vertical for various K/π ratios; experimental points via fig.4.3.

chapter 5 that $\xi \lesssim 0.4$ over the range of energy concerned. It is seen that the extension of μ^+/μ^- measurements to high energies near the vertical would be useful.

6.7 Discussion

The observed charge ratio cannot be accounted for by pion production within the framework of a statistical model even allowing for fluctuations in multiplicity, inelasticity and pion energy. A similar conclusion has been arrived at by Cohen et. al. (1965). If the charge excess among kaons observed at accelerator energies persists up to high energies, kaons may, within the assumptions adopted here, contribute a large part of the positive excess especially at high energies, but are unlikely to account for the experimental data at intermediate energies $E_\mu \sim$ 10-100 GeV. A further comment on the role of kaons will be made in chapter 8 after an investigation of the muon charge ratio in E.A.S. In the following chapter the consequences of less general dynamical models of particle production will be investigated.

CHAPTER 7

Other models of particle production and the μ^+/μ^- ratio

7.1 The isobar model

All the calculations so far are essentially within the framework of a statistical model, i.e. particle production results from the disintegration of a high temperature intermediate state. It has been known now for many years that such a model is not sufficient for a full description of particle production at accelerator energies. Considerable success has been attained in describing particle production at low energies below about 3 GeV in terms of the de-excitation of excited nucleon states, e.g. for single pion production the process

$$N\,N \rightarrow N\,N^{*} \rightarrow N\,N\,\pi$$

to which the state N^{*} $T = 3/2$, $J = 3/2$ contributes. In p-p scattering at higher energies peaks in the scattered proton intensities are observed at energies near the elastic peak, Cocconi et. al. (1964). These indicate that apart from the $N^{*}_{3/2,3/2}(1238)$ state there exist, at least two other states $N^{*}_{\frac{1}{2},3/2}(1512)$ and $N_{\frac{1}{2},5/2}(1690)$ which are excited with comparable cross-section. The experiment of these authors also indicated that excitation of the 3/2,3/2 state falls off with increasing E_o, as would be expected theoretically, Contogouris et. al. (1963), since the exchange of a quantum with non zero isospin is required to excite it. More recently in a bubble chamber experiment by Hien et. al. (1965), E_o = 6-30 GeV, these states have been observed, as was a state at ~ 1400 MeV of which Cocconi et. al. saw some signs, but no state at ~ 1920 MeV as observed in πN collisions. These latter authors also suggest that the cross-sections for

exciting the 3/2,3/2 and $\frac{1}{2}$,5/2 states are energy independent. Other more massive states T = 3/2, 2190 MeV and T = 3/2, 2360 MeV are observed in πN and γN scattering but will presumably have very small excitation cross-sections in NN collisions.

Henceforth we will only consider the excitation of T = $\frac{1}{2}$ states at high energies; the constraints on T = 3/2 production by the muon charge ratio have been discussed by Pal and Peters, (1963). If the excitation of isobaric states without exchange of isospin continues up to high energies, then, because the incident nucleons are predominantly positive the decay pions will have a large charge excess, and even for relatively small excitation cross-sections will have a very considerable effect on the muon charge excess because of the rather high energy obtained by such a pion, $\sim E_o/5$, and the rapidly falling primary spectrum. The effect of pion production by such a mechanism on the muon charge ratio has been considered by Ramana Murthy (1963), Pal and Peters (1963,1964) and Cohen et. al. (1965).

Considering only T = $\frac{1}{2}$ states, decaying by single pion emission, we have

$$p \rightarrow N^{*+} \rightarrow \tfrac{2}{3}\,\pi^{+}n + \tfrac{1}{3}\,\pi^{o}p$$

$$n \rightarrow N^{*o} \rightarrow \tfrac{2}{3}\,\pi^{-}p + \tfrac{1}{3}\,\pi^{o}n$$

Thus for such collisions π^{+}/π^{-} = p/n. To calculate the resultant muon charge ratio we must consider (i) the effect of isobar production on the charge composition of the nucleon beam and (ii) pions produced in other inelastic-pionisation-channels. We note that secondary nucleons from the above collisions have a charge excess of $-\delta_o/3$, nucleons from an i th

generation collision an excess of $\delta_0(-\frac{1}{3})^i$. If the inelasticity in this type of event is about the same as in 'normal' pionisation events, then, since the cross-section for isobar production is an order of magnitude down on that for pionisation the composition of the nucleon beam will be little altered. One should distinguish two possible cases, shown in fig. 7.1 (a),(b)

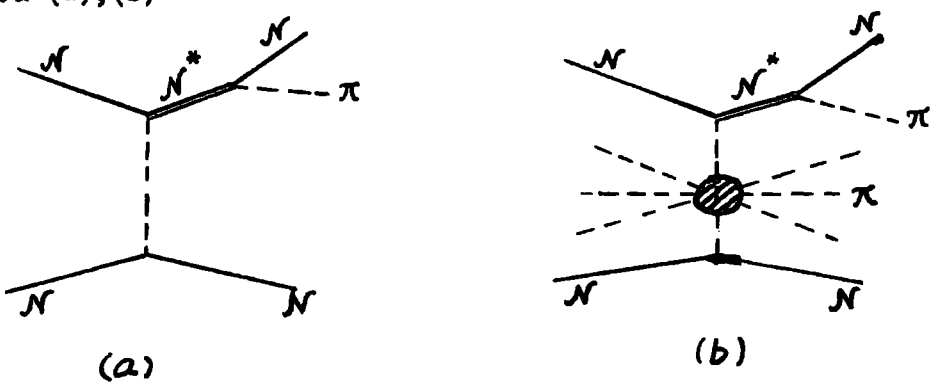

Fig. 7.1

(a) where the isobars are produced in quasi elastic collisions, and (b) where inelastic channels accompany the production of the isobar. While the case (b) is probably more likely at high energies we have at present no information on it. In case (b) the nucleon might not always retain its charge in the excited state, and the calculations would depend considerably on the associated inelasticity going into the pionisation.

Case (a) only will be considered, subject to the following assumptions; (i) the $(\frac{1}{2},3/2)$ and $(\frac{1}{2},5/2)$ isobars are produced with a total cross-section in the forward cone of 3 mbns., the cross-section observed at accelerator energies, independent of E_0, and in the ratio of their statistical weights $(2J+1) : (2T+1)$, i.e. 2:3. Cocconi et. al. (1964) find the $T = 5/2$ state more frequently produced than the $T = 3/2$ state but not by a factor of

3/2; this however is of little importance when only the pion decay modes are considered since the energy of the pion from both states is almost the same. (ii) The pionisation process occurs with a cross-section σ_p = 30 mbns; and is characterised by the most simple features, unique $n_\pi(E_o)$, k_π and equal energy distribution among pions in the forward cone, as considered in §5.3. Since $\sigma_I/\sigma_t \sim 0.1$, σ_t the total inelastic cross-section, and the inelasticity for pionisation is taken as 0.31 which is not very different from the effective inelasticity in quasi-elastic scattering, the effect on the nucleon charge composition will be neglected. Because the slight negative excess of those secondary nucleons resulting from isobar decay is neglected, and only case (a), fig. 7.1, is considered, the calculations will probably overestimate somewhat the charge excess for the adopted cross-section.

For the decay $N^* \rightarrow N + \pi$ we have a pion energy spectrum

$$\frac{\partial N}{\partial E_\pi}\, dE_\pi = \frac{dE_\pi}{2\gamma_I \beta_I p_\pi^*} \qquad \gamma_I(E_\pi^* - \beta_I p_\pi^*) \leq E_\pi \leq \gamma_I(E_\pi^* + \beta_I p_\pi^*)$$

where β_I is the velocity of the isobar in the laboratory system, $\gamma_I = E_I/m_I = (1-\beta_I^2)^{-\frac{1}{2}}$, and E_π^* and p_π^* are the energy and momentum of the pion in the rest frame of the isobar, $p_\pi^* = E_\pi^{*2} - m_\pi^2$. For isotropic decay

$$E_\pi^* = \frac{m_I^2 - m_p^2 - m_\pi^2}{2m_I}$$

whence $\frac{\partial N}{\partial E_\pi}\, dE_\pi = \frac{m_\pi}{2 E_\pi p_\pi^*} \frac{dE_\pi}{\sqrt{1 - 1/\gamma_I^2}}$, all charged states.

For $E_o \gtrsim 5$ GeV, $E_\pi \gtrsim 2$ GeV, we can neglect $1/\gamma_I^2$, and for quasi elastic scattering $E_I = E_o$. For pions from pionisation we have

where $\frac{\langle n \rangle}{2} E_\pi = k_\pi E_o \qquad \langle n \rangle = B E_o^\alpha$

$$E_o = \left(\frac{B}{2k_\pi}\right)^{1/1-\alpha} E_\pi^{1/1-\alpha}, \quad dE_o = \frac{1}{1-\alpha}\left(\frac{B}{2k_\pi}\right)^{1/1-\alpha}\left(\frac{E_\mu}{\tau}\right)^{\frac{\alpha}{1-\alpha}} \frac{dE_\mu}{\tau}$$

Then we have

$$\delta(E_\mu) = \mathcal{D}(E_\mu) \frac{\sum_I \int_{E_{o\,min}}^{E_{o\,max}} E_o^{-\gamma} 2\frac{\sigma_I}{3}\frac{m_I}{2E_o}\frac{dE_o}{\tau p_\pi^*} + \frac{\sigma_p}{1-\alpha}\left(\frac{B}{2k_\pi}\right)^{\frac{1-\gamma}{1-\alpha}}\left(\frac{E_\mu}{\tau}\right)^{\frac{\alpha-\gamma}{1-\alpha}} \frac{\langle n\rangle}{2\tau}\frac{\varphi(\langle n\rangle)}{2\langle n\rangle}}{\sum_I \int E_o^{-\gamma} 2\frac{\sigma_I}{3}\frac{m_I}{2E_o}\frac{dE_o}{\tau p_\pi^*} + \frac{B\sigma_p}{3(1-\alpha)}\left(\frac{B}{2k_\pi}\right)^{\frac{1+\alpha-\gamma}{1-\alpha}}\left(\frac{E_\mu}{\tau}\right)^{\frac{2\alpha-\gamma}{1-\alpha}}\frac{1}{\tau}} \quad \ldots\ldots (7.1)$$

where $E_{o\,max} = \dfrac{m_I E_\pi}{E_\pi^* - I p_\pi^*} \to \infty$, especially with the rapidly falling spectrum;

$$E_{o\,min} = \frac{m_I E_\pi}{E_\pi^* + I p_\pi^*} \approx \frac{m_I E_\pi}{2E_\pi^*}.$$

The parameters for the two states under consideration are tabulated below

N^*	m_I GeV	E_π^* GeV	p_π^* GeV	$E_{o\,min}$ GeV
$\frac{1}{2}$, 3/2	1.512	0.47	0.445	1.64 E_π
$\frac{1}{2}$, 5/2	1.690	0.59	0.574	1.45 E_π

$\sigma_I(\frac{1}{2},3/2) = \frac{6}{5}$ mbns, $\sigma_I(\frac{1}{2},5/2) = \frac{9}{5}$ mbns, $\sigma_p = 30$ mbns.

On evaluating the above expression for $\alpha = 0.25$, $\gamma = 2.58$, $B = 2.7$, $\tau = 0.76$, $k_\pi = 0.31$ and converting to muon charge ratio we get curve (a) in fig. 7.2. Due to the simple pionisation model used two other factors require attention. If a more realistic pionisation model were used the charge excess of the pions would be somewhat higher, but on the other hand the fluctuations in k_π and the spectrum in E_π, although having negligible effect on the computed charge excess, will result in an appreciably greater intensity of muons from pionisation than the simple case of no fluctuations, and will thus have a greater diluting effect on

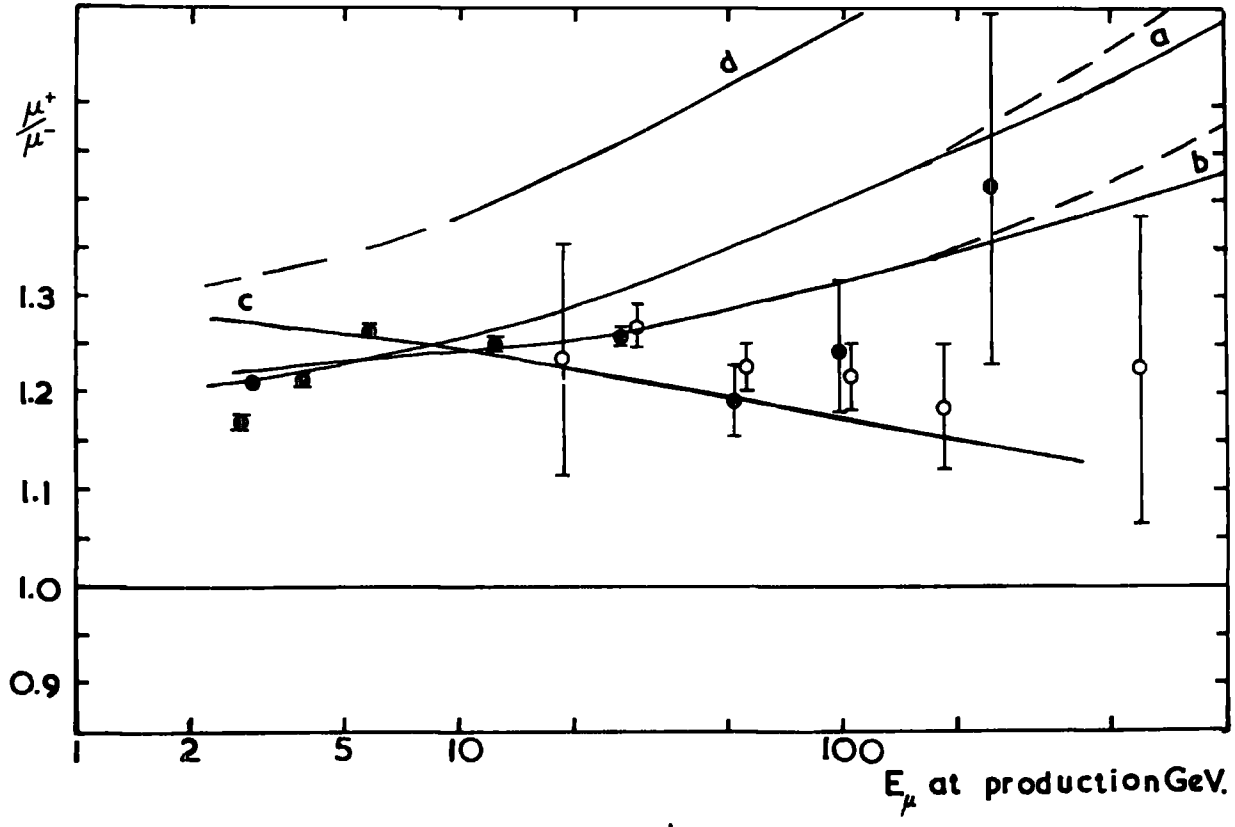

Fig.7.2 The calculated ratio for isobar production, (a), (b): σ_I constant; (c): $\sigma \sim 1/\ln E_0$; (d) O.P.E. model prediction.

the charge excess from isobar decay which will probably be much more serious than the slight increase due to fluctuations in n_π. It was noted in chapter 6 that the adopted multiplicity distribution underestimated the frequency of events with $n_s = 1.2$, i.e. $n_\pi \approx 1$ and we may consider these low multiplicities to arise from the decay of isobars. We can include fluctuations in the pionisation component to the degree considered in §6.5 as follows; if we write (6.5) as $\frac{3}{4}\,N/D$ then D is, to within a constant, the total number of charged pions; in fact

$$\pi^+ + \pi^- = \frac{\sigma_p}{3}\,(1+\beta)^2\,D = 250\,D \text{ for } \beta = 4$$

Thus the pionisation term, in the denominator of (7.1), is to be replaced by this, and the pionisation term in the numerator by $(\pi^+ + \pi^-)\delta_1(E_\mu) = 250\,D\delta_1(E_\mu)$ were $\delta_1(E_\mu)$ is the excess as calculated by (6.5). In this way we allow fully for the slightly greater charge excess due to fluctuations in n_π, and the increased dilution due to fluctuations in k_π and the spectrum in E_π in the pionisation component. The increased intensity of pionisation pions turns out to be ~ 1.5 times the intensity from simple considerations, slowly varying with energy. The resulting curve for the muon charge ratio at production is shown as curve (b) in fig. 7.2.

So far only single pion decay of these excited states has been considered, in fact some evidence for two pion decay modes exist, and also the $\frac{1}{2}$,5/2, 1690 MeV state has a Q value of $\sim$ 80 MeV for a decay into a kaon and a hyperon, $N^{**}_{5/2} \rightarrow K\Lambda$. The cross-section for the two pion mode is small and since it results in a further degradation in energy and charge excess it will have negligible effect on the computed ratio. The kaon mode may, however, be of greater importance since at very high energies

it can give rise to muons when pion interaction becomes predominant, even if its branching ratio is small as suggested by its Q value, and its effect on the computed ratio at high energies will be considered. The relevant decay mode is

$$N^{*+}_{5/2} \rightarrow K^+\Lambda \quad \hookrightarrow \mu^+\nu\ (58\%)$$

$$N^{*0}_{5/2} \rightarrow K^0\Lambda \quad \hookrightarrow \pi\ \mu\nu\ (13\%)$$

Negative kaons can only occur in $K\bar{K}$ pairs for which m_I must be in excess of 1960 MeV. All the other important modes involve intermediate pions, and in the second mode above $\tau_{K^0} \approx 2\tau_\pi$, thus since its branching ratio is also small all modes except the $K_{\mu 2}$ one will be neglected. The important Λ decay mode $p\pi^-(67\%)$ involves an intermediate pion and the direct $\Lambda \rightarrow p\mu\nu$ mode is completely negligible. If we denote by b the branching ratio for the $K\Lambda$ mode an additional term must be included in the numerator of (7.1) which is given by

$$\frac{0.83}{\delta_0} f_{K\mu_2}\, b \iint E_0^{-\gamma} \frac{1}{\dfrac{1+E_K/B_{K^+}}{1+E_K/B_\pi}}\, \sigma_I(1/2,3/2)\, N(E_K) N(E_\mu, E_K)\, dE_K\, dE_0$$

and a similar term, but without the δ_0, must be added to the denominator. $N(E_K)dE_K$ is the spectrum of kaons from isobar decay

$$N(E_K)dE_K = \frac{dE_K}{2\gamma_I p^*_K} = \frac{m_I dE_K}{2E_0 p^*_K}$$

$$E^*_K = \frac{m_I^2 - m^2 - m_K^2}{2m_I} = 0.548 \text{ GeV}, \quad p^*_K = 0.241 \text{ GeV/c}$$

also $E_{o\ min} = \frac{m_I E_K}{E_K^* + \beta_I p_K^*} = 2.14\ E_K$, $E_{o\ max} = \frac{m_I E_K}{E_K^* - \beta_I p_K^*} = 5.5\ E_K$

$N(E_\mu, E_K)dE_\mu$ is the spectrum of muons from $K_{\mu 2}$ decay

$$= \frac{1.049\ dE_\mu}{E_K} \qquad \frac{E_K}{21.58} \leq E_\mu \leq E_K$$

Then the term becomes

$$1.049 \frac{m_\Sigma}{2p_K^*} b\,\sigma_I(1/2, 5/2)\left(1 + \frac{E_\mu}{\tau B_\pi}\right)\frac{0.83}{\delta_o} f_{K_{\mu 2}} \int_{E_\mu}^{21.58E_\mu} \int_{2.14E_K}^{5.5E_K} \frac{E_o^{-\gamma}}{1 + \frac{E_K}{B_{K^*}}} \frac{dE_o}{E_o}\, dE_K$$

$$= \frac{1.049}{\tau} b\,\sigma_I(1/2, 5/2)\left(1 + \frac{E_\mu}{\tau B_\pi}\right)\frac{0.83}{\delta_o} f_{K_{\mu 2}} \frac{m_\Sigma}{2p_K^*}\frac{\tau}{\gamma}\left\{2.14^{-\gamma} - 5.5^{-\gamma}\right\} E_\mu^{-\gamma} I_{K_{\mu 2}}(E_\mu)$$

where $I_{K_{\mu 2}}$ is defined in §6.5 only $\eta \to \gamma$. The term is then

$$0.163\ \frac{b}{\tau}\left(1 + \frac{E_\mu}{\gamma B_\pi}\right) E_\mu^{-\gamma}\ I_{K_{\mu 2}}(E_\mu)$$

for $\sigma_I(\frac{1}{2}, 5/2) = \frac{9}{5}$ mbns, $f_{K_{\mu 2}} = 0.58$, $\gamma = 0.76$, $\delta_o = 0.74$, $\gamma = 2.58$. The resulting charge ratio for $\theta = 0^\circ$ is shown as the dashed curves in fig. 7.2 for a branching ratio $b = 0.10$. We see that the inclusion of the kaon mode does not have a very great effect in this case, as distinct from the calculations of Pal and Peters, (1964), where the inclusion of this mode has a very significant effect - fig. 7.3. This is because their adopted cross-section for isobar production is very much greater, ~ 75% of σ_{total}, and the kaons carry a charge excess ~ 3 times larger than the pions in their model. Recent experimental evidence suggests that the branching ratio for $K\Lambda$ is even smaller than assumed, ~ 2%.

It is interesting to see the effect of a decreasing cross-section for isobar production with nucleon energy and calculations have been

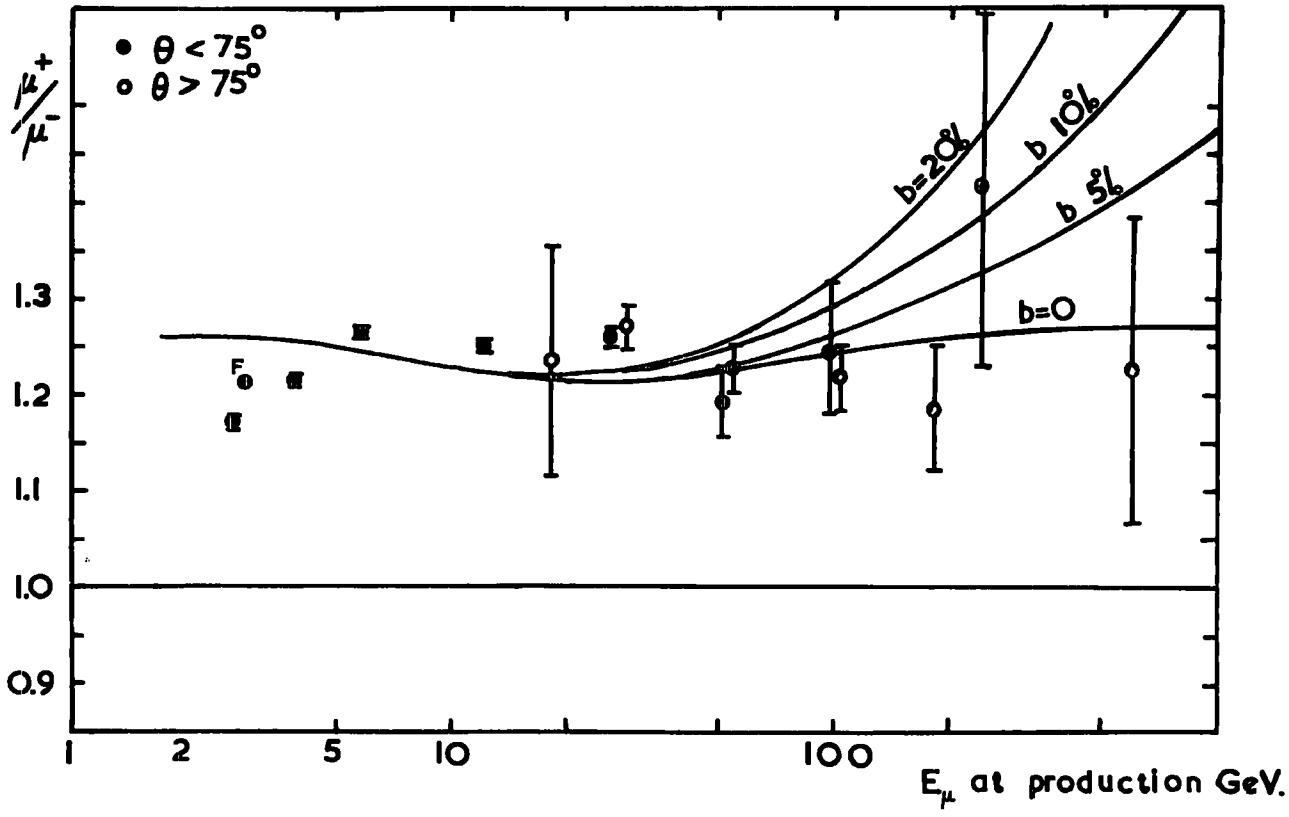

Fig.7.3 A comparison of the calculations of Yash Pal and Peters (1964) with the survey of the experimental data.

repeated for a cross-section varying as $^{1}/_{\ln E_o}$.

$\sigma_I = {}^{a}/_{\ln E_o} = 3$ mbms at 25 GeV sets a = 9.65

At very high energies a more rapidly decreasing cross-section is suggested by theoretical work of Contogouris et. al. (1963), and a slight decrease with E_o is indicated by the p p scattering of Cocconi et. al. (1964) but not by the work of Hien et. al. (1965). Using this cross-section, the first term in the numerator and in the denominator of (7.1) is replaced by the term

$$\sum_I \int_{E_{o\min}}^{E_{o\max}} \frac{a E_o^{-\gamma-1}}{\ln E_o} \frac{m_I}{2 P_K^*} \frac{dE_\mu}{\gamma} dE_o = -\sum_I \frac{a m_I}{2 P_K^*} \frac{dE_\mu}{\gamma} Ei(-\gamma \ln E_{o\min})$$

to be divided in the ratio 2:3 between the two states. Including the pionisation contribution with full fluctuations as in §6.5 the resulting muon charge ratio is shown as curve (c) in fig. 7.2.

7.2 The O.P.E. model

Among other models which have proved very useful at low energies there is the peripheral model but its extension to high energies leads to many difficulties. A particular version of the peripheral model is the diagram shown in fig. 7.4(a) the one pion exchange, (O.P.E.), model, where single pion production is effected by the diffraction of a pion of the target cloud of the incident nucleon, at the target nucleon. This

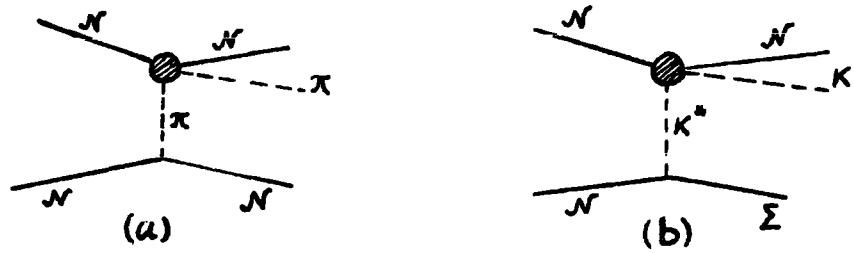

Fig. 7.4

diagram, phenomenologically modified for the πN scattering matrix element, (as indicated by the experimentally observed strong damping of large momentum transfers), and the virtuality of the pion, has been considered recently by Narayan (1964), Smrz (1964), and Takada and Bando (1965). The latter authors have shown, that with suitable modifications to the πN matrix element, cross-sections of the correct order to account for the observations on quasi elastic scattering at C.E.R.N. can be obtained. Narayan, making computational approximations which restrict the validity of his results to $E_o \gtrsim 100$ GeV has derived an expression for the distribution in laboratory inelasticity for events of this type. This may be written in the form, (in units with $c = \hbar = 1$),

$$\frac{d\sigma}{dk_\pi} = \frac{\alpha}{4}\frac{f^2}{(2\pi)^2}\frac{(M/\mu)^4}{a} M^2 \sigma_t^2 \, g(k_\pi)$$

with

$$g(k_\pi) = \frac{k_\pi \, e^{-\frac{1.1 k_\pi^2}{1-k_\pi}}}{1-k_\pi+\frac{M^2}{\mu^2}k_\pi^2}\left\{\left[1+\frac{\mu^2}{M^2}\frac{(1-k_\pi)(1+\lambda)}{k_\pi^2}\right]e^{\lambda} h(\lambda) - \frac{\mu^2}{M^2}\frac{1-k_\pi}{k_\pi^2}\right\}$$

where

$$\lambda = \frac{\mu^2}{M^2}\left(\frac{1.1}{1-k_\pi}+b\right)\left(1-k_\pi+\frac{M^2}{\mu^2}k_\pi^2\right), \qquad b \approx 6$$

$$h(\lambda) = -Ei(-\lambda) = \int_1^\infty \frac{e^{-\lambda y}}{y}\,dy$$

and f^2 is the pseudoscalar coupling constant, = 0.08, μ and M are the pion and nucleon masses, σ_t the total pion nucleon cross-section, a = 7.9 from experimental data on πN cross-sections, and α = 1 for π^o emission and 2 for $\pi^+(\pi^-)$ emission from an incident proton (neutron). This expression is only valid for $E_o \gtrsim 100$ GeV and $k_\pi \gtrsim 0.2$. For σ_t = 25 mbns we have

$$\frac{d\sigma}{dk_\pi} = 185\alpha \, g(k_\pi)$$

On integration, this expression yields a cross-section for $k_\pi \geq 0.2$ of 6 mbms for all charge states, and for $k_\pi \geq 0.6$, 0.12 mbms. The mean inelasticity, if a lower cut-off of 0.2 is adopted, is

$$\langle k_\pi \rangle = \frac{\int_{0.2}^{1} k_\pi\, g(k_\pi)\, dk_\pi}{\int_{0.2}^{1} g(k_\pi)\, dk_\pi} = 0.31$$

Thus while the cross-section here is about twice as great as that adopted for isobar production, because the mean inelasticity is so near the mean for pionisation type events, the effect on the charge composition of the nucleon beam will be small.

Assuming a lower cut-off at 0.2 the positive excess can be evaluated as for the case of isobar production, the first term in the numerator and denominator of (7.1) to be replaced by the term

$$dE_\pi \int E_0^{-\gamma} \frac{\partial \sigma^{\pm}(E_\pi)}{\partial E_\pi}\, dE_0$$

$E_\pi = k_\pi E_0 \quad \frac{\partial \sigma}{\partial E_\pi} = \frac{\partial \sigma}{\partial k_\pi}\frac{\partial k_\pi}{\partial E_\pi} = \frac{C}{E_0}\, g(k_\pi), \qquad C = 185\alpha$

and we get

$$C \left(\frac{E_\mu}{\gamma}\right)^{-\gamma} \frac{dE_\mu}{\gamma} \int_{0.2}^{1} k_\pi^{\gamma-1}\, g(k_\pi)\, dk_\pi$$

Inserting this term, with $\gamma = 2.58$, $\alpha = 2$, in the numerator and denominator of (7.1) in place of the isobar terms and including the simple pionisation dilution as given in this equation, the charge ratio has been calculated and is shown as curve (d) in fig. 7.2. It can be seen, that even if the more severe dilution from pionisation including fluctuations were included the computed ratio is appreciably greater than the observed. This arises from the fact that the cross-section is about twice as large as that adopted for isobar production, and also the energy spectrum of produced pions extends to E_0.

More recently Crossland and Fowler (1965), have repeated Narayan's work from a less phenomenological standpoint and find very good agreement with his results. There are, however, theoretical arguments against pion exchange at high energies, of which the disappearance of the 3/2, 3/2 isobar is probably an indication, and the above authors repeated the calculation for K^{*} exchange, leading to K^{*} production and they find σ_{K_K} (≥ 0.2) = 0.5 mbns for charged kaons. From symmetry considerations they also except a similar cross-section for pion production through ρ exchange.

7.3 Discussion

Because of the ambiguity in the experimental position it is difficult to draw conclusions from the comparison with the predictions of the isobar model. Since it seems, however, that the charge ratio is not increasing with energy the evidence is against a continuation of quasi elastic scattering with the cross-section observed at 25 GeV. A cross-section decreasing not quite as fast as $1/\ell n E_o$ would seem to account for the data, especially if the production of kaons in the inelastic channels were considered.

Pal and Peters, (1964), assumed isobar production in ~ 70% of all collisions, with masses $\geq$ 2300 MeV and a charge excess of produced pions of ~ $0.35\,\delta_o$. Their dilution from pionisation is also less than in our case because they have both a smaller fraction of energy going into pionisation and a greater multiplicity of pionisation pions. As can be seen from fig. 7.3 their calculations, assuming no kaon decay modes, are in sensible agreement with the experimental data, though if the isobars

were as massive as postulated the presence of such a decay mode might be expected. The evidence for isobars of any type at high energies is not very comprehensive; Kazuno (1964), from an analysis of jets argues in favour of appreciable isobar production above 10^{12}eV but her analysis is not sufficiently sensitive to the mass or decay modes of such isobars. Lattes et. al. (1964), at ultra high energies find events with $E_{\pi^0}/\sum E_{\pi^0} > 0.5$ but in all such cases $n_{\pi^0} < 3$. The occurrence of quasi elastic scattering, to the degree discussed in §7.1, because of its small cross-section, would not be inconsistent with observations on high energy events.

The charge excess predicted by the O.P.E. model is considerably greater than experimentally observed. The later results of Crossland and Fowler on K production, and π production via ρ exchange, might result in a better fit to the experimental data (through predicting lower ratios) though at the highest energies in contrast with observations, an increasing ratio would be expected since all the charged kaons would be positive.

CHAPTER 8

Conclusions

8.1 The Present Work: Experimental

In the work reported here the determination of the muon charge ratio has been extended up to the highest energies yet attained.

Since (i) the m.d.m. of the two spectrographs are 300 and 1950 GeV/c, (ii) good agreement exists between the predicted and observed intensities, and (iii) the ϵ distributions, and $R^{\pm}$, (Chapter 3), are sensibly symmetric we may be reasonably confident of the validity of the results. In the energy region where comparison with other workers can be made no significant disagreement obtains. No significant evidence for a minimum in the region 50-100 GeV (as found by some workers) appears, and a best fit line through the results, see fig. 3.4, would favour a charge ratio slowly decreasing with muon energy for $E_\mu \gtrsim 150$ GeV. The results do not favour a rapidly increasing ratio at high energies but are not inconsistant with a constant ratio from 30 - 1000 GeV.

8.2 The Present Experimental Position.

A best estimate of the behaviour of the charge ratio, on the basis of all the published data, has been derived in chapter 4. A best fit line through this survey is shown in fig. 8.1, with suggested upper and lower limits on its variation at the highest energies. No strong dependance on the zenith angle is observed, a feature also noted in the present work from a subdivision of the momentum cells by zenith angle, but in order to make more certain of this, greater accuracy of charge ratio measurements near the vertical is called for. Because of our ignorance of the behaviour at high energies no firm conclusions on the existence of a sharp minimum

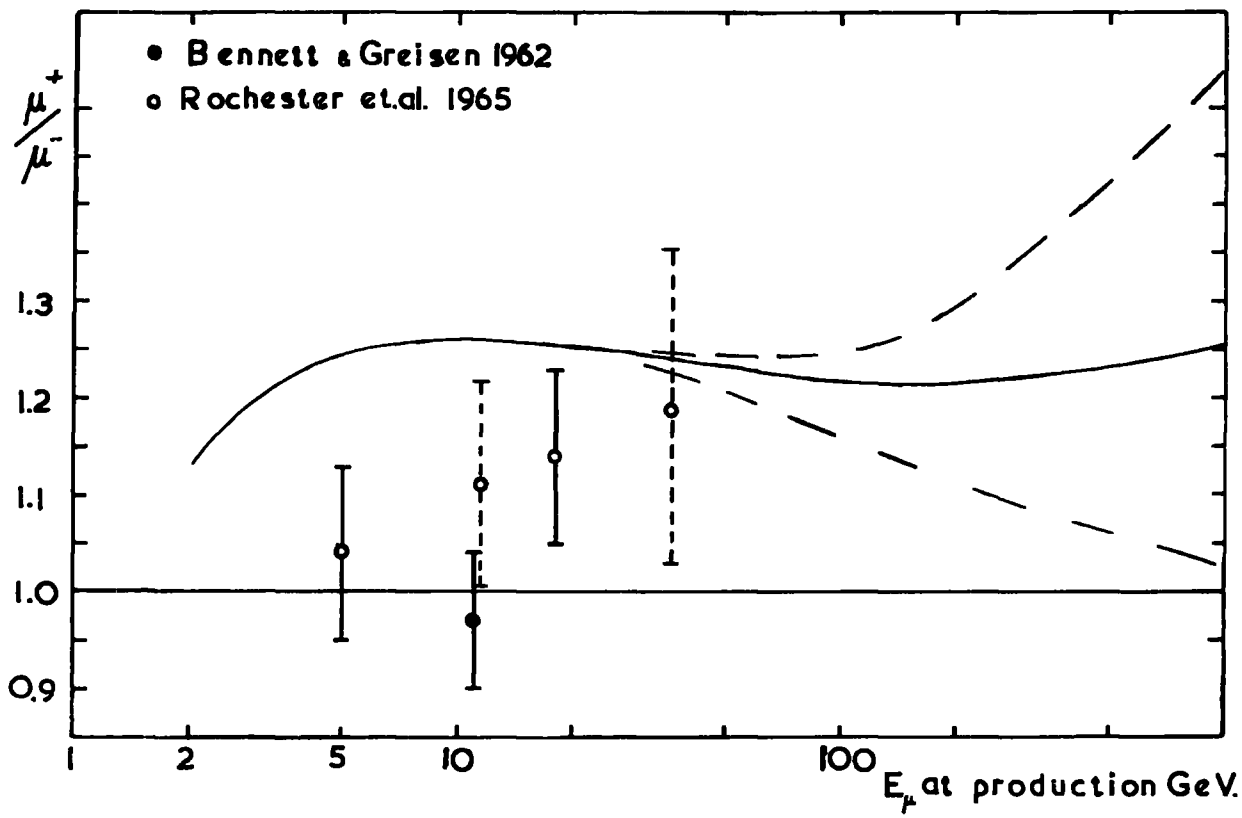

Fig. 8.1 A comparison of the charge ratio of muons in air showers with the charge ratio of unassociated muons.

in the region 50 - 100 GeV can be drawn, but the evidence slightly favours such a phenomenon.

8.3 The Present Work: Theoretical

The effect of the observed fluctuations in pion multiplicity from one event to another, within the framework of a statistical model is not sufficient to account for the experimental data. In such a model the effect of fluctuations in inelasticity and energy distribution is very small.

The effect of including kaons in such a model depends strongly on the assumptions made. For $K^+/K^- = 4$, and the charge excess uniformly distributed over the kaons a value of $(K/\pi)_{all} \approx 0.5$ is required for $E_0 \gtrsim 200$ GeV ($E_\mu \gtrsim 10$ GeV), see fig. 6.8, to account for the data a higher value than is suggested by the summary of the K/π ratio in § 5.6.3. While, in principle, more precise information on the contribution of kaons may be gained from the zenith angle effect, § 6.6, the experimental data at high energies are as yet too uncertain for such an analysis.

Another possible method of looking at the contribution of kaons is the investigation of the charge excess of muons in E.A.S. To date, only two such studies have been reported. Bennett and Greisen, (1962), and Rochester et al (1965), both of them at fairly low energies. Their results are shown in fig. 8.1 (plotted at an energy E_{median} + 2 GeV) where they can be compared with the best fit curve to the ratio for incoherent muons.

In air showers there are two factors to be considered. When one is sampling at a fixed shower size one is looking at a small band of primary energy, so that any effect which is emphasised by the steep slope of the primary spectrum will not be so pronounced as in the case of unassociated muons, as for example if the charge excess were preferentially distributed

among the high energy secondaries. A large fraction of the observed muons will have come from pion air-nucleus collisions. These two factors make more difficult a comparison between the associated and unassociated cases, but we can confidently say that if the charge ratio of unassociated muons is solely due to pions there should be negligible charge excess among muons in air showers. If, however, there is a significant contribution to the unassociated charge excess from kaons carrying a large charge excess at production the position is not as simple since we have not got very much information on the charge composition of kaons produced in pion nucleon collisions. Very little work on π^+ nucleon collisions is available but a kaon positive excess might be expected. For π^-p collisions we have data at E_π = 10 GeV, Bigi et al (1964), E_π = 11.6, 18.1 GeV Lloret et al (1964) and E_π = 16 GeV Bartke et al (1962). In table 8.1

Table 8.1

E_π	σ_{YK}	$\sigma_{K\bar{K}}$	$\sigma_{K\bar{K}}/\sigma_{YK}$	K^+/K^-
10	1.45 ±.17	1.97 ±.24	1.36 ±.23	1.74 ±.34
11.6	1.10 ±.16	1.71 ±.48	1.37 ±.43	1.73 ±.63
16	1.32 ±.15	2.21 ±.25	1.67 ±.27	1.60 ±.30
18.1	2.16 ±.30	2.96 ±.83	1.56 ±.47	1.64 ±.49

there are tabulated the cross-sections for the interactions

$$\pi^- p \longrightarrow Y K n(\pi) \quad , \sigma_{YK}$$

$$\pi^- p \longrightarrow K \bar{K} n(\pi) \quad , \sigma_{K\bar{K}}$$

as given by these authors, and the K^+/K^- ratio derived from them under the assumptions, (i) in the YK case K^o and K^+ are produced with the same frequency, as suggested by the work of Bigi et al and (ii) in the $K\bar{K}$ case

the four states $K^0 \bar{K}^0$, $K^0 K^-$, $\bar{K}^0 K^+$, $K^+ K^-$ are equally probable. We see that for $\pi^- p$ collisions a positive excess among the kaons obtains. For such collisions we also see that $(K/\pi)_{all} \lesssim 10\%$ at energies $E_\pi < 20$ GeV.

The experimental position on the μ^+/μ^- ratio in air showers is as yet unclear because of the poor statistics. Bennett and Greisen, in a rather broad interval of shower size, $N = 10^3 - 10^6$ particles, find a ratio of $0.969 \pm .072$ for muons with a median energy of 9 GeV. Rochester et al quote results for two shower sizes $N \simeq 2\ 10^7$ at 270m from the core, $E_{\mu\ \text{median}} \simeq 2.9$ GeV and $\mu^+/\mu^- = 1.041 \pm .090$ and $N \simeq 4\ 10^5$ at 37 m from the core, $E_{\mu\ \text{median}} \simeq 15.8$ GeV and $\mu^+/\mu^- = 1.137 \pm .089$. If the data at $N = 4\ 10^5$ are divided into two groups, $E_\mu < 20$ GeV and $E_\mu > 20$ GeV, the dashed points in fig. 8.1 follow. The results may indicate that the charge ratio is not unity but somewhere intermediate between unity and the value for unassociated muons, possibly increasing with energy. If this is so it may reflect a contribution from kaons with the charge excess shared preferentially among the high energy particles. Such kaons would presumably come from a kaonisation process rather than isobar decay, since energetic nucleon isobars in the laboratory would not be expected frequently in π- nucleon collisions. Thus if an appreciable charge excess of muons in air showers is observed it favours kaon production through a kaonisation process, with a large charge excess at production, in π-nucleon collisions, which would also be expected in nucleon-nucleon collisions. If this is not so a considerable contribution to the charge excess of unassociated muons might arise from kaons from isobar decay, which would have little effect in air showers.

Even the assumption of $K/\pi \approx 0.3$ and $K^+/K^- = 4$ is not sufficient to account for the observed charge ratio in the region 10 - 50 GeV, fig. 6.8, and some isobar production must be invoked to account for the data. This seems reasonable in view of the cross-sections for isobar production observed at accelerator energies, and it seems very likely that a cross-section falling off approximately as $1/\ln E_0$ (or possibly a constant cross-section with increasing accompaniment of inelastic channels) combined with all the other features of interactions at accelerator energies, K/π , $\frac{K^+}{K^-}(E_K)$, $N(E_\pi)dE_\pi$ $N(E_K)dE_K$ etc., if they were accurately known, would fully account for the experimental data within the errors.

While the present experimental data do not rule out such mechanisms as the heavy isobar model of Pal and Peters (1964) or the O.P.E. model of Narayan(1964) it is not essential at the present state of our knowledge, to invoke such models, though they might be important if the charge ratio does in fact increase at high energies, a behaviour which is unlikely but is not yet entirely ruled out by the present experimental position.

8.4 Future Work

With the present Mk 2 instrument the charge ratio may be established up to energies of ~500 GeV but at energies greater than this the rate is so low, ~3 per 100 hours, which is about a weeks running time, under the prevailing conditions, that an instrument of larger accepting power is imperative. Mindful that this must be accompanied by an increase in resolution an instrument with both a greater magnetic path length, and measuring elements with greater definition in location, would be necessary. However, before embarking on such a project it would be desirable to make a somewhat better estimate of the behaviour of the charge ratio with the present

instrument. Equally desirable would be an accurate determination of the μ^+/μ^- ratio up to 1000 GeV at the vertical, but because of the great flux of low energy particles, the rapidly falling spectrum and the reduced intensity of particles with energy $\gtrsim$ 100 GeV the realisation of such a measurement is a formidable task.

The charge ratio of muons in extensive air showers is a more feasible proposition, and reasonably accurate results on this may be expected in the near future. Of considerable interest would be an investigation of the charge ratio of the highest energy muons in E.A.S. by studying the multiply penetrating particles observed underground in association with air showers.

A much more sensitive indication of the contribution of kaons to the charge ratio than any so far discussed would be the charge ratio of muons produced by neutrino interactions at great depths underground. This arises from the fact that neutrinos from K_{μ_2} decay are about twice as energetic on average as those from π decay. The $(\mu^+/\mu^-)_\nu$ ratio will be the same as the $\bar{\nu}/\nu$ ratio which will be very appreciably less than the μ^-/μ^+ ratio in the atmosphere for a reasonable kaon contribution. For $K/\pi = 0.2$ and $K^+/K^- = 4$ at production, the pions having no charge excess, the ratio for neutrino induced muons would be $(\mu^+/\mu^-)_\nu \simeq \frac{1}{1.6} = 0.62$ if the mean energy of neutrinos were $\approx$20 GeV and $\simeq$0.48 at $E_\nu \approx$100 GeV.

Acknowledgements

The author is greatly indebted to Professor G.D. Rochester, F.R.S. for the facilities provided, and has much appreciated his constant interest throughout the progress of the work. He is likewise extremely grateful to Professor A.W. Wolfendale, his supervisor, for invaluable guidance and his constant co-operation, without which the work would not have been possible.

To his colleagues, Professor Y. Kamiya, Mr. G.N. Kelly, Mr. J.B.M. Pattison, Dr. P.V. Ramana Murthy, Mr. S.S. Said, Professor N.S. Sinha and Dr. J. Wdowczyk, who at various times by word and deed contributed to the final results, the author is very grateful. The author also appreciates the valuable discussions he has had with Dr. F. Ashton, Mr. A. Aurela, Dr. G.N. Fowler and Mr. J.L. Osborne.

The collaboration and effort of the technical staff, notably Mrs. E.M. Graham, Mr. W. Leslie, Mr. E.W. Lincoln, Mr. W.D. Threadgill and Mr. R. White is appreciated, and particular thanks are expressed to Miss Carole Guyll for her ready attention to the thankless tasks of scanning the films and punching data and to Mr. Peter Finley for his amiable and ready assistance in the day to day running of the spectrographs.

The staff of the University Computing Laboratory, in particular its supervisor, Mrs. E. Templeton, are thanked for their co-operation and assistance.

For their painstaking efforts in typing this thesis Miss P. Stewart and Miss A. Parnaby are sincerely thanked.

Finally, for the essential financial assitance, the European Office, Aerospace Research of the U.S. Air Force, and the Science Research Council of the United Kingdom are thanked for the award of Research Studentships during the period of the work.

References

P.E.P.C.R.P. ≡ Progress in Elementary Particle and Cosmic Ray Physics, Eds. Wilson, J.G. and Wothuysen, S.A. (Amsterdam: North Holland).

Proc. Jaipur Conf. ≡ Proceedings of International Conference on Cosmic Rays, Jaipur, 1963. (Bombay: Commercial Printing Press).

Lond. Conf. ≡ Proceedings of International Conference on Cosmic Rays, London, 1965. (Proc. Phys. Soc. in the Press).

Achar, C.V., Menon, M.G.K., Narashimam, V.S., Ramana Murthy, P.V., Sreekantan, B.V., Hinotani, K., Miyake, S., Creed, D.R., Osborne, J.L., Pattison, J.B.M. and Wolfendale, A.W.,(1965), Phys. Lett. 18, 196.
Ibid., 19, 78.

Alikhanian, A.I. and Vaisenberg, A.O.,(1957), Zhurn. Eksp. Teor. Fiz., 32, 413, (Sov. Phys. J.E.T.P., 5, 349).

Allen, J.E. and Apostolakis, A.J., (1961), Proc. Roy. Soc., A265, 117.

Allkofer, O.C., (1960), Z. Physik, 158, 274.

Allkofer, O.C. and Trumper, J., (1964), Zeits. fur Naturforschung, 19, 1304.

Aly, H.H., Kaplon, M.F., and Shen, M.L., (1964), Nuovo Cim., 32, 905.

Ashton, F., and Wolfendale, A.W., (1963), Proc. Phys. Soc., 81, 596.

Ashton, F., MacKeown, P.K., Ramana Murthy, P.V., Pattison, J.B.M. and Wolfendale, A.W., (1963), Phys. Lett. 6, 259.

Ashton, F., Kamiya, Y., MacKeown, P.K., Pattison, J.B.M., Ramana Murthy, P.V., and Wolfendale, A.W., (1965), Proc. Phys. Soc.,in the press.

Aurela, A., (1965), Ph.D. Thesis, Univ. of Durham.

Babayan, Kh.P., Grigorov, N.L., Mamidjanian, E.A., Shestoperov, V.Ya. and Tretyakova, Ch.A., (1963b), Proc. Jaipur Conf., 5, 248.

Babayan, Kh.P., Brikker, S.I., Grigorov, N.L., Podgurskaya, A.V., Savelyeva, A.I., and Shestoperov, V.Ya., (1963a), Proc. Jaipur Conf., 5, 51.

Baradzei, L.T., Rubstov, V.I., Smorodin, Yu.A., Solob'ev, M.V., and Tolkachev, B.V., (1964), Trudy Lebedev Inst., 26, 224.

Barkow, A.G., Chamany, B., Haskin, D.M., Jain, P.L., Lohrmann, E., Teucher, M.W., and Schein, M., (1961), Phys. Rev., 122, 617.

Barrett, P.H., Bellinger, L.M., Cocconi, C., Eisenberg, Y., and Greisen, K., (1952), Rev. Mod. Phys., 24, 133.

Bartke, J., Budde, R., Cooper, W.A., Filthuth, H., Goldschmidt-Clermont, Y., Macleod, G.R., deMarco, A., Minguzzi-Ranzi, A., Montanet, L., Morrison, D.R.O., Nillson, S., Peyrou, C., Sosnowski, R., Bigi, A., Carrara, A., Franzinetti, C., Mannelli, I., Brautti, G., Ceschia, M., and Chersovani, L., (1962), Nuovo Cim., 24, 876.

Bassi, P., Clementel, E., Filosofo, I., and Puppi, G., (1949), Nuovo Cim., 6, 484.

Belenkii, S.Z., Maksimenko, V.M., Nikishchov, A.I., and Rozental, L., (1957), Uspechii Fiz. Nauk, 62, (2), 1.

Bennett, S., and Greisen, K., (1961), Phys. Rev., 124, 1982.

Beretta, E., Filosofo, I., Sommacal, B., and Puppi, G., (1953), Nuovo Cim., 10, 1354.

Bigi, A., Brandt, S., deMarco-Trabucco, A., Peyrou, Ch., Sosnowski, R., and Wroblewski, A., (1964), Nuovo Cim., 33, 1249, 1265.

Blackett, P.M.S., (1937), Proc. Roy. Soc., A159, 1.

Borog, V.V., Kirillov-Ugrymov, V.G., Petrukhin, A.A., Rozental, I.L., and Shestakov, V.V., (1965), London Conf., Proc. Phys. Soc. (in the press).

Boult, J., Bowler, M.G., Fowler, P.H., Hackforth, H.L., Keereetaveep, J., Mayes, V.M.,and Tovey, S.N., (1964), preprint Univ. of Bristol.

Bowler, M.G., Fowler, P.H., and Perkins, D.H., (1962), Nuovo Cim., 26, 1182.

Brandt, S., Peyrou, Ch., Sosnowski, R., and Wroblewski, A., (1963), Proc. Sienna Conf. Elem. Particles, 1, 676.

Brode, R.B., (1949), Suppl. Nuovo Cim., 6, 465.

Brode, R.B., and Weber, M.J., (1955), Phys. Rev., 99, 610.

Brooke, G., Gardener, M., Lloyd, J.L., Kisdnasamy, S., and Wolfendale, A.W., (1962a) Proc. Phys. Soc., 80, 674.

Brooke, G., Haymna, P.J., Taylor, F.E., and Wolfendale, A.W., (1962b), unpublished.

Brooke, G., and Wolfendale, A.W., (1964a), Proc. Phys. Soc., 83, 843.

Brooke, G., and Wolfendale, A.W., (1964b), Nature, 202, 480.

Brooke, G., Hayman, P.J., Kamiya, Y., and Wolfendale, A.W., (1964a), Proc. Phys. Soc., 83, 853.

Brooke, G., Meyer, M.A., and Wolfendale, A.W., (1964b), Proc. Phys. Soc., 83, 871.

Bull, R.M., Baber, S.R., Nash, W.F., and Rastin, B.C., (1965), London Conf., Proc. Phys. Soc., (in the press).

Caldirola, P., and Loinger, A., (1950), Nuovo Cim., 7, 1.

Campbell, M.J.T., (1962), Ph.D. Thesis Univ. of Sydney.

Campbell, M.J., Murdoch, H.S., Ogilvie, K.W., and Rathgeber, H.D., (1962), Nuovo Cim., 24, 37.

Caro, D.E., Parry, J.K., and Rathgeber, H.D., (1951), Aust. J.Sci.Res. 4, 16.

Chernavsky, D.S., and Feinberg, E.L., (1963), Proc. Jaipur Conf., 5, 395.

Cini, M., and Wataghin, G., (1950), Nuovo Cim., 7, 135.

Cocconi, G., Koester, L.J., and Perkins, D.H., (1961), UCLRL High Energy Physics, Study Seminars No. 28 Part 2.

Cocconi, G., Lillethun, E., Scanlon, J.P., Stahlbrandt, C.A., Ting, C.C., Walters, J., and Wetherell, A.M., (1964), Phys. Lett., 8, 134.

Cohen, L., Fowler, G.N., and Poulopous, P., (1964), preprint Univ. of Newcastle.

Contogouris, A.P., Frautschi, S.C., and How-Sen Wong (1963), Phys. Rev., 129, 974.

Conversi, M., (1949), Phys. Rev., 76, 311.

Correll, M., (1947), Phys. Rev., 72, 1054.

Coxell, H., (1961), Ph.D. Thesis Univ. of Durham.

Coxell, H., and Wolfendale, A.W., (1960), Proc. Phys. Soc., 75, 378.

Crossland, A.D. and Fowler, G.N., (1965), London Conf., Proc. Phys. Soc. (in the press).

Dekkers, D., Geibel, J.A., Mermod, R., Weber, G., Willits, T.R., Winter, K., Jordan, B., Vivargent, M., King, N.M., and Wilson, E.J.N., (1965), Phys. Rev., 137, 962.

Diddens, A.N., Galbraith, W., Lillethun,E., Manning, G., Parham, A.G., Taylor, A.E., Walker, T,G., and Wetherell, A.M., (1964), Nuovo Cim., 31, 961.

Dodd, P., Jobes, M., Kinson, J., Tallini, B., French, B.R., Sherman, H.J., Skillicorn, I.C., Davies, W.T., Derrick, M., and Radojicic, D., (1961), Proc. Aix-en-Provence Conf., 1, 433.

Duthie, J., Fowler, P.H., Kaddoura, A., Perkins, D.H., and Pinkau, K., (1962), Nuovo Cim., 24, 122.

Fast, G., and Hagedorn, R., (1963), Nuovo Cim., 27, 208, 856.

Filosofo, I., Pohl, E., and Pohl-Rühling, J., (1954), Nuovo Cim., 12, 809.

Fowler, G.N., and Wolfendale, A.W., (1961), Handb. der Physik, 46, 272 (Springer, Berlin).

Fowler, P.H., and Perkins, D.H., (1964), Proc. Roy. Soc., A278, 401.

Frautschi, S.C., (1963), Nuovo Cim., 28, 409.

Frishman, Y., and Yeivin, Y., (1965), preprint Hebrew Univ. of Jerusalem.

Gardener, M., Kisdnasamy, S. Rössle, E., and Wolfendale, A.W., (1957), Proc. Phys. Soc., A70, 687.

Grigorov, N.L., (1963), Zhurn. Eksp. Teor. Fiz., 45, 1544, (Sov. Phys. J.E.T.P., 18, 1063).

Grigorov, N.L., and Shestoperov, V.Ya., (1963), Proc. Jaipur Conf., 5, 268.
(1964) Nucleonica 9, 307.

Grigorov, N.L., Nesterov, V.E., Rapoport, I.D., Savenko, I.A., and Skuridin, G.A., (1965), London Conf., Proc. Phys. Soc. (in the press).

Grigorov, N.L., Erofeeva, I.N., Mitshenko, L.G., Mursin, V.S., Rapoport, I.D., Saricheva, L.I., and Bashindjagian, G.L., (1965), Lond.Conf.(in the press).

Groetzinger, G., and McClure, G.W., (1950), Phys. Rev., 7, 777.

Guseva, V.V., Dobrotin, N.A., Zelevinskaya, N.G., Kotelnikov, K.A., Lebedev, A.M., and Slavatinski, S.A., (1961), J. Phys. Soc. Japan (Suppl. A.3), 17, 375.

Hayman, P.J., (1962), Ph.D. Thesis Univ. of Durham.

Hayman, P.J., and Wolfendale, A.W. (1962a), Nature, 195, 166.
(1962b), Proc. Phys. Soc., 80, 710.

Hayman, P.J., Palmer, N.S., and Wolfendale, A.W., (1963), Proc. Roy. Soc., A.275, 391.

Hien, N.C., Carrigan, R., Edelstein, R., McMahon, T., Nadelhaft, I., Anderson, E.W., Bleser, E., Collins, G.B., Fujü, T., Menes, J., Turkot, F., and Fischer, J., (1965), Proc. Oxford Conf. on Elementary Particles (to be published).

Higashi, S., Kitamura, T., Watase, Y., Oda, M., and Tanaka, Y., (1964), Nuovo Cim., 32, 1.

Holmes, J.E.R., Owen, B.G., and Rodgers, A.L.,(1961a), Proc. Phys. Soc.,78, 496.
(1961b), Proc. Phys. Soc.,78, 505.

Huggett, R.W., (1965), London Conf., Proc. Phys. Soc., (in the press).

Hughes, D.J., (1940), Phys. Rev., 57, 592.

Hyams, B.D., Myroli, M.G., Owen, B.G., and Wilson, J.G., (1950), Proc. Phys. Soc., A63, 1053.

I.C.E.F. Results, (1964), Nuovo Cim.(Suppl. 1), 31, 1.

Imaeda, K., and Kazuno, M., (1964), Nuovo Cim. (Suppl. 1), 31, 83.

Jain, P.L., Glahe, H.C., Srivastava, G.N., and Bharadwaj, P.D., (1961), Nuovo Cim., 21, 859.

Jakeman, D., (1956), Can. J. Phys., 34, 432.

Jones, H., (1939), Rev. Mod. Phys., 11, 235.

Judge, R.J.R., and Nash, W.F., (1965), Nuovo Cim., 35, 1025.

Kamiya, Y., (1963), J. Geomag. Geolect, 14, 191.

Kamiya, Y., Ueno, H., Sagisaka, S., and Sekido, Y., (1963), Nuovo Cim., 30, 1.

Kawaguchi, S., Sakai, T., Oda, H., Ueno, H., and Kamiya, Y.,(1965), London Conf., Proc. Phys. Soc. (in the press).

Kazuno, M., (1964), Nuovo Cim., 34, 303.

Kim, C.O., (1964), Phys. Rev., 136, B515.

Koba, Z., and Krzywicki, A., (1963), Nucl. Phys., 46, 471, 485.

Koba, Z., (1965), London Conf., Proc. Phys. Soc. (in the press).

Kobayashi, T., Namiki, M., and Ohba, I., (1964a), Prog. Theor. Phys., 31, 840.

Kobayashi, T., Namiki, M., Ohba, I., and Orito, S. (1964b), Prog. Theor. Phys., 32, 738.

Kotov, Yu,D.. and Rozental, I.L., (1962), Zhurn. Eksp. Teor. Fiz., 43, 1411, (Sov. Phys., J.E.T.P., 16, 1001)

Krisch, A.D., (1964), Phys. Rev., 135, B1456.

Krzywicki, A., (1963), preprint (CERN).

Lal, S., Subramanian, A., Tonwar, S.C., and Vatcha, R.H., (1965), Phys. Lett., 14, 332.

Lattes, C.M.G., Orsini, C.Q., Pacca, I.G., daCruz, M.T., Okuno, E., Fujimoto, Y., Hasegawa, S., and Yokoi, K., (1964), Nuovo Cim., 33, 680.

Leprince Ringuet, L., and Crussard, J. (1937) J. de Phys. et Rad., 8, 207.

Lewis, H.W., Oppenheimer, J.R., and Wouthuysen, S.A., (1948), Phys. Rev. 73, 127.

Lloret, A., Bezagnet A., Block, M., Drigard, D., Morellet, D., Orkin-Lecourtois, A., Rousset, A., and Veillet, J.J., (1964), Nuovo Cim., 31, 541.

Lloyd, J.L., (1960), Proc. Phys. Soc., 75, 387.

Lohrmann, E., Teucher, M.W., and Schein, M., (1961), Phys. Rev., 122, 672.

MacKeown, P.K., Said, S.S., Wdowczyk, J., and Wolfendale, A.W., (1965), Lond. Conf., Proc. Phys. Soc., (In the press).

Maeda, K., (1960), J. Atmosph. Terr. Phys. , 19, 184.
(1964), J. Geophys. Res., 69, 1725.

Malhotra, P.K., (9163), Nucl. Phys., 46, 559.

Malhotra, P.K., Shukla, P.G., Stephenson, S.A., Vijayalskshmi, B., Boult, J., Bowler, M.G., Fowler, P.H., Hackforth, H.L., Keereetaveep, J., Mayes, V.M., and Tovey, S.N., (1965), London Conf., Proc. Phys. Soc. (in the press).

McCusker, C.B.A., (1963), Proc. Jaipur Conf., 4, 35.

McCusker, C.B.A., and Peak, L.S., (1964), Nuovo Cim., 31, 525.

Melkman, A., Meroz, I., and Yeivin, Y. (1965), London Conf., Proc. Phys. Soc., (in the press).

Miyake, S., (1963), J. Phys. Soc. Japan, 18, 1226.

Miyake, S., Narashimam, V.S., and Ramana Murthy, P.V., (1964), Nuovo Cim., 32, 1524.

Morewitz, H.A., and Shamos, M.H (1953), Phys. Rev. 92, 134.

Moroney, J.R., and Parry, J.K., (1954), Aust. J. Phys., 7, 423.

Morrison, D.R.O., (1963), Com. to Bristol Conf. (CERN/TC/PHYS 63-1) unpublished.

Mursin, V.S., (1965), Yadernaya Fiz., 1, 835.

Narayan, D.S., (1964), Nuovo Cim., 34, 981.

Neddermeyer, S.H. and Curtis, S.B., (1963), Phys. Rev., 131, 835.

Nereson, N., (1948), Phys. Rev., 73, 565.

Nicolic, (1965), P.E.P.C.R.P., 8, 125.

O'Connor, P.V., and Wolfendale, A.E., (1960), Nuovo Cim., 15, (Suppl.2), 202.

Okuda, H., (1963), Proc. Cosmic Ray Lab., Nagoya Univ., 10, 1.

Osborne, J.L., (1964), Nuovo Cim., 32, 816.

Osborne, J.L. and Wolfendale, A.W., (1964), Proc. Phys. Soc., 84, 901.

Osborne, J.L., Wolfendale, A.W., and Palmer, N.S., (1964), Proc. Phys. Soc., 84, 911.

Owen, B.G., and Wilson, J.G., (1951), Proc. Phys. Soc., 64, 417.

Pais, A., (1960), Ann. Phys., 9, 548.
(1963), Ann. Phys., 22, 274.

Pak, W., Ozaki, S., Roe, B.P., and Greisen, K., (1961), Phys. Rev., 121, 905.

Yash Pal, and Peters, B., (1963), Comm. to Bristol Conf., unpublished.
(1964), Mat. Fys. Medd. Dan. Vid. Selsk., 33, No. 15.

Pattison, J.B.M., (1963), M.Sc. Thesis, Univ. of Durham.

Perkins, D.H., (1961), P.E.P.C.R.P., 5, 259.

Pine, J., Davisson, R.J., and Greisen, K., (1959), Nuovo,Cim., 14, 1181.

Pinkau, K., (1964), Fort. der Physik, 12, 139.

Puppi, G., and Dallaporta, N., (1952), P.E.P.C.R.P., 1, 317.

Quercia, I.F., and Rispoli, B., (1953), Nuovo. Cim. 10, 1142.
(1954), Nuovo. Cim. 12, 490.

Ramana Murthy, P.V., (1963), NuovoCim., 30, 762.

Rastin, B.C., (1964), Ph.D. Thesis, Univ. of Nottingham.

Rastin, B.C., Baber, S.R., Bull, R.M., and Nash, W.F., (1965), London Conf., Proc. Phys. Soc. (in the press)

Rochester, G.D., Somogyi, A.J., Turver, K.E., and Walton, A.B., (1965), London Conf., Proc. Phys. Soc., (in the press)

Rodgers, A.L., (1957), Ph.D. Thesis, Univ. of Manchester.

Rossi, B., (1952), High Energy Particles (New York, Prentice-Hall).

Rossi, B., and Greisen, K., (1941), Rev. Mod. Phys., 13, 240.

Smith, J.A., and Duller, N.M., (1959), J. Geophys. Res., 64, 2297.

Smrz, P., (1964), Zhurn. Eksp. Teor. Fiz., 47, 1736, (Sov. Phys. JETP, 20, 1168).

Subramanian, A., (1962), Ph.D. Thesis, Univ. of Madras.

Takada, Y., and Bando, M., (1965), Prog. Theor. Phys., 33, 657.

Volkova, L.V., and Zatsepin, G.T., (1965), London Conf., Proc. Phys. Soc. (in the press).

Waddington, C.J., (1960), Prog. Nucl. Phys., 8, 1.

Wilson, B.G., (1959), Can. J. Phys., 37, 19.

Wolter, W., (1964), Nucleonica, 9, 265.

Yeivin, Y., (1955), Nuovo Cim., 2, 658.
(1956), Ph.D. Thesis, Hebrew Univ. of Jerusalem.

Zatsepin, G.T., and Kuzmin, V.A., (1961), Zhurn. Eksp. Teur. Fiz., 39, 1677, (Sov. Phys. JETP, 12, 171).

Zatsepin, G.T., Nikolskii, S.I., and Khristiansen, G.B., (1963), Proc. Jaipur Conf., 4, 100.

Appendix

The Average charge distribution in the final state in pionization

For a calculation of the positive excess in a statistical model we need to know the average charge excess of produced pions as a function of pion multiplicity. For proton nucleon collisions we have

$$p + N \longrightarrow N + N + n(\pi)$$

and the initial and final pair of nucleons may be in isospin states T = 0 or 1. Consequently the pion assembly may be in a state of isospin T = 0, 1 or 2. We require the average $\langle \pi^+ - \pi^- \rangle$ for such an assembly, commonly taken as $\frac{1}{2}$, independant of multiplicity. For n = 1 and 2 the branching ratios for decay of the pion assembly may be obtained directly from the Clebsch-Gordan coefficients. For $n \geqslant 3$ such a simple procedure cannot be adopted because for such multiplicities the overall symmetry of the pion wave function rather than its isospin must be taken into account. This was considered by Belenkii et al (1957), who derived the various charge states of the final assembly for multiplicities up to 5. For multiplicities $n > 5$ the position is even more complicated because then the symmetry is not uniquely correlated with the isospin of the system and we find multiple occurrence of isospin values for a given symmetry class for T = 2. This has been considered in full detail by Pais (1960, 1963), who derives the branching ratios $\langle [\lambda], T \mid i+T_3, i, n-2i-T_3 \rangle$ for the allowed partitions $[\lambda]$ of an assembly of n pions in a state of isospin T. By summing over all the partitions $[\lambda]$ weighted according to their multiplicity ρ_λ we can find the overall charge distributions. For p - n collisions we find $\langle \pi^+ - \pi^- \rangle \equiv 0$ and for p - p collisions $\langle \pi^+ - \pi^- \rangle = \varphi(n)$. Thus for p - N collisions $\langle \pi^+ - \pi^- \rangle = \varphi(n)/2$.

The several complicating factors outlined above have been overcome recently by Frishman and Yeivin (1965), who, using the elegant methods of tensor operator algebra have derived a closed formula for $\varphi(n)$ for p - nucleon collisions, viz

$$\frac{\varphi(n)}{2} = \langle \pi^+ - \pi^- \rangle = \frac{3}{4} \frac{g_{n+2}(0) - g_n(0)}{g_{n+2}(0) + g_{n+1}(0)}$$

where $$g_n(S) = (2S + 1) \sum_j \frac{(-1)^{n+j}}{2j+1} \binom{n}{j} \binom{2j+1}{j-S}$$

For $n \gtrsim 10$ this may be written in the assymptotic form

$$\frac{\varphi(n)}{2} \approx \frac{1}{2} - \frac{3}{8n} + \frac{15}{64n^2} + \cdots\cdots$$

The exact values of $\varphi(n)$ up to n = 10 are given in table 5.1, and their effect on the charge ratio considered in § 5.4. The effect was seen not to be very great, resulting in a reduced charge excess. The effect is greater when fluctuations in multiplicity are included, since great importance then attaches to the lowest multiplicities where $\varphi(n)/2$ is appreciably different from $\frac{1}{2}$.